Partial Core Power Transformer

Ming Zhong, B.E.(Hons)

A thesis submitted in partial fulfillment
of the requirement for the degree of
Master of Engineering
in
Electrical and Computer Engineering
at the
University of Canterbury,
Christchurch, New Zealand.

April 2012

Abstract

This thesis describes the design, construction, and testing of a 15kVA, 11kV/230V partial core power transformer (PCPT) for continuous operation. While applications for the partial core transformer have been developed for many years, the concept of constructing a partial core transformer, from conventional copper windings, as a power transformer has not been investigated, specifically to have a continuous operation. In this thesis, this concept has been investigated and tested.

The first part of the research involved creating a computer program to model the physical dimensions and the electrical performance of a partial core transformer, based on the existing partial core transformer models.

Also, since the hot-spot temperature is the key factor for limiting the power rating of the PCPT, the second part of the research investigates a thermal model to simulate the change of the hot-spot temperature for the designed PCPT. The cooling fluid of the PCPT applied in this project was BIOTEMP®**.** The original thermal model used was from the IEEE Guide for Loading Mineral-Oil-Immersed transformer. However, some changes to the original thermal model had to be made since the original model does not include BIOTEMP® as a type of cooling fluid. The constructed partial core transformer was tested to determine its hot-spot temperature when it is immersed by BIOTEMP®, and the results compared with the thermal model.

The third part of the research involved using both the electrical model and the thermal model to design a PCPT. The PCPT was tested to obtain the actual electrical and the thermal performance for the PCPT.

The overall performance of the PCPT was very close to the model estimation. However, cooling of the PCPT was not sufficient to allow the PCPT to operate at the design rated load for continuous operation. Therefore, the PCPT was down rated from 15kVA to maintain the hot-spot temperature at 100˚C for continuous operation. The actual rating of the PCPT is 80% of the original power rating, which is 12kVA.

Acknowledgements

The final reading of this thesis has reminded me every moment of the most enjoyable time at University of Canterbury. I am very happy with the outcome of this thesis. The years spent as a post-graduate student and under-graduate at University of Canterbury has been some of the best of my life so far.

None of this would have been possible without the technical and social support of the other students and staff. First and foremost, my sincere thanks must go to my supervisor Professor Pat Bodger and co-supervisor Dr Wade Enright for their academic guidance, support, encouragement and inspiring discussions. Also thanks to the technicians, especially Jac Woudberg and David Healy for helping to build the transformer, and Ken Smart for general transformer testing setup and loaning of testing equipment.

I am very grateful to ABB New Zealand for providing the material which I needed to build my transformer. I would never have been able to build this transformer without the help from ABB New Zealand. I would like to acknowledge the financial support I received through the scholarship from Electric Power Engineering Centre.

Thanks to all my post-graduate colleagues in the Department of Electrical and Computer Engineering for their help, support, and friendship. Special mention must go to Dr Keliang Zhou, Dr Yonghe Liu, Jinyuan Pan, Michael Hwang, Kalyan Malla, Andrew Lapthorn, Lisiate Takau, Jonathan Tse, Parash Acharya, and Bhaba Das.

Finally I would like to thank my parents, for their enduring love, support, and patience. I would not have achieved all of this without the opportunities given by them. I love you Mum and Dad.

Ming Zhong

Table of Contents

Abstract i

Acknowledgements iii

GLOSSARY ix

CHAPTER 1 INTRODUCTION 1

1.1 General Overview 1

1.2 Thesis Objectives 2

1.3 Thesis Outline 3

CHAPTER 2 TRANSFORMER DESIGN MODEL 5

2.1 Introduction 5

2.2 Configurations 6

2.3 Computer Model for the Electrical Performance of Partial Core Transformers 7

2.3.1 Ideal Partial Core Transformer 7

2.3.2 Characteristics of a Non-ideal Partial Core Transformer 10

2.3.3 Partial Core Transformer Equivalent Circuits 11

2.4 Calculation of Partial Core Transformer Values 12

2.4.1 Winding Resistance 17

2.4.2 Leakage Reactance of Both Windings 18

2.4.3 Magnetising Reactance Component 19

2.4.4 Core Loss Component 22

2.4.5 Eddy Current Power Losses and Resistance 22

2.4.6 Hysteresis Power Loss and Resistance Model 23

2.5 Performance tests 24

2.5.1 Open Circuit Model 24

2.5.2 Short Circuit Model 26

2.5.3 Loaded Circuit Model 27

2.6 Discussion and Conclusion 29

CHAPTER 3 OIL-IMMERSED PARTIAL CORE POWER TRANSFROMER (PCPT) COOLING MODEL DESIGN AND TESTING....31

3.1 Introduction 31

3.2 Oil Immersed PCPT Cooling Model 31

3.3 Type of Transformer Cooling..... 31

3.4 Hot-spot Temperature Calculation 31

3.5 Average Winding Temperature Rise of Both Windings..... 33

3.5.1 Winding Hot-spot Temperature 36

3.6 Average Oil Temperature..... 38

3.7 Top and Bottom Oil Temperatures..... 40

3.8 Stability Requirements..... 40

3.9 Oil Viscosity and Specific Heat of BIOTEMP® 40

3.9.1 Including BIOTEMP® into the Thermal Model 41

3.9.2 Summary of Exponents for BIOTEMP® 42

3.10 Thermal Model Corrections and Modifications 42

3.11 Thermal Model Test..... 44

3.12 Discussion and Conclusion 50

CHAPTER 4 DESIGN AND CONSTRUCTION OF THE PARTIAL CORE POWER TRANSFORMER (PCPT) 51

4.1 Introduction 51

4.2 Computer Design Modeling and Results 51

4.3 Thermal Modeling Results..... 55

4.4 Construction of the Core, Windings and Tank..... 56

4.4.1 Construction of the Core..... 56

4.4.2 Winding Construction..... 58

4.4.3 Overall Assembly of the Transformer Core and Winding in the Tank..... 61

4.5 Discussion and Conclusion 63

CHAPTER 5 TESTING THE PARTIAL CORE POWER TRANSFORMER (PCPT) ……..65

5.1 Introduction 65

5.2 Winding Insulation Test..... 65

5.3 Routine Tests..... 67

5.3.1 Winding Resistance Test..... 67

5.3.2 Voltage Ratio and Open Circuit Test Results 68

5.3.3 Short Circuit Test..... 77

5.3.4 Load Circuit Test for PCPT 78

5.4 Weight of Core Components..... 83

5.5 Winding Temperature Testing Results 84

5.6 Experimental Winding Temperature Test..... 84

5.7 Finding a New Power Rating for the Designed PCPT..... 86

5.8 Discussion and Conclusion 87

CHAPTER 6 DISCUSSION AND FUTURE WORK..... 91

6.1 General Conclusions..... 91

6.2 Electrical Model 91

6.3 Thermal model..... 92

6.4 Transformer Design and Construction..... 92

6.5 Transformer testing and results 93

6.6 Future work 95

APPENDIX A LIST OF FIGURES 97

APPENDIX B LIST OF TABLES 99

APPENDIX C THERMAL PROGRAM CODE 101

REFERENCES 111

GLOSSARY

Table of Symbol for the Electrical Model

Equation and programme	Description
A_c	Actual area of the core
D_c	Diameter of the core
A'_c	Area of the core steel
SF_c	Stacking factor of the transformer's core
B_{mc}	Maximum flux density
WT_c	Weight of the core material
l_c	Length of the core
γ_c	Density of the core material
CT_c	Cost per unit weight of the core material
N_{lam}	Number of laminations
LT_c	Thickness of a lamination
Φ	Flux
f	Operating frequency
ω	Angular frequency
e_1	EMF generated by the inside winding
e_2	EMF generated by the outside winding
N_1	Number of turns on the inside winding
N_2	Number of turns on the inside winding
V_1	Voltage of the inside winding
V_2	Voltage of the outside winding
I_1	Current of the inside windings
I_2	Current of the outside windings
a	Turns ratio of the inside and the outside winding
Z_1	Impedance of the inside winding
Z_2	Impedance of the outside winding
WC_1	Thickness of the inside winding wire
W_1	Inside winding conductor diameter
A_1	Cross-sectional area of the inside winding

WC_2	Thickness of the outside winding wire
W_2	Outside winding conductor diameter
A_2	Cross-sectional area of the outside winding
Ly_1	Number of the inside winding layers
Ly_2	Number of the outside winding layers
D_1	Outside diameter of the inside winding
WI_1	Insulation for the inside winding conductor
IC_1	Insulation thickness between the core and the inside winding
IL_1	Insulation for the inside winding layer
LE_1	Length of the inside winding
D_2	Outside diameter of the outside winding
WI_2	Insulation for the outside winding conductor
I_{12}	Inter-winding insulation between the inside and outside windings
IL_2	Insulation for the outside winding
LE_2	Length of the outside winding
WW	Winding width
Vol_1	Volume of the inside winding
$Volw_1$	Volume of the inside winding wire
γ_1	Density of the inside winding material
Sp_1	Spacing factor of the inside winding
Vol_2	Volume of the outside winding
$Volw_2$	Volume of the outside winding wire
γ_2	Density of the outside winding material
Sp_2	Spacing factor of the outside winding
W_{e1}	Weight of the inside winding
W_{e2}	Weight of the outside winding
R_1	Inside winding resistance
ρ_1	Inside winding operating resistivity at temperature T1˚C
$\Delta\rho_1$	Thermal resistivity coefficient of the inside winding material
T_1	Operating temperature of the inside winding
$\rho_{1\text{-}20^{\circ}C}$	Inside winding material resistivity at 20˚C

R_2	Outside winding resistance
ρ_2	Outside winding operating resistivity at temperature T2˚C
$\Delta\rho_2$	Thermal resistivity coefficient of the outside winding material
T_2	Operating temperature of the outside winding
$\rho_{2\text{-}20^{\circ}C}$	Outside winding material resistivity at 20˚C
X_{12}	Leakage reactance of both windings
X_1	Leakage reactance of the inside winding
X_2	Leakage reactance of the outside winding
μ_0	Permeability of free space (air)
l_1	Mean circumferential length of the inside winding
l_2	Mean circumferential length of the outside winding
l_{12}	Mean circumferential length of the inter-winding space
d_1	Inside winding thickness
d_2	Outside winding thickness
R_{core}	Reluctance of the core
R_{air}	Reluctance of the air
μ_{rc}	Relative permeability of the material for the core
X_m	Magnetizing reactance of the core
P_{ec}	Eddy current power loss
R_{ec}	Eddy current resistance
η	Eddy current resistance correction factor
ρ_c	Core operating resistivity at temperature TC˚C
$\Delta\rho_c$	Thermal resistivity coefficient of core material
T_c	Operating temperature of core
$\rho_{c\text{-}20^{\circ}C}$	Core material resistivity at 20˚C
P_h	Hysteresis real power loss
k	Hysteresis loss constant
x	Steinmetz factor
W_{Tc}	Weight of the core
R_h	Hysteresis resistance
R_c	Total core resistance

S_{oc}	Open circuit apparent power
P_{oc}	Open circuit real power
pf_{oc}	Open circuit power factor
Z_{wl}	Inside winding impedance
Y_{core}	Core admittance
Z_{core}	Core impedance
Z_{oc}	Total open circuit impedance looking from the inside winding
Y_{oc}	Open circuit admittance
G_{oc}	Open circuit conductance
B_{oc}	Open circuit susceptance
R_{oc}	Open circuit equivalent shunt resistance
X_{oc}	Open circuit equivalent shunt reactance
$\tilde{I}_{oc1}$	Complex open circuit inside winding current
I_{oc1}	Magnitude of open circuit inside winding current
$\tilde{S}_{oc}$	Complex open circuit apparent power
$\tilde{I}^{*}_{oc1}$	Complex conjugate of the open circuit inside winding current
$\tilde{e}_1$	Induced emf across the core
$Z_2^{'}$	Outside winding impedance
$R_2^{'}$	Outside winding resistance referred to the inside winding
$X_2^{'}$	Outside winding leakage reactance referred to the inside winding
$Y_2^{'}$	Outside winding admittance referred to the inside winding
$Y_{core,2}$	Total admittance of both the core and the Outside winding without the load
$Z_{core,2}$	Total impedance of both the core and the Outside winding without the load
Z_{sc}	Total short circuit impedance
R_{sc}	Total short circuit resistance
X_{sc}	Total short circuit reactance
$\tilde{I}_{sc1}$	Complex short circuit inside winding current
I_{sc1}	Magnitude of the short circuit inside winding current
$\tilde{S}_{sc}$	Complex short circuit apparent power
$\tilde{I}^{*}_{sc1}$	Complex conjugate of the short circuit inside winding current

P_{sc}	Short circuit real power loss
pf_{sc}	Short circuit power factor
Z_L	Impedance of the load
R_L	Resistance of the load
X_L	Reactance of the load
$Z_L^{'}$	Load impedance referred to the inside winding
$Z_{2,L}^{'}$	Combined outside winding and load impedances referred to the inside winding
$Y_{2,L}^{'}$	Admittance of the outside winding and load impedances referred to the inside winding
$Z_{core,2,L}$	Impedance of the outside winding with the load and the core
$Y_{core,2,L}$	Admittance of the outside winding with the load and the core
Z_{loaded}	Loaded circuit impedance referred to the outside winding
$\tilde{I}_{L1}$	Loaded circuit Complex inside winding current
I_{L1}	Magnitude of the loaded circuit inside winding current
$\tilde{S}_1$	Complex apparent power of the loaded circuit
$\tilde{I}_{L1}^{*}$	Complex conjugate of the loaded circuit inside winding current
P_1	Inside winding real power loss
pf_1	Inside winding power factor
$\tilde{I}_{L2}^{'}$	Complex outside current at loaded condition referred to the inside winding
$I_{L2}^{'}$	Magnitude of the secondary winding current at loaded condition referred to the inside winding
$\tilde{V}_L^{'}$	Complex load voltage referred to the primary winding
$V_L^{'}$	Magnitude of complex load voltage
I_{L2}	Outside winding current at loaded condition
V_L	Load voltage
$VREG(\%)$	Voltage regulation
P_L	Real power dissipated across the load
$EFF(\%)$	Efficiency

Table of Symbols for the Thermal Model

Equation	Program	Description
—	A	Ageing acceleration factor
—	AEQ	Equivalent ageing acceleration factor over a complete load cycle
—	ASUM	Equivalent insulation ageing over load cycle, hr
—	AMB()	Ambient point on input of load cycle curve, °C
D	B	Constant in viscosity equation
G	C	Constant in viscosity equation
Cp_{CORE}	—	Specific heat of the core, W-min/lb °C. Steel = 2.43
Cp_{OIL}	CPF	Specific heat of the oil, W-min/lb °C
—	CPST	Specific heat of the steel, W-min/lb °C
Cp_{TANK}	—	Specific heat of the tank, W-min/lb °C
Cp_W	CpW	Specific heat of the winding material, W-min/lb °C. Copper = 2.91
E_{HS}	PUELHS	Eddy loss at winding hot-spot location, per unit of I2R loss
—	GFLUID	Oil volume, gallons
H_{HS}	HHS	Per unit of winding height to hot spot location
—	JJ	Number of points on load cycle
I_R	—	Rated current
K_{HS}	TKHS	Temperature correction for losses at hot spot location
—	LCAS	Loading case 1 or 2
K	PL	Per unit load
—	PUL()	Per unit load point on load cycle curve
—	MA	Cooling code, 1=ONAN
—	MC	Conductor code, 2=copper
—	MCORE	Core over excitation occurs during load cycle, 0=no, 1=yes
—	MF	Oil code, 1=BIOTAMP
—	MPR1	Print temperature Table, 0=no, 1=yes
—	MPR	Print temperature Table, 0=no, 1=yes
M_{CC}	WCC	Core and coil mass, lb
M_{CORE}	WCORE	Mass of the core, lb
M_{OIL}	WFL	Mass of the oil, lb

M_{TANK}	WTANK	Mass of the tank, lb
M_W	WWIND	Mass of the windings, lb
$M_W Cp_W$	XMCP	Winding mass specific heat , W-min/°C
Σ_{MCP}	SUMMCP	Total mass specific heat of the oil, tank and core, W-min/°C
$P_{C.R}$	PC	Core(no-load) loss, W
$P_{C.OE}$	PCOE	Core loss when over excitation occurs, W
P_E	PE	Eddy current loss of the windings at rated load, W
P_{EHS}	PEHS	Eddy current loss at rated windings at reated load and rated winding hot –spot temperature, W
P_S	PS	Stray losses at rated load, W
P_T	PT	Total losses at rated load, W
P_W	PW	Winding I2R loss at rated load, W
P_{HS}	PWHS	Winding I2R loss at rated load and rated hot-spot temperature, W
Q_C	QC	Heat generated by the core, W-min
$Q_{GEN,HS}$	QHSGEN	Heat generated at hot spot temperature, W-min
$Q_{GEN,W}$	QWGEN	Heat generated by windings, W-min
$Q_{LOST,HS}$	QLHS	Heat lost for hot-spot calculation, W-min
$Q_{LOST,O}$	QLOSTF	Heat lost by the oil to ambient, W-min
$Q_{LOST,W}$	QWLOST	Heat lost by the winding, W-min
Q_S	QS	Heat generated by stray losses, W-min
—	RHOF	The oil density, lb/in3
—	SL	Slope of line between two load points of load cycle curve
—	SLAMB	Slope of line between two ambient temperature points of load cycle curve
Δ_t	DT	Time increment for calculation, min
—	DTP	Time increment for printing calculation, min
—	TIM()	Value of time point on load cycle
—	TIMHS	Time during load cycle when maximum hot spot occurs, hour
—	TIMP()	Times when results are printed, min
—	TMP	Time to print a calculation, min
—	TIMCOR	Time when core over excitation occurs, hour
—	TIMTO	Time during load cycle when maximum top oil temperature occurs, hour
—	TIMS	Elapsed time, min

	TIMSH	Elapsed time, hour
x	X	Exponent for duct oil rise over bottom oil, 0.5 for ONAN
y	YN	Exponent for average oil rise with heat loss, 0.8 for ONAN
z	Z	Exponent for top to bottom oil temperature difference, 0.5 for ONAN
Θ	T	Temperature to calculate viscosity, °C
Θ_A	TA	Ambient temperature, °C
$\Theta_{A.R}$	TAR	Rated ambient at kVA base for load cycle, °C
Θ_{BO}	TBO	Bottom oil temperature, °C
$\Theta_{BO.R}$	TBOR	Bottom oil temperature at rated load, °C
Θ_{DAO}	TDAO	Average temperature of oil in cooling ducts, °C
$\Theta_{DAO.R}$	TDAOR	Average temperature of oil in cooling ducts at rated load, °C
Θ_{TDO}	TTDO	Oil temperature at top of duct, °C
$\Theta_{TDO.R}$	TTDOR	Oil temperature at top of duct at rated load, °C
Θ_H	THS	Winding hot spot temperature, °C
—	THSMAX	Maximum hot-spot temperature during load cycle, °C
—	THSR	Winding hot spot temperature at rated load, °C
Θ_K	TK	Temperature factor for resistance correction, °C
—	TKHS	Correction factor for correction of losses to hot spot temperature
—	TKVA1	Temperature base for losses at base kVA input
—	TMU	Temperature in viscosity function, °C
Θ_{AO}	TFAVE	Average oil temperature in the tank and the radiator, °C
—	TFAVER	Average oil temperature in the tank and the radiator at rated load, °C
Θ_{TO}	TTO	Top oil temperature in the tank and the radiator, °C
—	TTOMAX	Maximum top oil temperature in the tank during load cycle, °C
$\Theta_{TO.R}$	TTOR	Top oil temperature in the tank and the radiator at rated load, °C
Θ_W	TW	Average winding temperature, °C
Θ_{WO}	TWO	Temperature of oil adjacent to winding hot spot, °C
$\Theta_{WO.R}$	TWOR	Temperature of oil adjacent to winding hot spot at rated load, °C
—	TWR	Rated average winding temperature at rated load, °C
$\Theta_{W.R}$	TWRT	Average winding temperature at rated load tested, °C
$\Delta\Theta_{AO.R}$	—	Average oil temperature rise over ambient at rated load, °C

$\Delta\Theta_{BO}$	—	Bottom oil temperature rise over ambient, °C
$\Delta\Theta_{BO.R}$	THEBOR	Bottom oil temperature rise over ambient at rated load tested, °C
$\Delta\Theta_{DO.R}$	THEDOR	Temperature rise of oil at top of duct over ambient at rated load, °C
$\Delta\Theta_{DO/BO}$	DTDO	Temperature rise of oil at top of duct over bottom oil, °C
$\Delta\Theta_{H/A}$	THEHSA	Winding hot spot rise over ambient, °C
$\Delta\Theta_{H/WO}$	—	Winding hot spot temperature rise over oil next to hot spot location ,°C
$\Delta\Theta_{T/B}$	DTTB	Temperature rise of oil at top of radiator over bottom oil, °C
$\Delta\Theta_{TO}$	—	Top oil temperature rise over ambient, °C
$\Delta\Theta_{TO,R}$	THETOR	Top oil temperature rise over ambient at rated load, °C
—	THKAV2	Rated ave. winding temperature rise over ambient at kVA base of load cycle, °C
$\Delta\Theta_{W/A,R}$	THEWA	Tested or rated average winding temperature rise over ambient, °C
$\Delta\Theta_{WO/BO}$	—	Temperature rise of oil at winding hot spot location over bottom oil, °C
μ	FNV(B,C,T)	Viscosity, cP
μ_{HS}	VISHS	Viscosity of oil for hot spot calculation, cP
$\mu_{HS,R}$	VIHSR	Viscosity of oil for hot spot calculation at rated load, cP
μ_{W}	VIS	Viscosity of oil for average winding temperature rise calc. cP
$\mu_{W,R}$	VISR	Viscosity of oil for average winding temperature rise at rated load, cP
t_W	TAUW	Winding time constant, min
—	XKVA1	kVA base for losses in input data
—	XKVA2	kVA base for load cycle curve
Suffixes		**Description**
1		Initial time
2		At the next instant of time
R		At rated load
/		over

CHAPTER 1

INTRODUCTION

In modern power system networks, alternating current (AC) supply systems are important due to their power transfer capabilities. The distribution parts of power networks require different voltage levels from the generation systems, and these are different to the high voltage levels used in transmission. Therefore, the AC voltage must be varied up or down to satisfy loading voltage requirements. In order to solve this issue, transformers that change the AC voltage to desired voltage levels are required.

Power transformers are devices in which power supplied at one voltage is converted to a second voltage with a minimum amount of power loss. The fundamental principle of power transformers was discovered by Michael Faraday in 1831[1]. A basic characteristic of power transformers is that they can only operate on AC voltages.

Power system and high voltage testing transformers are usually designed with full iron cores. Their construction, transportation and maintenance are generally expensive and complex. To minimise these costs, the physical size of transformers needs to be diminished by reducing the core size of transformers. Partial core transformers are well-suited for this size reduction. This physical advantage makes the partial core transformers to suit as an emergency power transformer. The aim of this research was to develop a 15kVA; 11kV/ 230V partial core power transformer (PCPT) for continuous operation.

1.1 General Overview

The project has been divided into three parts. They are the PCPT modeling, the PCPT manufacturing and the PCPT testing. A flow chart of the project activities is shown in Figure 1.1.

The project starts with the modeling section. This has been separated into two different phases, being the electrical model and the thermal model. The electrical model evaluates the physical dimensions and the electrical performance for the PCPT. The electrical model is based on what material is available for building the tank, the core, the former, the inside winding, the outside winding, and the winding layer insulation to determine its electrical performance and physical dimensions. The thermal model is based on the transformer cooling

type and the cooling fluid, and calculates the thermal performance of the PCPT. The second part of the project is manufacturing a PCPT. The manufacturing of the PCPT is divided into three sections. They are the core construction, winding construction and the tank construction. The final stage of the project is the testing of the PCPT. There are six tests that determine the overall electrical and thermal performance of the PCPT. They are the winding insulation test, the winding resistance test, the open circuit test, the short circuit test, the load circuit test, and the winding thermal test.

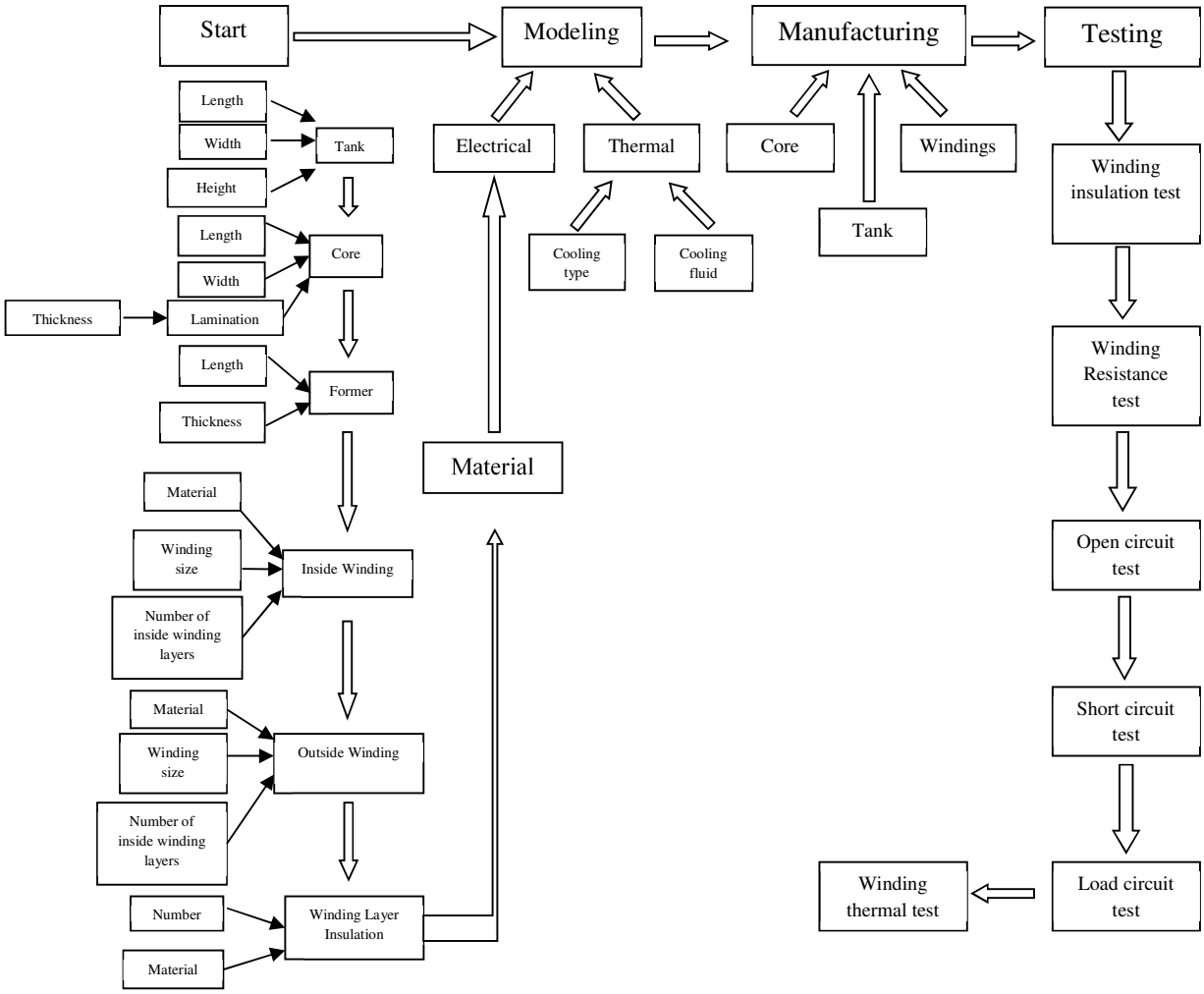

Figure 1.1 Flow chart of the project overview.

1.2 Thesis Objectives

The aim of the research was to construct a 15kVA 11000/230V PCPT for continuous operation. The major challenge was the investigation of an oil-immersed transformer thermal model to calculate the temperature rise of the PCPT. Also, the thermal model had to incorporate the thermal characteristics of BIOTEMP®. BIOTEMP® was the cooling fluid

chosen for this project. The model was used to design a power transformer that could be operated under normal temperature conditions for a long time. The last stage of this research was to build a PCPT transformer and obtain its experimental electrical and thermal performances.

1.3 Thesis Outline

Chapter 2 gives a summary of an electrical model for building a partial core power transformer. The ideal partial core transformer and the non-ideal partial core transformer are introduced in this chapter. The open circuit test, the short circuit test, and the load circuit test models are developed from the electrical model for the partial core power transformer.

Chapter 3 gives a summary of developing and testing a thermal model for the oil-immersed partial core power transformer. The cooling concept for an oil-immersed full core transformer model is introduced, and applied for estimating the winding thermal performance of the partial core oil-immersed transformer. The original thermal model was modified with the thermal characteristics of BIOTEMP®. Also, a hot-spot temperature test on a built PCPT was under taken to evaluate the accuracy of the thermal model.

Chapter 4 shows how to use the two models which were introduced in chapter 2 and chapter 3 to model and to design a PCPT. Also, the construction of this designed of PCPT is also introduced in this chapter. The construction procedure for the PCPT is the core, the winding, and the transformer tank.

Chapter 5 presents the testing of the partial core power transformer. This includes the transformer winding insulation test, the winding resistance test, the open circuit test, the short circuit test, the load circuit test and the winding thermal test. Each test has been introduced in this chapter including their setup, test standards and test results.

Chapter 6 presents the main conclusions of this thesis and discusses possible directions for future research.

CHAPTER 2

TRANSFORMER DESIGN MODEL

2.1 Introduction

The aim of this research was to design a 15kVA partial core power transformer (PCPT). In order to build such a transformer, the overall design model is divided into two parts. The first part of the transformer design model determines the electrical performance, physical dimensions and weight. The second part of the transformer design model determines the winding and oil temperatures of the desired transformer. The modeling technique and details of the electrical performance, the physical dimensions and the weight for PCPT is introduced in this chapter. The modeling of the open circuit test, the short circuit test and the load circuit test for PCPT is also given in this chapter.

Partial core transformers do not have outer limbs and connecting yokes as do full-core transformers. Therefore, the magnetic circuit of a partial core transformer has both the core and the surrounding air as the flux path. Thus, the flux path reluctance is greater than if just core material is used. Consequently, the magnetising reactance of the partial-core transformer is lower than that for the full-core transformer [2].

Partial core transformers have been designed as step-up transformers for energising capacitive loads, where they are referred to as partial core resonant transformers (PCRTXs). A partial core resonant transformer model is illustrated in Figure 2.1. By matching the inductive reactance of the secondary winding to the capacitive reactance of the load, the reactive power drawn from the primary winding can be reduced to almost zero [2]. Applications include high-voltage testing of hydro generator stators [3] [4] and energising arc-signs [5] [6]. In these examples, the advantages over conventional equipment, a full-core step-up transformer and a separate full-core transformer, are significant reductions in weight and cost, and increased portability. Due to these advantages, the partial core transformer design is suitable for a portable emergency power transformer. Also due to the size reduction of the transformer, the partial core transformer has an advantage use as an emergency power transformer application.

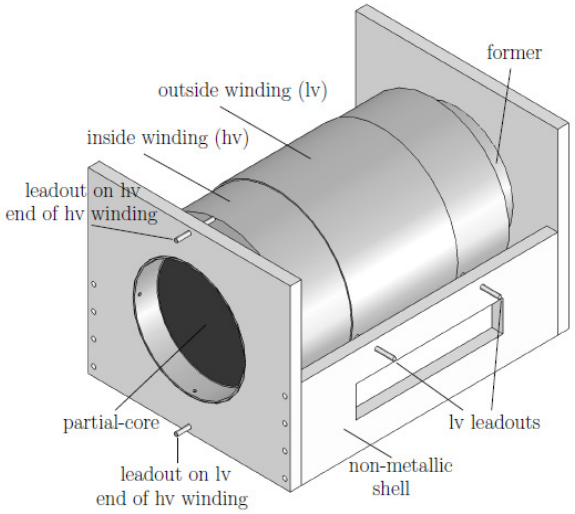

Figure 2.1 3D model of a partial core resonant transformer [2].

2.2 Configurations

A cross-sectional view of a partial core transformer is shown in Figure 2.2. The special physical feature of a partial core transformer is that the laminated core only occupies the central space. The yokes and limbs are not present. The windings are wrapped around the core. For the particular example shown, the high voltage winding is on the outside, and the low voltage winding is on the inside. This was a convenient arrangement for the intended use of the power transformer.

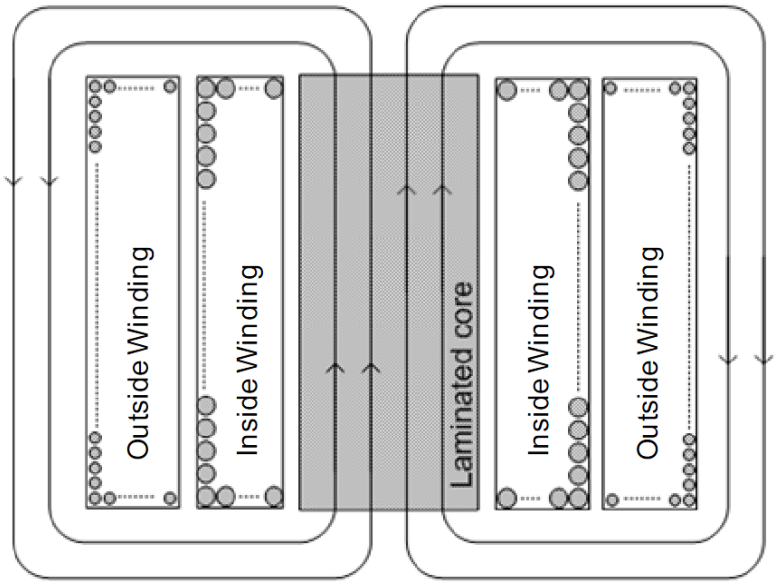

Figure 2.2 Partial core transformer cross sectional view [1].

2.3 Computer Model for the Electrical Performance of Partial Core Transformers

In order to develop a computer model for a partial core transformer, the basic theory for an ideal partial core transformer needs to be introduced [1].

2.3.1 Ideal Partial Core Transformer

Generally, a single phase partial core transformer is constructed with two windings and a core, with both windings wound around the core. Exciting one winding by connecting it to an AC voltage source means a magnetic flux can be generated in the core [7]. The magnetic flux flows inside the second winding, and generates an electromotive force (emf). The emf creates the current in the second winding if the second winding circuit is closed with load impedance. Power losses are always associated with this movement of EMF.

It is appropriate to start the modeling of a transformer with its ideal performance, and take into account the factors that make it into a real device. A 3D schematic and equivalent circuit of an ideal, two-winding, single phase partial core transformer are shown in Figure 2.3.

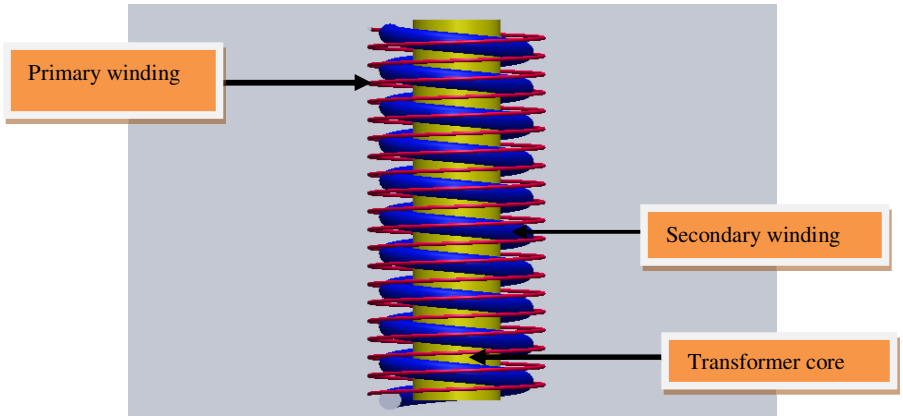

(a) Schematic

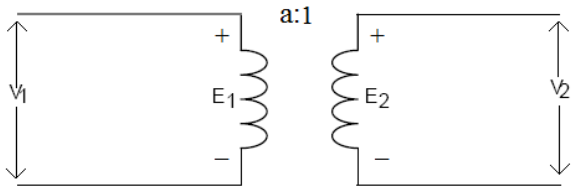

(b) Equivalent circuit

Figure 2.3 An ideal partial core transformer.

.

The fundamental components are the partial core, the inside winding with N_1 turns and the outside winding with N_2 turns. The basic operation of both full core transformers and partial core transformers is the same. According to Faraday's law [2], the emfs on each winding are expressed as the number of turns for each winding multiplied by a finite rate of change of flux Φ such that

$$e_1 = N_1 \frac{d\Phi}{dt} \tag{2.1}$$

and

$$e_2 = N_2 \frac{d\Phi}{dt} \tag{2.2}$$

The direction of e_1 is such that it produces a current which opposes the flux change, according to Lenz's law [2]. From equations 2.1 and 2.2,

$$\frac{e_1}{e_2} = \frac{N_1}{N_2} = a \tag{2.3}$$

where a is the nominal turns ratio.

If E_1 and E_2 are the RMS values of e_1 and e_2 respectively, then

$$\frac{E_1}{E_2} = \frac{N_1}{N_2} \tag{2.4}$$

Also, since $e_1 = v_1$ and $e_2 = v_2$ for an ideal partial core transformer, then

$$\frac{V_1}{V_2} = \frac{N_1}{N_2} \tag{2.5}$$

The flux and voltage are related by

$$\Phi = \frac{1}{N_1} \int e_1 dt = \frac{1}{N_2} \int e_2 \, dt \tag{2.6}$$

In general terms, if the flux varies as a sine function such that

$$\Phi = \Phi_m \sin \omega t \tag{2.7}$$

then the corresponding voltage V for linking an N/turn winding is given by Faraday's law as

$$V = \omega N \Phi_m \cos \omega t \tag{2.8}$$

The RMS value of the induced voltage is thus Φ

$$V = \frac{\omega N \Phi_m}{\sqrt{2}} = 4.44 f N \Phi_m \tag{2.9}$$

where $\omega = 2\pi f$

f is the frequency (Hz)

Equation 2.9 is known as the emf or transformer equation.

For an ideal partial core transformer, the magneto motive force (mmf) required to produce the working flux is negligibly small. This mmf is the resultant of the mmf due to the primary current and that due to the secondary current such that

$$N_1 i_1 = N_2 i_2 \tag{2.10}$$

Therefore

$$\frac{i_1}{i_2} = \frac{N_2}{N_1} = \frac{1}{a} \tag{2.11}$$

Multiplying Equations 2-5 and 2-11 together,

$$v_1 i_1 = v_2 i_2 \tag{2.12}$$

Thus, the apparent powers through both the primary and secondary windings are equal. This is the power rating of a transformer. The functionality of the primary winding is to absorb the power from the power sources; at the same time the secondary winding delivers the power to the load. In the definition of an ideal transformer, no power is lost internally due to the windings and core so that the two quantities are equal.

From Equations 2.5 and 2.11, it can be shown that if load impedance $Z_2 = \frac{v_2}{i_2}$ is connected to the secondary, the impedance Z_2' seen at the primary is

$$\frac{Z_2'}{Z_2} = \left(\frac{N_1}{N_2}\right)^2 = a^2 \tag{2.13}$$

2.3.2 Characteristics of a Non-ideal Partial Core Transformer

Modeling a practical partial core transformer is more complex than modeling an ideal partial core transformer. There are several losses associated with designing a real partial core transformer, and these losses are mainly created by the core and windings of the transformer. The equivalent circuit of a non-ideal partial core transformer is shown in Figure 2.4. This equivalent circuit is relevant for low frequency modeling of power transformers.

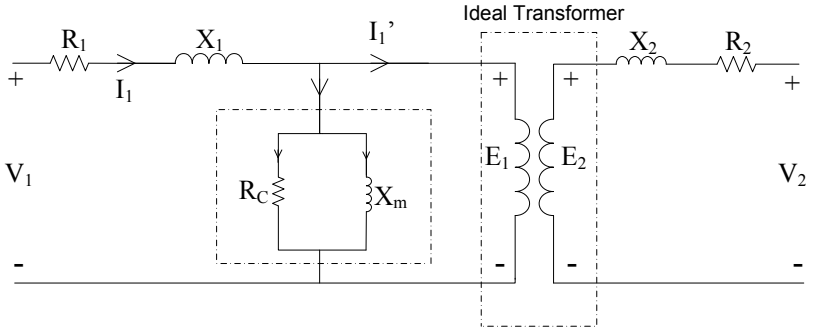

Figure 2.4 Equivalent circuit of a non-ideal partial core transformer operating at low frequency [8].

The most obvious loss is created by the current in the primary winding, even when the secondary winding is open circuited. This current has two components. The first component is the magnetising current, which is generated by having a core of finite permeability. A significant magnetising force is required to produce an operating flux. This is modeled as a magnetising reactance, which is illustrated as a shunt reactance path (designated by X_m) on the primary side of the partial core transformer [8].

The second component current of the current represents two losses inside the transformer's core which are hysteresis losses and eddy current losses, such that some real power is absorbed even at no-load. These losses can be modeled by the addition of a shunt resistance (designated by R_c) on the primary side, through which a core loss current flows.

The real power losses of both windings are other significant components modeled to account for the performance of a real partial core transformer. These can be modeled as a series resistance for each winding (R_1 and R_2 respectively).

When current flows through the primary and secondary side of the transformer, there is some leakage flux which passes through the air surrounding each winding instead of going through the core. Since there is very little reluctance created by the magnetic path through the iron core compared to the reluctance generated by the air path around each winding, the leakage flux is usually quite small. However, the leakage flux cannot be ignored since it links with the turns in each winding, and establishes emf's that oppose the flow of current through each winding. Therefore, the leakage flux has the same effect as an unwanted inductance in series with each winding. The unwanted inductance is also termed the leakage inductance, which is represented by reactance's X_1 and X_2 in the primary and secondary windings respectively [8].

In addition, capacitance exists between turns, between one winding and another, between windings and the core, as well as between windings and the tank. However, these capacitances need to be considered only at relatively high frequencies. For the particular design, the capacitances are ignored. This is a reasonable approximation for power transformers operating at mains frequency which in New Zealand is 50Hz [27].

2.3.3 Partial Core Transformer Equivalent Circuits

In order to simplify the equivalent circuit of Figure 2.4, the parameters of the secondary circuitry can be referred to the primary, as shown in Figure 2.5. The ideal transformer is eliminated so that the transformer can be represented exclusively by an RL circuit. Such a representation involves simpler circuit analysis than that for the circuit of Figure 2.4.

The equivalent circuit of a partial core transformer is particularly useful in determining its performance and characteristics. Voltage regulation and efficiency are two important measures for evaluating the quality of the designed transformer [8].

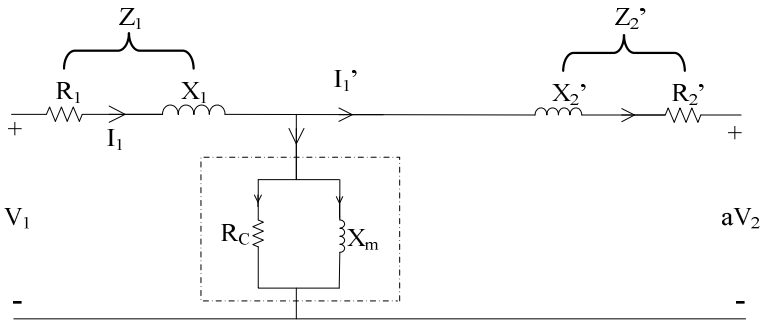

Figure 2.5 Transformer equivalent circuit referred to the primary side [8].

2.4 Calculation of Partial Core Transformer Values

To determine the components of the equivalent circuit, the transformer needs to be designed. From the dimensions used of material sued for the core and windings, the values of these components can be determined.

The physical structure of the transformer is a combination of laminated core, winding wire, and insulation. Figure 2.6 illustrates the dimensions of the winding wires, the laminated core, the number of layers and insulation. Since both windings are wound around the laminated core, the dimensions of the core have to be determined before those of the windings.

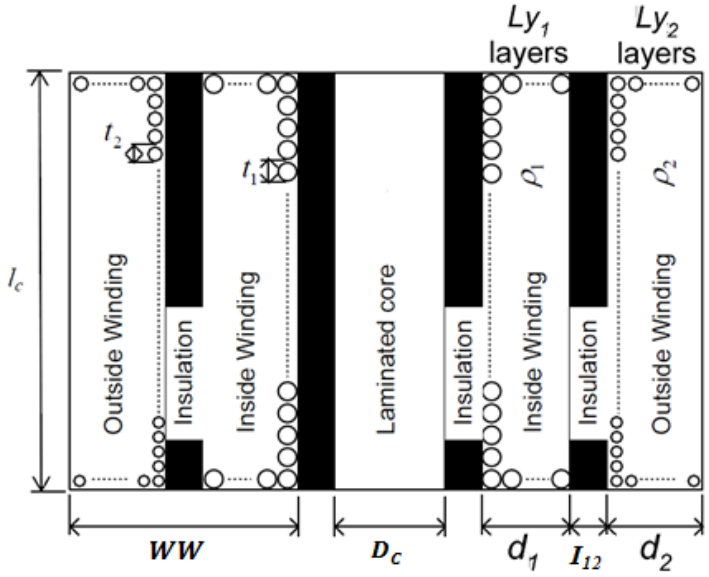

Figure 2.6 Centre limb of a partial core transformer showing component dimensions and material properties [8].

The area of the core is:

$$A_c = \pi D_c^2/4 \tag{2.14}$$

where

D_c is the diameter of the core

The steel core of the transformer has insulation between the laminations; therefore, the actual area of the core steel is

$$A_c' = A_c \times SF_c \tag{2.15}$$

where

SF_c is the stacking factor of the transformer's core to account for the insulation

The maximum flux density is

$$B_{mc} = \frac{\sqrt{2}V_1}{\omega N_1 A_c'} \tag{2.16}$$

The maximum flux density needs to be less than 1.89T for Kawasaki lamination steel with 0.23mm thickness [9].

The core volume is

$$V_c = A_c^{'} \times l_c \tag{2.17}$$

The weight of the core material is a product of the material density DN_c and the core volume.

$$WT_c = DN_c \times V_c \tag{2.18}$$

The cost of the core material is

$$CT_c = C_c \times WT_c \tag{2.19}$$

where

C_c is the cost per unit weight of the core material.

The number of laminations is:

$$N_{lam} = \frac{D_c}{SF_c \times LT_c} \tag{2.20}$$

where

LT_c is the thickness of the lamination

For the winding calculations, the thickness of the both windings has to be specified. The thickness of the inside winding wire is

$$WC_1 = W_1 + 2*WI_1 \tag{2.21}$$

where

W_1 is the diameter of the inside winding wire

WI_1 is the insulation of the inside winding wire

Hence, the cross-sectional area of the inside winding is

$$A_1 = \frac{WC_1{}^2 \times \pi}{4} \tag{2.22}$$

The thickness of the outside winding wire is

$$WC_2 = W_2 + 2 * WI_2 \tag{2.23}$$

where

W_2 is the diameter of the outside winding wire

WI_2 is the insulation of the outside winding wire

Hence, the cross-sectional area of the outside winding is

$$A_2 = \frac{WC_2{}^2 \times \pi}{4} \tag{2.24}$$

The number of turns for the inside winding is

$$N_1 = Ly_1 \times \frac{l_c}{WC_1} \tag{2.25}$$

where

Ly_1 is the number of winding layers on the inside winding

l_c is the length of the transformer core

and the number of turns for the outside winding is

$$N_2 = Ly_2 \times \frac{l_c}{WC_2} \tag{2.26}$$

where

Ly_2 is the number of winding layers on the outside winding

Hence the turn's ratio is

$$a = N_1/N_2 \tag{2.27}$$

This assumes that the lengths of both the inside and outside windings are the same as the core length, as shown in Figure 2.7.

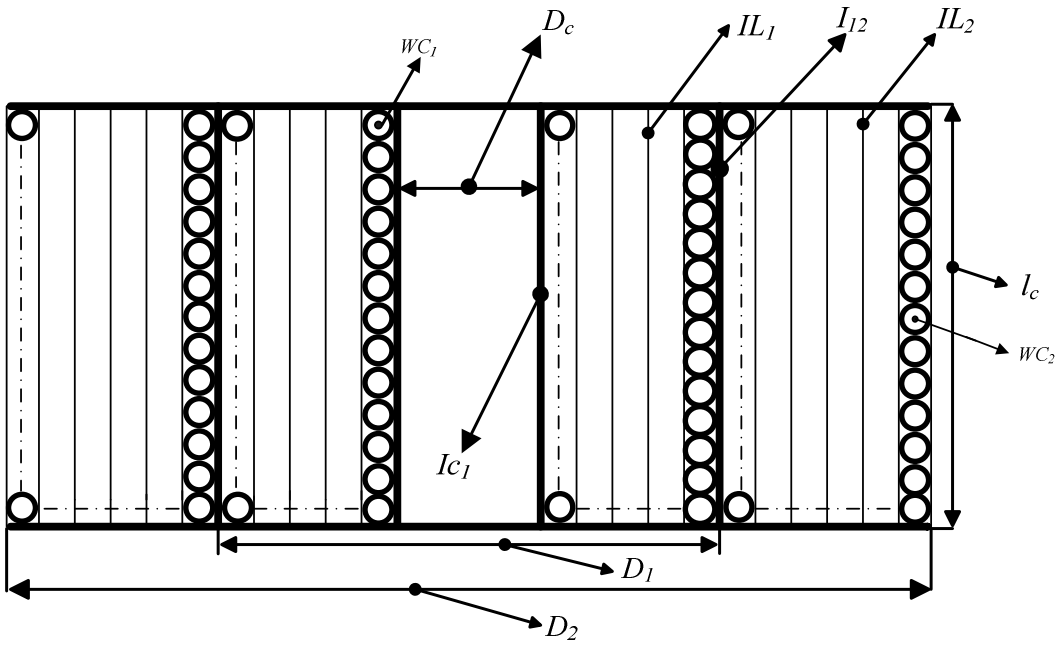

Figure 2.7 Dimensions of a partial core transformer.

In the partial core model, the transformer is constructed from the core out to the windings. Given the core length and diameter, the inside winding (usually the low voltage winding) is constructed by winding it layer by layer around the core. Insulation is placed between the core, the inside winding (former), and between each layer for both windings. Insulation can also be placed between each winding.

The outer winding (usually the HV winding) is wound over this, with insulation between layers according to the voltage between them. According to Figure 2.7 and with reference to Figure 2.6 the diameter of the inside winding is

$$D_1 = D_c+2.0*((Ic_1+ Ly_1*(WC_1+IL_1)) - IL_1) \tag{2.28}$$

where

Ic_1 - core/inside winding insulation thickness

IL_1 - inside winding layer insulation

The length of the inside winding wire is

$LE_1=N_1*\pi*(Ic_1+D_C)/2.0$

(2.29)

The diameter of the outside winding is

$D_2 = D_1+2.0*((I_{12}+ Ly_2*(WC_2+IL_2)) -IL_2)$ (2.30)

where

WI_2 –conductor insulation for the outside winding

I_{12} –insulation between the inside and outside winding

IL_2 – secondary winding layer insulation

The length of the outside winding wire is

$LE_2=N_2* \pi *(D_2+D_1+I_{12})/2.0$ (2.31)

The winding width (*WW*) of the transformer windings is

$$WW = (\frac{D_2-D_c}{2})$$ (2.32)

Given the material densities and the costs per unit weight, the amount of material required for the windings can be determined.

The volume of the inside winding wire is

$$Vol_{w1} = LE_1 \times A_1$$ (2.33)

The volume of the inside winding which includes its insulation is

$$Vol_1 = \frac{L_c}{4}(D_1^2 - (D_c + I_{c1})^2)\pi$$ (2.34)

The spacing factor of the inside winding is

$$Sp_1 = \frac{Vol_{w1}}{Vol_1}$$ (2.35)

The weight of the inside winding wire is

$$We_1 = Vol_{w1} \times \gamma_1$$ (2.36)

where

γ_1 is the density of the inside winding material.

The volume of the outside winding wire is:

$$Vol_{w2} = LE_2 \times A_2 \tag{2.37}$$

The volume for the outside winding which includes its insulation is

$$Vol_2 = \frac{L_c}{4}(D_2^2 - (D_1 + I_{12})^2)\pi \tag{2.38}$$

The spacing factor of the outside winding is

$$Sp_2 = \frac{Vol_{w2}}{Vol_2} \tag{2.39}$$

and the physical weight of the outside winding wire is

$$We_2 = Vol_{w2} \times \gamma_2 \tag{2.40}$$

where

γ_2 is the density of the outside winding material.

From all the dimensions, the metal physical characteristics and the number of turns, the equivalent circuit parameters of the transformer can be calculated, and its electrical performance predicted.

2.4.1 Winding Resistance

The inside winding resistance is [8]

$$R_1 = \frac{\rho_1 LE_1}{A_1} \tag{2.41}$$

The operating resistivity at temperature T_1 °C is calculated as

$$\rho_1 = \rho_{1-20^{\circ}\mathrm{C}}\,(1 + \Delta\rho_1(T_1 - 20)) \tag{2.42}$$

where

$\Delta\rho_1$ is the thermal resistivity coefficient of the inside winding material.

ρ_{1-20^0C} is the inside winding material resistivity at 20°C.

The outside winding resistance is [8]

$$R_2 = \frac{\rho_2 L E_2}{A_2} \tag{2.43}$$

The operating resistivity at temperature T_2°C is calculated as [8]

$$\rho_2 = \rho_{2-20°C}\,(1 + \Delta\rho_2(T_2 - 20)) \tag{2.44}$$

where

$\Delta\rho_2$ is the thermal resistivity coefficient of the outside winding material.

ρ_{2-20^0C} is the outside winding material resistivity at 20°C.

2.4.2 Leakage Reactance of Both Windings

The leakage flux path for a partial core transformer is shown in Figure 2.8 [8]. This model was used in preference to those developed in [2] because of its simplicity for inclusion into an analytically closed form solution model of the transformer. This made such modelling consistent with the form of the thermal model also used in this thesis.

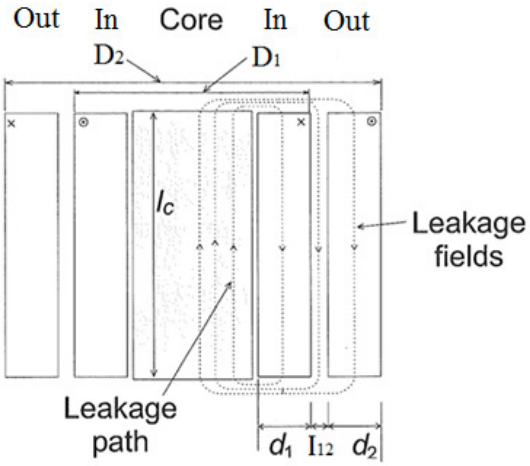

Figure 2.8 Calculate the leakage reactance for both windings [8].

The inside and outside winding leakage reactances are calculated from a total leakage reactance. The equation of the total transformer leakage reactance is [8]

$$X_{12} = \frac{\omega\mu_o N_1^2}{l_c}\left[\frac{l_1 d_1 + l_2 d_2}{3} + l_{12} I_{12}\right] \tag{2.45}$$

where

μ_o is the permeability of free space (air)

l_1 is the mean circumferential length of the inside winding .

$$l_1 = \pi\left(D_c + \frac{WW}{2}\right) \tag{2.46}$$

l_2 is the mean circumferential length of the outside winding.

$$l_2 = \pi\left(D_c + \frac{3WW}{2}\right) \tag{2.47}$$

l_{12} is the mean circumferential length of the inter-winding space.

$$l_{12} = \pi(D_c - WW) \tag{2.48}$$

$d_1 = \frac{D_1 - D_c}{2}$

d_1 is the inside winding thickness

$d_2 = \frac{D_2 - D_1}{2}$

d_2 is the outside winding thickness

I_{12} is the insulation between the inside and the outside windings

The inside and outside winding leakage reactances are usually taken as being equal. Therefore

$$X_1 = X_2 = X_{12}/2 \tag{2.49}$$

2.4.3 Magnetising Reactance Component

The magnetising current reactance of a partial core transformer is different to that of the full core transformer, since the flux of a partial transformer not only goes through the core, but also flows in the air around the core. This is shown in Figure 2.9.

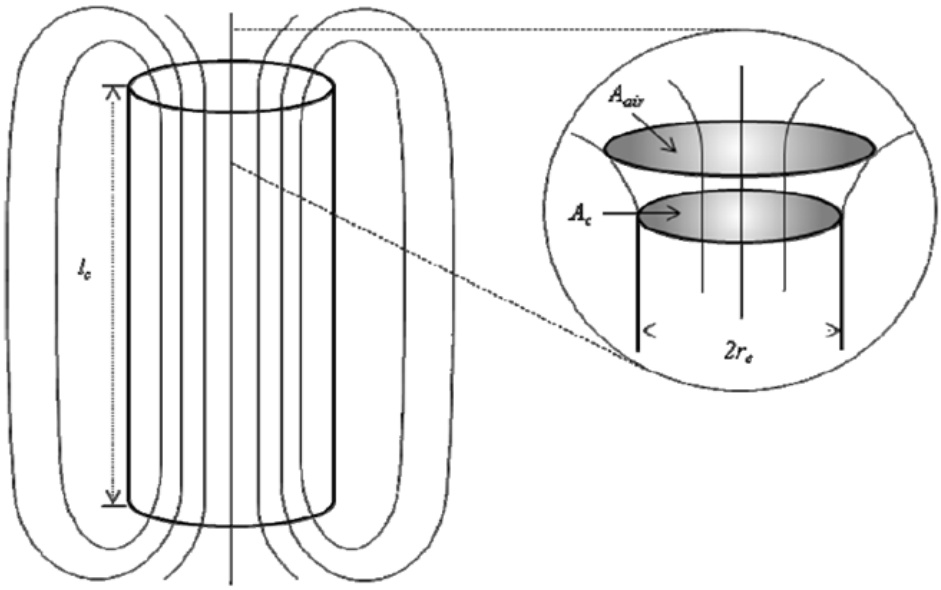

Figure 2.9 Axial flux view of the core for the partial core transformer [8].

A method to calculate the magnetising reactance specifically for partial core transformer has been developed [8]. Again, this model was used in preference to those developed in [2] because of its simplicity for inclusion into the analytically closed form solution model of the transformer. It assumes that the reluctance of the air is only in the regions at the ends of the core. The reluctance of the air at one end of the partial core transformer is

$$R_{air} = 1.69356 \times 10^5 \left(\frac{1}{A_c'}\right)^{0.345} \left(\frac{1}{l_c}\right)^{0.31} \tag{2.50}$$

The reluctance of the core is

$$R_{core} = \frac{l_c}{\mu_0 \mu_{rc} A_c'} \tag{2.51}$$

where

μ_0 is the permeability of free space (air)

μ_{rc} is the relative permeability of the material for the core

The equivalent magnetic circuit of the partial core transformer is illustrated in Figure 2.10.

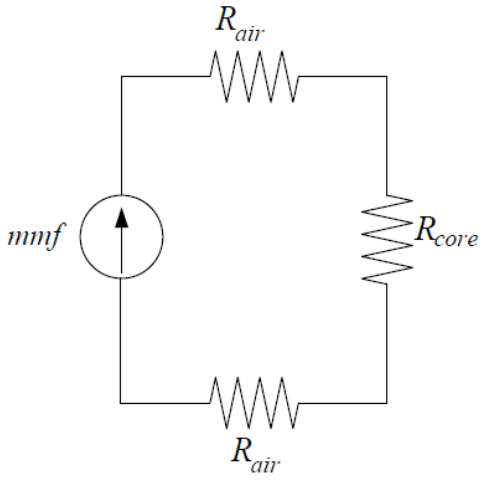

Figure 2.10 Magnetic circuit of the partial core transformer.

The overall reluctance of the partial core transformer is [8]

$$R_T = R_{core} + 2R_{air} \tag{2.52}$$

This is equivalent to a flux path through a homogeneous medium of relative permeability μ_{rT}

$$R_T = \frac{l_T}{\mu_0 \mu_{rT} A_T} \tag{2.53}$$

where l_T = overall flux path length

$= l_c + 2l_{air}$

$\approx l_c$ (since $l_c \gg 2l_{air}$)

$A_T =$ overall cross-sectional area of the transformer

$\approx A_c$

Rearranging equation 2-53 gives

$$\mu_{rT} = \frac{l_c}{\mu_0 R_T A_c} \tag{2.54}$$

The magnetising reactance of a partial core transformer is

$$X_m = \frac{\omega N_1^2 \mu_0 \mu_{rT} A_c}{l_c} \tag{2.55}$$

2.4.4 Core Loss Component

In general, the core loss of a full core power transformer is associated with the weight of material used in the construction of the core. The typical expression for calculating the core loss of a full core power transformer is [15]

$$P_c = P_{c/_{kg}} \times W_{c_{kg}} \tag{2.56}$$

where

$P_{c_{/kg}}$is the core loss per kilogram

$W_{c_{kg}}$is the total weight of the core

However, the core construction of a partial core power transformer is quite different to that of a full-core power transformer. Therefore, the flux path of the partial core transformers is not the same as the full core transformers. This means that the general expression for core losses for a full core transformer is not ideal for estimating the core losses for a partial core transformer. Therefore, it is necessary to develop core losses models for the partial core power transformer.

The core losses of all types of transformer are attributed to two components; they are the eddy current power loss and hysteresis power loss.

2.4.5 Eddy Current Power Losses and Resistance

The eddy current resistance is derived from consideration of the core resistivity, the induced emf in a lamination, the current flow in the laminations, and the associated dimensions of the core and laminations [8].

The eddy current power loss can be expressed as

$$P_{ec} = \frac{LT_c^2}{12\rho_c} \times \frac{l_c}{N_1^2 A_c'} e_1^2 \tag{2.57}$$

Hence the eddy current resistance for the transformer equivalent circuit is then

$$R_{ec} = \frac{e_1^2}{P_{ec}} \tag{2.58}$$

$$= \frac{N_1^2 A_c'}{l_c} \times \frac{12\rho_c}{LT_c^2} \tag{2.59}$$

However, the value for the eddy current resistance of the partial core transformers determined from test results is much smaller than that from equation 2.59 [8]. This is because in practice there are eddy current losses in the ends of the core due to the flux direction having a significant radial component in these regions, rather than being along the core, as assumed in theory.In order to match the test and model results, equation 2.59 has to be multiplied by a correction factor η. The actual eddy current resistance for the partial core transformer model is

$$R_{ec} = \frac{N_1^2 A_c'}{L_c} \times \frac{12\rho_c}{LT_c^2} \times \eta \qquad (2.60)$$

For the core laminations used in the partial core transformers fabricated and tested during the project, the average value of η is 60. This value is used in this project. However, the change in eddy current losses does not hold a linear relationship. Therefore, equation 2.59 cannot model all types of partial core transformers. An alternative model for estimating eddy current losses for partial core transformers is given by Huo Xi Ting [10]. It has not been incorporated into the design model in this project because it had not been published when the project was started. Incorporating the new eddy current model into the partial core transformer design model and improving the accuracy of eddy current losses is for a future project. The alternative of using a radially stacked core [2] was not practical for the particular partial core power transformer designed and built because the diameter of the partial core was too small.

The operating resistivity at temperature T_c°C is calculated as:

$$\rho_c = \rho_{c-20^0C}\,(1 + \Delta\rho_c(T_c - 20)) \qquad (2.61)$$

where

$\Delta\rho_c$ is the thermal resistivity coefficient of the core material

ρ_{c-20^0C} is the core material resistivity at 20°C

2.4.6 Hysteresis Power Loss and Resistance Model

Steinmetz formulated the hysteresis loss for the partial core transformer as [8]

$$P_h = k_h f B_{mc}^x V_c \gamma_c \qquad (2.62)$$

where

k is a constant dependent on the core material

x is the Steinmetz factor

This model was developed to model the hysteresis power loss for the full core transformers. In order to match the performance of the partial core transformer, for the core material used in the transformers fabricated and tested at the University of Canterbury, the average value of the x is 1.85 and hence this value is used in this project [8]. The k value is taken as 0.11[8]. However, a new hysteresis power loss model for partial core transformer is required in the future work.

Thus the hysteresis resistance is

$$R_h = e_1^2/P_h \tag{2.63}$$

Both R_h and R_{ec} can be included in the transformer equivalent circuit model as the core loss resistance R_C in parallel with X_m.

$$R_c = \frac{R_h R_{ec}}{R_h + R_{ec}} \tag{2.64}$$

2.5 Performance tests

Using the model for each component of the partial core transformer, the performance of the designed partial core transformer can be modelled in three different tests. They are the open circuit model, the short circuit model and the load circuit model. As the project required the design of an 11kV to 230V single phase power transformer, the outside high voltage winding is modelled as the primary winding and the inside low voltage winding is modelled as the secondary winding in the test models.

2.5.1 Open Circuit Model

An open circuit model is defined by the equivalent circuit shown in Figure 2.11 [8].

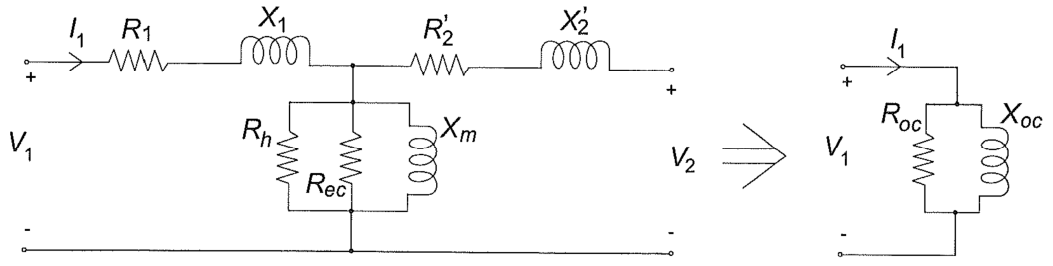

Figure 2.11 Open circuit transformer equivalent circuit [8].

The primary winding impedance is

$$Z_{w1} = R_1 + jX_1 \tag{2.65}$$

The core admittance is

$$Y_c = \frac{1}{R_c} - j\frac{1}{X_m} \tag{2.66}$$

from which the core impedance is calculated:

$$Z_c = \frac{1}{Y_c} \tag{2.67}$$

The total open circuit impedance looking from the primary side is

$$Z_{oc} = Z_{w1} + Z_c \tag{2.68}$$

The open circuit admittance is thus

$$Y_{oc} = \frac{1}{Z_{oc}} \tag{2.69}$$

The open circuit conductance and susceptance are

$$G_{oc} = Re(Y_{oc}) \tag{2.70}$$

and

$$B_{oc} = Im(Y_{oc}) \tag{2.71}$$

where

Re () denotes the real part

Im () denotes the imaginary part

The equivalent open circuit components are thus

$$R_{oc} = \frac{1}{G_{oc}} \tag{2.72}$$

and

$$X_{oc} = -\frac{1}{B_{oc}} \tag{2.73}$$

The complex open circuit primary current is calculated as

$$\tilde{I}_{oc1} = V_1 Y_{oc} \tag{2.74}$$

The magnitude of the open circuit primary current is

$$I_{oc1} = |\tilde{I}_{oc1}| \tag{2.75}$$

The complex open circuit apparent power is

$$\tilde{S}_{oc} = V_1 \tilde{I}^*_{oc1} \tag{2.76}$$

where $\tilde{I}^*_{oc1}$ is the complex conjugate of $\tilde{I}_{oc1}$

The open circuit real power loss is

$$P_{oc} = \frac{V_1^2}{R_{oc}} \tag{2.77}$$

The open circuit power factor is

$$pf_{oc} = \frac{P_{oc}}{|\tilde{S}_{oc}|} \tag{2.78}$$

The induced emf across the core is

$$\tilde{e}_1 = V_1 - \tilde{I}_{oc1} Z_1 \tag{2.79}$$

2.5.2 Short Circuit Model

The equivalent circuit used for the short circuit analysis is shown in Figure 2.12 [8].

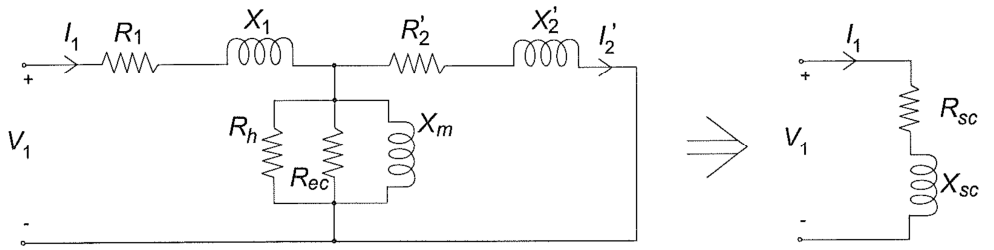

Figure 2.12 Short circuit transformer equivalent circuit [8].

For a short circuit condition, the load impedance is zero

$$Z_L = 0 \tag{2.80}$$

The secondary winding impedance is

$$Z_2^{'} = R_2^{'} + jX_2^{'} \tag{2.81}$$

From which the corresponding admittance is

$$Y_2' = \frac{1}{Z_2'} \tag{2.82}$$

It can be seen that Y_2' is in parallel with Y_c. Thus the equivalent admittance is calculated as

$$Y_{c,2} = Y_c + Y_2^{'} \tag{2.83}$$

The corresponding impedance is

$$Z_{c,2} = \frac{1}{Y_{c,2}} \tag{2.84}$$

The total short circuit impedance looking from the primary side is

$$Z_{sc} = Z_1 + Z_{c2} \tag{2.85}$$

Hence, the equivalent short circuit components are

$$R_{sc} = Re(Z_{sc}) \tag{2.86}$$

and

$$X_{sc} = Im(Z_{sc}) \tag{2.87}$$

The complex short circuit primary current is calculated as

$$\tilde{I}_{sc1} = \frac{V_1}{Z_{sc}} \tag{2.88}$$

The magnitude of the short circuit primary current is calculated using

$$I_{sc1} = |\tilde{I}_{sc1}| \tag{2.89}$$

The complex short circuit apparent power is

$$\tilde{S}_{sc} = V_1 \tilde{I}^*_{sc1} \tag{2.90}$$

where $\tilde{I}^*_{sc1}$ is the complex conjugate of $\tilde{I}_{sc1}$

The short circuit real power loss is

$$P_{sc} = I^2_{sc1} R_{sc} \tag{2.91}$$

The short circuit power factor is

$$pf_{sc} = \frac{P_{sc}}{|\tilde{S}_{sc}|} \tag{2.92}$$

2.5.3 Loaded Circuit Model

A load $Z_L = R_L + jX_L$ is placed across the secondary terminals. The load, referred to the primary side, $Z_L^{'}$, is calculated as [8].

$$Z_L^{'} = a^2 Z_L \tag{2.93}$$

The equivalent circuit used for the loaded circuit analysis is shown in Figure 2.13.

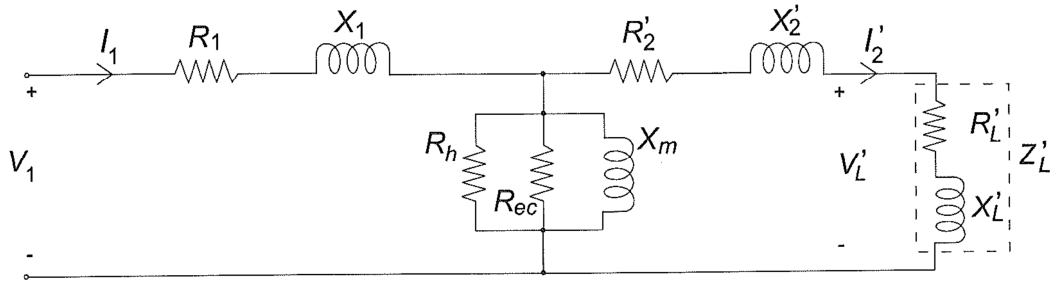

Figure 2.13 Loaded circuit transformer equivalent circuit [8].

The secondary winding impedance $Z_2^{'}$ is in series with $Z_L^{'}$

$$Z_{2L}^{'} = Z_2^{'} + Z_L^{'} \tag{2.94}$$

From which the corresponding admittance is

$$Y_{2L}^{'} = \frac{1}{Z_{2L}^{'}} \tag{2.95}$$

It can be seen that $Y_{2L}^{'}$ is in parallel with Y_c. Thus the equivalent admittance is calculated as

$$Y_{c2L} = Y_c + Y_{2L}^{'} \tag{2.96}$$

The corresponding impedance is

$$Z_{c2L} = \frac{1}{Y_{c2L}} \tag{2.97}$$

The loaded circuit impedance looking from the primary side is

$$Z_{loaded} = Z_1 + Z_{c2L} \tag{2.98}$$

The complex loaded circuit primary current is calculated as

$$\tilde{I}_{L1} = \frac{V_1}{Z_{loaded}} \tag{2.99}$$

The magnitude of the loaded circuit primary current is calculated using

$$I_{L1} = |\tilde{I}_{L1}| \tag{2.100}$$

The complex apparent power is

$$\tilde{S}_1 = V_1 \tilde{I}_{L1}^* \tag{2.101}$$

where $\tilde{I}_{L1}^*$ is the complex conjugate of $\tilde{I}_{L1}$

The total real power loss is

$$P_1 = I_{L1}^2 Re(Z_{loaded}) \tag{2.102}$$

The power factor is

$$pf_1 = \frac{P_1}{|\tilde{S}_1|} \tag{2.103}$$

The induced emf across the core is

$$\tilde{e}_1 = V_1 - \tilde{I}_{L1} Z_1 \tag{2.104}$$

The referred complex secondary current is

$$\tilde{I}'_{L2} = \frac{\tilde{e}_1}{Z'_{2L}} \tag{2.105}$$

The magnitude of the referred secondary current is therefore

$$I'_{L2} = \left|\tilde{I}'_{L2}\right| \tag{2.106}$$

The referred complex load voltage is

$$\tilde{V}'_L = \tilde{I}'_{L2} Z'_L \tag{2.107}$$

from which the magnitude is calculated as

$$V'_L = \left|\tilde{V}'_L\right| \tag{2.108}$$

The corresponding secondary current and load voltage are

$$I_{L2} = aI'_{L2} \tag{2.109}$$

and

$$V_L = \frac{V'_L}{a} \tag{2.110}$$

The voltage regulation is calculated using

$$VREG(\%) = \frac{V_1 - V_L'}{V_1} \times 100 \quad (2.111)$$

The real power dissipated in the load is

$$P_L' = I'^2_{L2} R_L' \quad (2.112)$$

The transformer efficiency is therefore

$$EFF(\%) = \frac{P_L'}{P_1} \times 100 \quad (2.113)$$

2.6 Discussion and Conclusion

In this chapter, the basic principles and the modeling for an ideal partial core transformer was introduced. The modeling for the physical dimensions and the electrical performance of the non-ideal partial core transformer was developed. The open circuit, the short circuit, and the load circuit tests were incorporated with the electrical performance of the partial core transformer into the calculation. However, when modeling the eddy current losses, the eddy current model used in this project is for full core transformers. The value for the eddy current resistance of the partial core transformers determined from test results is much smaller than that from the model. In order to account for this, a multiplication correction factor η was used in the model. This method is not very accurate because the eddy current loss for the partial core transformers does not have a linear relationship with load. A more accurate model [10] has been developed, and could be included in future work. The hysteresis power loss model used is based on the Steinmetz model. The Steinmetz model has two constants *k* and *x*. For the material used in the partial core transformers fabricated and tested at the University of Canterbury, the average value of *x* is 1.85. The *k* value is chosen as 0.11 in this project. It is the same as used in full core transformer models. However, the values of *k* for transformers are significantly different from one another [7]. This suggests that the Steinmetz hysteresis loss model may not be particularly accurate for partial core transformers. A new mathematical expression for the constant value *k* is required for the partial core transformer design.

CHAPTER 3
OIL-IMMERSED PARTIAL CORE POWER TRANSFROMER (PCPT) COOLING MODEL DESIGN AND TESTING

3.1 Introduction

In this chapter, the cooling method for the PCPT in this project is given. Also, the PCPT cooling model is developed, which is a modification of the model used for a full core oil immersed power transformer [1]. The cooling oil used in this project is BIOTEMP®. Its characteristics are implemented into the thermal model to determine the thermal performance of the PCPT cooled by BIOTEMP®.

3.2 Oil Immersed PCPT Cooling Model

The cooling system of the PCPT needs to be designed to dissipate the heat created in steady state so that it can operate effectively. While the physical structure of a full core transformer is slightly different to a partial core transformer, the heat transfers for these two types of transformers have similar characteristics. The heat dissipation model for the partial core transformer is developed from the heat dissipation model for the full core transformer, since there is no existing heat dissipation model for the partial core transformer. The full core transformer thermal model is derived from the IEEE Guide for Loading Mineral-Oil-Immersed transformers [11].

3.3 Type of Transformer Cooling

There are four models generally used for cooling oil-immersed transformers such as oil natural air natural (ONAN), oil natural air forced (ONAF), oil directed air forced (ODAF), and oil forced air forced (OFAF). In this particular project, the ONAN cooling method is selected for cooling the partial core power transformer since this is especially suitable for low power rating transformers.

3.4 Hot-spot Temperature Calculation

The mathematical representation of the hot-spot temperature θ_H is the sum of the ambient temperature, the bottom oil temperature, the temperature rise of the oil at the winding hot-spot location over the bottom oil temperature, and the winding hot-spot temperature rise over the oil next to the hot-spot location temperature [11].

$$\theta_H = \theta_A + \theta_{BO} + \Delta\theta_{WO/BO} + \Delta\theta_{H/WO} \text{ (°C)} \quad (3.1)$$

A pictorial representation for the components of equation 3.1 is shown in Figure 3.1.

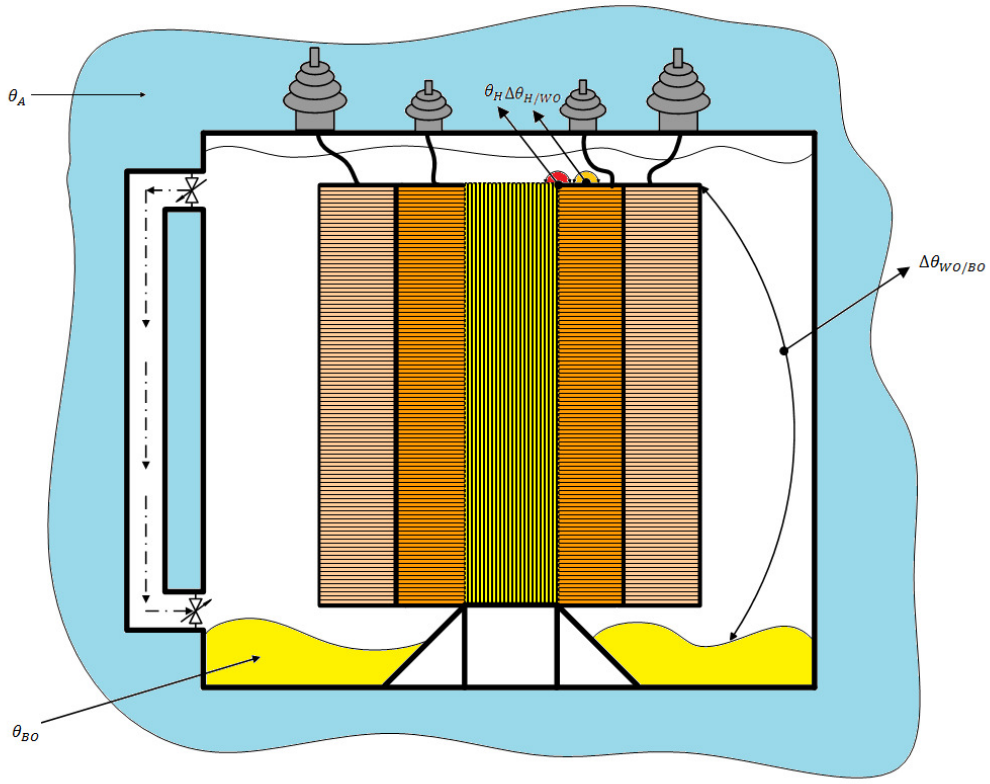

Figure 3.1 Graphical representation of the hot-spot temperature and its components.

θ_H is the hot-spot temperature,°C

θ_A is the ambient temperature,°C

θ_{BO} is the bottom oil temperature,°C

$\Delta\theta_{WO/BO}$ is the temperature rise of the oil at the winding hot-spot location over the bottom oil temperature,°C

$\Delta\theta_{H/WO}$ is the winding hot-spot temperature rise over the oil temperature next to the hot-spot location,°C

The oil temperature can be presented as the average oil temperature in the tank and radiators. Thus, the temperatures of the top and bottom oil are [11].

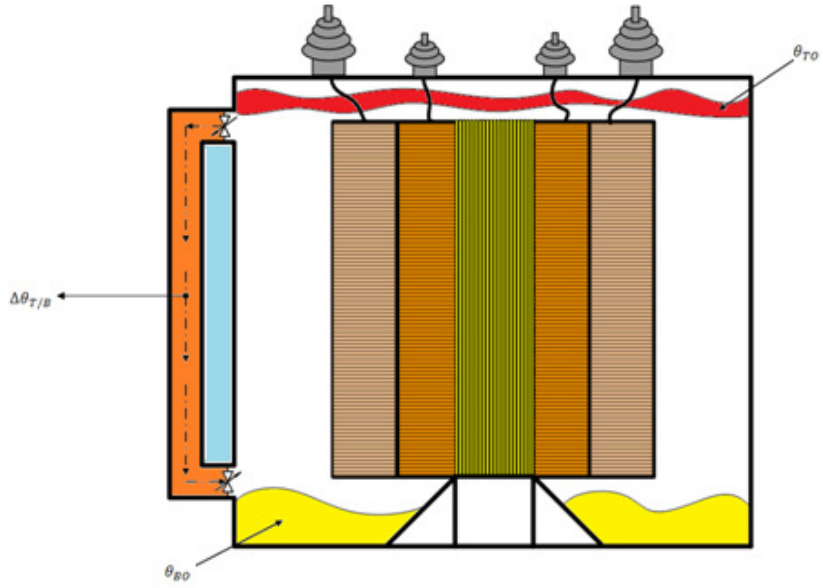

Figure 3.2 Graphical presentation of the top and bottom oil temperatures.

$$\theta_{BO} = \theta_{AO} - \frac{\Delta\theta_{T/B}}{2} \text{ (°C)} \quad (2.2)$$

$$\theta_{TO} = \theta_{AO} + \frac{\Delta\theta_{T/B}}{2} \text{ (°C)} \quad (2.3)$$

where

θ_{AO} is the average oil temperature in the tank and the radiator,°C

$\Delta\theta_{T/B}$ is the temperature rise of the oil at the top of the radiator over the temperature of the bottom oil,°C

θ_{TO} is the top oil temperature in the tank and the radiator,°C

θ_{AO} is the average oil temperature in the tank and the radiator,°C

$\Delta\theta_{T/B}$ is the temperature rise of the oil at the top of the radiator over the temperature of the bottom oil,°C

3.5 Average Winding Temperature Rise of Both Windings

The thermal system inside the transformer oil is a dynamic system. This is because the resistances of both windings increase as the temperature rises inside the transformer.

Consequently, the winding losses are not constant during the temperature variations of the windings. Thus, a temperature correction factor K_W is calculated so that a more accurate value for heat generated by the windings can be obtained [11].

$$K_W = \frac{\theta_{W,1}+\theta_K}{\theta_{W,R}+\theta_K} \tag{3.4}$$

where

$\theta_{W,1}$ is the initial temperature on both windings,°C

$\theta_{W,R}$ is the average temperature of both windings at the rated load tested,°C

θ_K is the temperature factor for resistance, °C, which is 234.5 for copper [11]

The temperatures of the winding hot-spot and oil inside a PCPT are obtained using the conservation of heat energy during a small instant of time, Δt. In this time step, the last calculated temperatures are used to calculate the temperatures for the next time step. Therefore, the system of equations constitutes a transient forward-marching finite difference calculation procedure. Therefore, the heat generated $Q_{GEN,W}$ by both windings during the time t_1 to t_2 is [11].

$$Q_{GEN,W} = K^2\left[P_W K_W + \frac{P_E}{K_W}\right]\Delta t \quad \text{(W-min)} \tag{3.5}$$

where

P_W is the I^2R loss of both windings, W

P_E is the eddy current loss of both windings, W

For the ONAN cooling modes, the heat lost by both windings is [11]

$$Q_{LOST,W} = \left(\frac{\theta_{W,1}-\theta_{DAO,1}}{\theta_{W,R}-\theta_{DAO,R}}\right)^{\frac{5}{4}}\left(\frac{\mu_{W,R}}{\mu_{W,1}}\right)^{\frac{1}{4}}(P_W + P_E)\Delta t \quad \text{(W-min)} \tag{3.6}$$

where

$\theta_{DAO,1}$ is the initial temperature of the oil in the cooling ducts ,°C

$\theta_{DAO,R}$ is the average temperature of the oil in the cooling ducts at the rated load,°C

$\mu_{W,R}$ is the viscosity of the oil at the average temperature rise of both windings at rated load.

$\mu_{W,1}$ is the viscosity of the oil for the initial temperature rise of both windings

The thermal capacitance of a winding is the ability of a winding to store thermal energy. It is estimated from the winding time constant, which is the time period for the simulation. It is determined from the cooling curves obtained during factory heat run testing, or approximate values may be used. The winding mass multiplied by the specific heat Cp_W may be determined from [11].

$$M_W Cp_W = \frac{(P_W+P_E)\tau_W}{\theta_{W,R}-\theta_{DAO,R}} \text{ (W-min/°C)} \quad (3.7)$$

where

τ_W is the winding time constant, min

The average temperature of both windings at time t=t_2 is [11]

$$\theta_{W,2} = \frac{Q_{GEN,W}-Q_{LOST,W}+M_W Cp_W \theta_{W,1}}{M_W Cp_W} \quad (°C) \quad (3.8)$$

The winding duct oil temperature rise over the bottom oil temperature is [11]

$$\Delta\theta_{DO/BO} = \theta_{TDO} - \theta_{BO} = \left[\frac{Q_{LOST,W}}{(P_W+P_E)\Delta t}\right]^x (\theta_{TDO,R} - \theta_{BO,R}) \ (°C) \quad (3.9)$$

where

x is 0.5 for ONAN.

$\Delta\theta_{DO/BO}$ is the temperature rise of the oil at the top of the duct over the bottom oil temperature ,°C

θ_{TDO} is the oil temperature at the top of the duct ,°C

$\theta_{TDO,R}$ is the oil temperature at the top of the duct at rated load ,°C

$\theta_{BO,R}$ is the bottom oil temperature at rated load ,°C

For the ONAN cooling modes, the duct top-oil temperature $\theta_{TDO,R}$ at rated load is assumed equal to the tank top oil temperature.

During an increase in load, the hot-spot location in the winding does not necessarily stay at the top of the winding [2]. The oil temperature at the hot-spot position is given by [11]

$$\Delta\theta_{WO/BO} = H_{HS}(\theta_{TDO} - \theta_{BO}) \ (°C) \quad (3.10)$$

where

H_{HS} is the per unit of winding height to hot-spot location.

The temperature of oil adjacent to the winding hot spot, °C is then [11]

$$\theta_{WO} = \theta_{BO} + \Delta\theta_{WO/BO} \quad (3.11)$$

When the winding duct-oil temperature is less than the temperature of the top oil in the tank, the oil temperature adjacent to the hot spot is assumed to be equal to the top-oil temperature, since the upper portion of the winding may be in contact with the hotter top oil.

If $\theta_{TDO} < \theta_{TO} \ \Rightarrow \ \theta_{WO} = \theta_{TO}$

where

θ_{TO} is the top oil temperature in the tank and radiator ,°C

3.5.1 Winding Hot-spot Temperature

To account for the additional heat generated at the hot-spot, it is necessary to adjust the winding losses using the average winding temperature. The resistance of the winding and core changes with temperature. The viscosity of the oil also varies with temperature. These factors affect the temperature calculation.

The winding I^2R loss at rated load and hot-spot temperature is [11]

$$P_{HS} = \left(\frac{\theta_{H,R}+\theta_K}{\theta_{W,R}+\theta_K}\right) P_W \ (W) \quad (3.12)$$

where

$\theta_{H,R}$ is the rated winding hot-spot temperature ,°C

The eddy loss at the rated winding hot-spot temperature is [11]

$$P_{EHS} = E_{HS}P_{HS} \ (W) \quad (3.13)$$

E_{HS} is the per unit value of the winding height to the hot-spot location

If E_{HS} is unknown, it may be estimated; however, it should be equal to or greater than $P_{E,R}$ divided by $P_{W,R}$. Hence, at each time step, the losses of the windings and the core are calculated for a particular load, and corrected for the change in resistance with temperature. The heat generated at the hot spot temperature is [11]

$$Q_{GEN,HS} = K^2 \left[P_{HS}K_{HS} + \frac{P_{EHS}}{K}\right]\Delta t \ \text{(W-min)} \tag{3.14}$$

where

K_{HS} is the temperature correction for losses at the hot-spot location [11]

$$K_{HS} = \frac{\theta_{H,1}+\theta_K}{\theta_{H,R}+\theta_K} \tag{3.15}$$

where

$\theta_{H,1}$ is the initial winding hot-spot temperature ,°C

Corrections for oil viscosity changes with temperature are also incorporated into the equations. The required accuracy is achieved by selecting a small value for the time increment Δt. For the ONAN modes, the heat lost at the hot spot location is given by [11]

$$Q_{LOST,HS} = \left[\frac{\theta_{H,1}-\theta_{WO,1}}{\theta_{H,R}-\theta_{WO,R}}\right]^{5/4}\left[\frac{\mu_{HS,R}}{\mu_{HS,1}}\right]^{1/4}(P_{HS}+P_{EHS})\Delta t \ \text{(W-min)} \tag{3.16}$$

where

$\theta_{WO,1}$ is the initial temperature of oil adjacent to the winding hot spot ,°C

$\theta_{WO,R}$ is the temperature of oil adjacent to the winding hot spot at rated load ,°C

$\mu_{HS,R}$ is the viscosity of the oil for the hot-spot calculation at rated load, cP

$\mu_{HS,1}$ is the viscosity of the oil for the hot-spot calculation at the initial time, cP

Δt is the time increment for the calculations, min

The winding hot-spot temperature at time t_2 is [11]

$$\theta_{H,2} = \frac{Q_{GEN,HS} - Q_{LOST,HS} + M_W Cp_W \theta_{H,1}}{M_W Cp_W} \quad (°C) \tag{3.17}$$

3.6 Average Oil Temperature

The heat lost by the windings to the duct oil and the heat generated by both the core and stray losses is absorbed by the bulk oil in the main tank. This heat is then lost to the ambient air. The heat generated by the core varies slightly with temperature, however, it is assumed constant for the analysis.

For normal excitation, the heat generated by the core is [11]

$$Q_C = P_{C,R} \Delta t \quad \text{(W-min)} \tag{3.18}$$

where

$P_{C,R}$ is the core (no-load) loss, W

The heat generated by the stray loss is [11]

$$Q_S = \left[\frac{K^2 P_S}{K_W}\right] \Delta t \quad \text{(W-min)} \tag{3.19}$$

where

P_S is the stay losses, W

The temperature correction, K_W for the stray loss is given by equation 3.4 and assumes that the temperatures of the structural parts are the same as the average winding temperature.

The power lost from the oil is [11]

$$P_T = P_W + P_E + P_S + P_C \quad \text{(W)} \tag{3.20}$$

The heat lost from the oil to the ambient surroundings is [11]

$$Q_{LOST,O} = \left[\frac{\theta_{AO,1} - \theta_{A,1}}{\theta_{AO,R} - \theta_{A,R}}\right]^{1/y} P_T \Delta t \quad \text{(W-min)} \tag{3.21}$$

where

$\theta_{AO,1}$ is the initial oil temperature in the tank and the radiator ,°C

$\theta_{A,1}$ is the initial ambient temperature ,°C

$\theta_{AO,R}$ is the average oil temperature in the tank and the radiator at rated load ,°C

$\theta_{A,R}$ is the rated ambient temperature at the nominal kVA base for the load cycle ,°C

y is the exponent of the average oil rise with heat loss; 0.8 is for ONAN [11]

To determine the core mass, it is necessary to subtract the mass of the windings used in 3.22 from the total core, and coil mass given on the outline drawing supplied by the manufacturer. This is internal to the thermal program.

The mass of windings [11]

$$M_W = \frac{M_W Cp_W}{Cp_W} \text{ (lb)} \tag{3.22}$$

where

$M_W Cp_W$ is the winding mass times the specific heat, W-min/°C

Cp_W is the specific heat of the winding material, W-min/lb°C

The mass of the core is [3]

$$M_{CORE} = M_{CC} - M_W \text{ (lb)} \tag{3.23}$$

where

M_{CC} is the mass of core and coil, lb

The total mass times the specific heat of the tank, core, and oil is [11]

$$\sum MCp = M_{TANK} Cp_{TANK} + M_{CORE} Cp_{CORE} + M_{OIL} Cp_{OIL} \text{ (lb)} \tag{3.24}$$

where

M_{TANK} is the mass of the tank, lb

Cp_{TANK} is the specific heat of the tank, W-min/lb°C

Cp_{CORE} is the specific heat of the core, W-min/lb°C

M_{OIL} is the mass of the oil, lb

Cp_{OIL} is the specific heat of the oil, W-min/lb°C

The average oil temperature for the tank and radiator at time t_2 is [11]

$$\theta_{AO,2} = \frac{Q_{LOST,W} + Q_S + Q_C - Q_{LOST,O} + (\sum MCp)\theta_{AO,1}}{\sum MCp} \ (°C) \tag{3.25}$$

3.7 Top and Bottom Oil Temperatures

The top and bottom oil temperatures are determined by an equation similar to that for the duct oil rise.

The temperature rise of the oil at the top of the radiator over the bottom oil temperature, °C [11] is

$$\theta_{T/B} = (\theta_{TO} - \theta_{BO}) = \left[\frac{Q_{LOST,O}}{P_T \Delta t}\right]^z \left(\theta_{TO,R} - \theta_{BO}\right) \ (°C) \tag{3.26}$$

where

z is 0.5 for ONAN.

3.8 Stability Requirements

For the ONAN cooling modes, the system of equations is stable if the following criteria are met [11]

$$\frac{\tau_W}{\Delta t} > \left(\frac{\theta_{W,1} - \theta_{DAO,1}}{\theta_{W,R} - \theta_{DAO,R}}\right)^{1/4} \left(\frac{\mu_{W,R}}{\mu_{W,1}}\right)^{1/4} \tag{3.27}$$

and $\frac{\tau_w}{\Delta t} > 1$

For the computer program, a time increment of Δt=0.5 min is used. The following criterion used for stability accuracy for all four cooling modes is

$\frac{\tau_w}{\Delta t} > 9$

If required, the value of Δt is reduced to meet the stability requirement.

3.9 Oil Viscosity and Specific Heat of BIOTEMP®

BIOTEMP® Transformer oil is expected to function both as an insulating medium and a heat transfer agent. Viscosity is an important parameter in design calculations for heat transfer by either natural convection in smaller self-cooled transformers or forced convection in larger

units with pumps. Viscosity is also the quantity that describes oil's resistance to flow. It is the factor of denseness and internal friction for all oils. The greatest ease of movement for fluids will occur with low viscosity fluids. In addition, viscosity influences pressure drop, flow, and cooling rates in a circulating oil system. The cooling mode of the partial core transformer is natural convection flow of oil through the windings. Viscosity changes with a change in temperature for a specific liquid. This factor directly affects the thermal performance of the BIOTEMP®. Hence, the viscosity of the BIOTEMP® has to be calculated as the temperature rises.

3.9.1 Including BIOTEMP® into the Thermal Model

Oil viscosity is highly temperature dependent. The oil viscosity μ at any temperature θ is [11]

$$\mu = D\ EXP^{G/(\theta+273)} \tag{3.28}$$

where

D is a constant

G is a constant

θ is the temperature for the viscosity calculation

The viscosity μ is evaluated at a temperature equal to the average of both winding temperatures plus the average oil duct temperature divided by two. The temperatures used to calculate the viscosity are given in Table 3.1. The viscosity of BIOTEMP® is 10 at 100˚C and 45 at 40˚C [12]. Based on equation 3.28, the viscosity equation parameters of *D* and *G* for BIOTEMP® can be calculated. The results for both parameters are shown in Table 3.2.

The specific heat of a material does not change with temperature variation, so that a constant value of specific heat can be used [11]. The specific heat of mineral oil is 13.92 W-min./lb˚C [11] or 0.43 cal/gr/˚C [12]. However, the specification data sheet of BIOTEMP® was only offered that the specific heat of BIOTEMP® is 0.47cal/gr/˚C [12]. To convert the BIOTEMP® value to fit with the calculations of the thermal model, the specific heat of BIOTEMP® is determined to be 12.73 W-min./lb˚C which is based on the conversion rate of the mineral oil.

The temperature for different viscosity calculations in the thermal model is shown in Table 3.1. The values of the constants *D* and *G* for BIOTEMP® were derived from specification data [11] [13] shown in Table 3.2.

Table 3.1 Temperatures for calculating viscosity for the PCPT thermal model.

Viscosity term in the model	Temperature for viscosity calculation
$\mu_{W,R}$	$(\theta_{W,R} + \theta_{DAO,R})/2$
$\mu_{W,1}$	$(\theta_{W,1} + \theta_{DAO,1})/2$
$\mu_{HS,R}$	$(\theta_{H,R} + \theta_{WO,R})/2$
$\mu_{HS,1}$	$(\theta_{H,1} + \theta_{WO,1})/2$

Table 3.2 Specific heat and constants for BIOTEMP® viscosity calculation.

Material	Cp	unit	D	unit	G	unit
BIOTEMP®	12.73	W-min./lb˚C	0.0054292	Pa·s	2800	/°C

3.9.2 Summary of Exponents for BIOTEMP®

Values of the exponents used in the temperature calculations are summarised in Table 3.3. The computer program allows changing the *y* exponent for cases for which test data is available.

Table 3.3 Exponent temperature parameters for ONAN cooling method [11].

Exponent	Used for	ONAN
x	Duct oil rise	0.5
y	Average oil rise	0.8
z	Top to bottom oil rise in radiator	0.5

3.10 Thermal Model Corrections and Modifications

The thermal model of the IEEE standard as published is not functional since the model has a number of errors in the program coding and input data which prevents the simulation program from operating. In addition, the thermal model does not include BIOTEMP® as a type of cooling medium for power transformers. However, this research requires the use of BIOTEMP® as the cooling liquid to stabilise the power transformer temperature for long term operation. Thus, correcting the errors and adding BIOTEMP® characteristics into thermal model is a new development for this research.

The error in the input data is the number of points on the load cycle. The original figure is 12. However, this figure does not match with the load cycle duration. The actual load cycle duration is 24 hours. Thus, the value for the number of points on the load cycle was changed to 24.

There are errors that appear in the code of the simulation programme which stop the program compiling. They are listed in Table 3.4.

Table 3.4 Thermal program coding errors, adjustment and their corrections.

Line	Error	Correction
2140	PRINT # I, " TEMPERATURE DURING LOAD CYCLE : "	PRINT # 1, " TEMPERATURE DURING LOAD CYCLE : "
180	FOR J=1 TO JJ	FOR J=0 TO JJ
1360	FOR K=1 TO KK	FOR K=0 TO KK
1530	J=1: K=1: TIMS=0:TIMSH=0:ASUM=0	J=0: K=0: TIMS=0:TIMSH=0:ASUM=0

After fixing the program errors and the input error, the thermal temperature program was compiled. The output results of the program for the mineral oil exactly matched the example give in the IEEE Guide for loading mineral-oil-immersed transformers [11].

In this project, the cooling oil is BIOTEMP®. To simulate the thermal performance of the BIOTEMP® in the thermal model, the characteristics of BIOTEMP® based on Table 3.2 were added into the thermal program. This modification for the thermal model is shown in Table 3.5.

Table 3.5 Thermal program modification for BIOTEMP®.

Line	Original	Modification
560	CPF=13.92: RHOF=0.031621:C=2797.3:B=0.0013473	CPF=12.73:RHOF=0.031621:C=2800:B= 0.0054292
570	PRINT #1,"COOLING FLUID IS TRANSFORMER OIL": GOTO 620	PRINT #1," COOLING FLUID IS BIOTEMP®": GOTO 620

Since the specific heat for the mineral oil and BIOTEMP® are very similar, the thermal model temperature setting for BIOTEMP® was modified from the temperature setting of the mineral

oil, based on IEC 60067-2 [14] and the IEEE Guide for loading mineral-oil-immersed transformers [11]. The rated average winding rise over ambient is 65 °C. The test average winding rise over ambient is 65 °C. The hottest spot rise over ambient is 80 °C. The top fluid rise over ambient is 60 °C. The bottom fluid rise over ambient is 25 °C. The rated ambient temperature is 20 °C.

3.11 Thermal Model Test

Once the thermal model was corrected, the accuracy of the thermal model with the experimental thermal result could be examined. Hence, an existing partial core power transformer was selected, and tested under load conditions. The partial core power transformer specifications and the computer model results are listed in Tables 3.6, 3.7, and 3.8.

Table 3.6 Design specification of the PCPT.

Core parts		
Length	0.345	m
Breadth	0.044	m
Width	0.044	m
Lamination thickness	0.00054	m
Relative permeability	5000	
Resistivity of the core material at 20°C	1.60E-07	Ωm
Coefficient of thermal resistivity	6.50E-03	$°C^{-1}$
Operating temperature	50	°C
Material density	7650	kg/m^3
Stacking factor	0.99	
Former		
Length	0.234	m
Thickness	0.002	m
Inside winding		
Length	0.234	m
Thickness of wire	0.002	m
Number of layers	6	
Resistivity of the wire at 20°C	1.72E-08	Ωm
Coefficient of thermal resistivity	0.0039	$°C^{-1}$
Operating temperature	50	°C
Material density	8960	kg/m^3
Outside winding		
Length	0.234	m
Thickness of conductor	0.002	m
Total number of layers	7	
Resistivity of wire at 20°C	1.72E-08	Ωm
Coefficient of thermal resistivity	0.0039	$°C^{-1}$
Operating temperature	50	°C
Material density	8960	kg/m^3

Table 3.7 1 p.u load circuit test results from the electrical model.

Parameter		
Flux density	0.85	T
Inside winding turns	702	
Outside winding turns	819	
Outside voltage	300	V
Inside load voltage	230	V
Inside winding current	15	A
Outside winding current	10	A
Inside winding apparent power	3.45	kVA
Inside winding real power	3.36	kW
Inside winding power factor	0.98	
Outside winding apparent power	3	kVA
Outside winding real power	3	kW
Outside winding power factor	1	
Total power deliver to the load	3	kW
Core loss	16	W
Total winding loss	348	W
Inside current density	5.7	A/mm^2
Outside current density	3.84	A/mm^2
Efficiency	89	%
Voltage regulation	14	%

Table 3.8 Weights for each component of the PCPT generated by the electrical model.

Component	Weight	
Core	5	kg
Both windings	20	kg
Total	25	kg

A cross-section of the PCPT is shown in Figure 3.3.

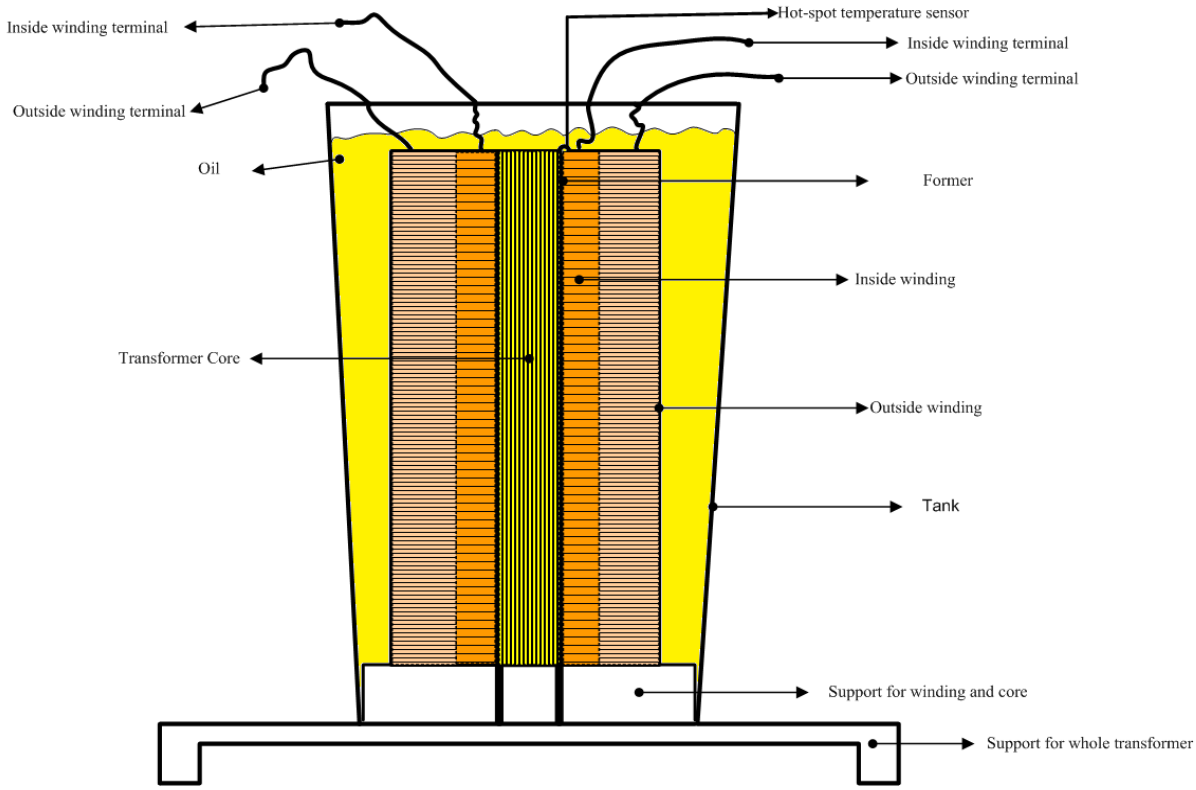

Figure 3.3 A side view of the tested after PCPT.

The transformer tank is a double layer plastic container. A plastic tank is necessary with a partial core transformer because flux emanating from the partial core can penetrate through the tank. If the tank was metallic, additional eddy current losses would occur due to induction heating. A plastic tank prevents this. The advantages of using a double layer plastic container are that it has a good insulation level, is light weight, and it prevents oil leaks. The PCPT is set in the middle of the container. The core and windings have been placed on the top of a plastic base for support. The transformer tank is fastened to a wooden base structure to prevent the transformer toppling and oil spilling. The physical structure was subjected to a large number of earthquakes (over 10000 aftershocks) in Christchurch during 2010 to 2012. It remained upright for the entire period.

After obtaining the electrical and physical model results for the PCPT, the next step in testing the accuracy of the developed thermal model was to run the program and compare the modeling results with actual thermal experimental results. The mathematical models of winding eddy current losses and stray losses for partial core transformers have not been developed in the electrical model. Therefore, these two losses are set as zero in this project.

The assumptions are valid since the majority of the winding losses are the I^2R losses. However, the winding eddy current losses and stray losses models are not zero in reality. The thermal model was used to model the heat dissipation in the transformers. In this project, the plastic tank was used and the radiator was not added to the transformer. In fact, Heat dissipation through metal is much faster than heat dissipation through plastic, and a radiator. Hence, the thermal model needs to be modified to account a plastic tank and the partial core transformer without the radiators. This is the future work. The input data for the thermal model is generated by the electrical model. These are listed in Table 3.9.

Table 3.9 Input specification for PCPT of the developed thermal model.

Program input	**Value**
base of losses kVA	3.46
Temperature base for losses at this kVA,˚C	75
I^2R losses, P_W, Watts	348
Winding eddy current losses, P_E, Watts	0
Stray losses, P_S, Watts	0
Core losses, P_{CR}, Watts	16
1 per unit kVA base for load cycle	3.46
Rated average winding temperature rise over ambient, ˚C	65
Tested or rated average winding temperature rise over ambient , $\Delta\Theta_{W/A,R}$,˚C	63
Tested or rated hot-spot temperature rise over ambient, $\Delta\Theta_{H/A,R}$,˚C	80
Tested or rated top-oil temperature rise over ambient, $\Delta\Theta_{W/A,R}$, ˚C	55
Tested or rated bottom oil temperature rise over ambient, $\Delta\Theta_{W/A,R}$, ˚C	25
Rated ambient temperature, $\Theta_{A,R}$, ˚C	30
Winding conductor, 2=copper	1
Per unit eddy current losses at winding hot-spot	0
Winding time constant, $t_{W,}$ minutes	1
Per unit winding height to hot-spot height, H_{HS}	1
Mass of core and coil, M_{CC}, lb	55
Mass of tank and fittings, M_{Tank}, lb	15
Type fluid, 1= BIOTEMP®	2
Oil volume (US gallons)	10
Over excitation occurs, 0=yes, 1=yes	0

Time when over excitation occurs, h	0
Core loss during over excitation, $P_{C,OE,}$ W	8.7
Loading case	2
Initial winding hot spot temperature, $\Theta_{HS,}$˚C	20
Initial average winding temperature, $\Theta_{W,}$˚C	20
Initial top oil temperature, $\Theta_{TO,}$˚C	20
Initial top duct oil temperature, $\Theta_{TDO,}$˚C	20
Initial bottom oil temperature, $\Theta_{BO,}$˚C	20
Type of cooling for load cycle , 1=ONAN	1
Print temperature Table,1=yes	1
Time increment for printing, minutes	60
Number of points on load cycle	24
Ambient temperature ˚C	20
Per unit of load	1

Using results from the electrical model as inputs into the thermal model was deemed appropriate as this was to be the process followed in the design of a new transformer. However, this does not separately verify the thermal model, as any errors in the electrical model values are carried forward, and the thermal model outputs are a combination of both electrical and thermal models. It would be more correct to verify the thermal model by using actual measured electrical values as its inputs. Since the thermal model examines the thermal performance of the PCPT from when it starts at turn on to the full load operation, the loading case in the model menu has to choose 2. The initial testing temperature condition has to be included in the input data for the thermal model. The input for the loading case is shown in Table 3.10.

Table 3.10 Initial loading case input setting.

Loading case input setting	Value
Initial winding hot-spot temperature, °C	20
Initial average winding temperature, °C	20
Initial top oil temperature in the tank and the radiator, °C	20
Initial oil temperature at top of duct, °C	20
Initial bottom oil temperature, °C	20
Cooling model 1= ONAN	1
Print the Table 1=yes	1
Time increment for printing calculation, (min)	60
Number of points on load cycle, (hours)	24

During the PCPT thermal testing, the load was always 1 per unit load; and the laboratory temperature was 20°C. The testing period is 24 hours.

Since the project applies only one thermal testing method and processes, the input load case and loading input is always the same for different PCPTs. After inputting these data into the program, the hot-spot thermal performance of the PCPT was estimated using the model. The results are shown in Figure 3.4. The red line represents the hotspot temperature estimated by the thermal model. This shows the hot-spot temperature is 105 ˚C after 10 hours. For the testing PCPT, the hot-spot temperature sensor was set into the top slot between the inside winding and the winding former as shown in Figure 3.3. The thermal test lasted 10 hours under full load conditions. The results are also shown in Figure 3.4. As the blue line in Figure 3.4 shows, the measured hot-spot temperature rises faster than the estimated temperature from the computer model. This is due to the limitation of the thermal model. The thermal model was used to model the heat dissipation by using the metal tank. In this project, the plastic tank was used. However, the measured hot-spot temperature converges to estimate values from the computer model. Therefore, the thermal model is considered sufficient for predicting the maximum hotspot temperature to overcome the cooling issues as the project required.

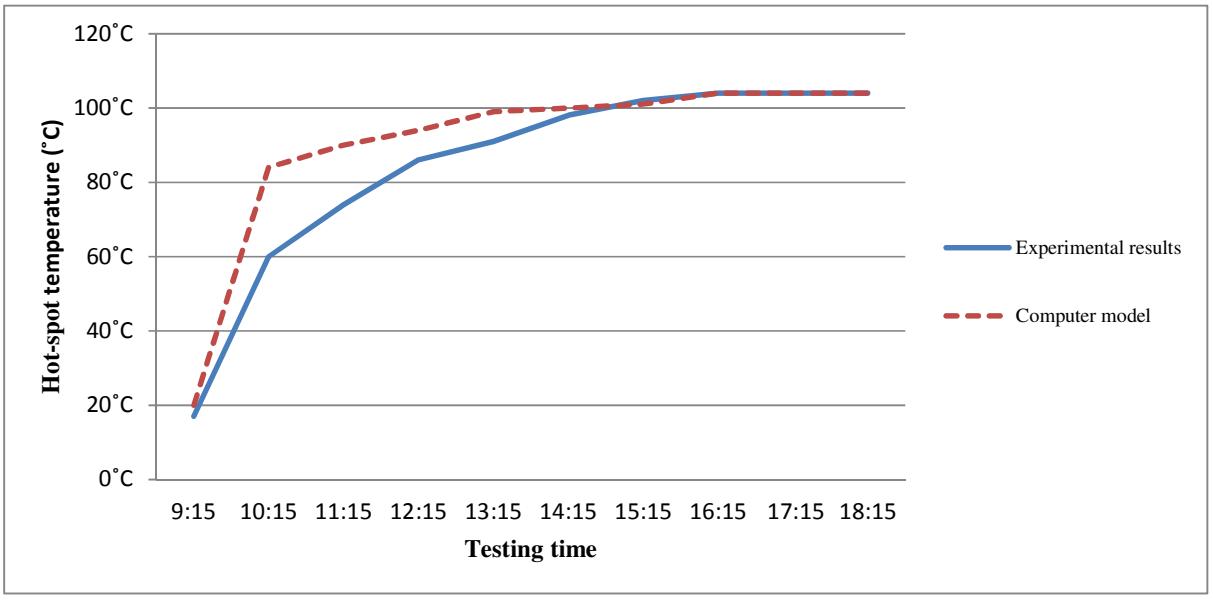

Figure 3.4 Hot-spot temperature for both experiment and computer model.

3.12 Discussion and Conclusion

In this chapter, the original full core transformer thermal model from the IEEE Guide for Loading Mineral-oil-Immersed Transformers [1] was successfully corrected. The error in the program input was discovered, and fixed. It was due to the unmatched load cycle duration. Also, there were a few coding errors which were explored, and are corrected. These errors and their corrections are shown in Table 3.4. After correcting these errors, the modification of the thermal characters then for BIOTEMP® were successfully programmed into the original model, based on a thermal characteristic comparison between BIOTEMP® and mineral oil. However, the new thermal model needs to have a few modifications as future work. The first modification is to include a plastic tank for the partial core transformer. The second modification is to calculate the heat dissipation when the PCPT does not have radiators. The constructed PCPT was used to test the accuracy of the new thermal model.

The thermal model testing results showed that the model can accurately estimate the maximum hot-spot temperature for the tested PCPT. Having successfully developed and tested the model, the process of designing and manufacturing a new PCPT could be started. The variation of estimating the transient performance for the hot-spot temperature is an important issue for the future project. However, it does not affect the steady state performance.

CHAPTER 4

DESIGN AND CONSTRUCTION OF THE PARTIAL CORE POWER TRANSFORMER (PCPT)

4.1 Introduction

Since both the electrical and the thermal model have been developed, and tested, the manufacturing processes of the PCPT are presented in this chapter. The overall processes are divided into two consecutive parts. The first procedure is designing a required PCPT by using the electrical model, and testing its thermal performance with the thermal model. The second part is the construction processes. This includes the core construction, winding construction, and tank construction. The production details of each component are listed in this chapter.

4.2 Computer Design Modeling and Results

The specifications of the PCPT are 15kVA; 11kV/230V; 50Hz; single phase. There are six main parts for building a PCPT. These are the tank, core, former, inside winding, outside winding, and winding layer insulation. These are the key inputs for the electrical model and determine the electrical performance of the PCPT. All the design inputs are listed in Table 4.1. After inputting the physical parameters into the computer model, the model generates the results for the open circuit, short circuit and load tests. These results are shown in Tables 4.2, 4.3, 4.4, and 4.5.

Table 4.1 Design specification for the PCPT.

Material		
Tank		unit
Breadth	0.51	m
Width	0.45	m
Height	0.84	m
Core		
Length	0.5	m
Diameter	0.055	m
Lamination thickness	0.00023	m
Stacking factor	0.965	
Relative permeability of the core material	5000	
Resistivity of the core material at 20°C	1.60E-07	Ωm
Coefficient of thermal resistivity of the core material	6.50E-03	$°C^{-1}$
Operating temperature	50	°C

Material density	7650	kg/m³
Former		
Length	0.65	m
Inside diameter	0.06	m
Thickness	0.0015	m
Inside winding		
Length	0.55	m
Thickness of the winding wire	0.004	m
Total number of layers	2	
Resistivity of the winding wire at 20°C	1.72E-08	Ωm
Coefficient of thermal resistivity of the winding wire	0.0039	°C⁻¹
Operating temperature	50	°C
Winding material density	8960	kg/m³
Outside winding		
Length	0.55	m
Thickness of the winding wire	0.00063	m
Total number of layers	17	
Resistivity of the winding wire at 20°C	1.72E-08	Ωm
Coefficient of thermal resistivity of the wire winding	0.0039	°C⁻¹
Operating temperature of the winding	50	°C
Winding material density	8960	kg/m³
Outside winding insulation		
Total layers of insulation	17	
Insulation thickness	0.00023	m

Table 4.2 Open circuit results from computer modeling.

Open circuit test results		
Voltage on the outside winding	11968	V
Voltage on the inside winding	230	V
Open circuit current on outside winding	0.7	A
Apparent power	8377	VA
Real power loss	167	W
Power factor	0.02	

In the model, the inside winding was energized. The model results of the open circuit test show that the voltage on the outside winding is 11968 V. This is 8.8 % above the design requirement of 11 kV. However, considering the differences between the design and

construction of the windings as well as the limitation of the thicknesses for the winding wire at the university, a tolerance range of the design was set at 10 %. Therefore, the open circuit voltage is within an acceptable range. The open circuit real power loss known as the core losses is 167W and the power factor is 0.02. The calculated core resistance based on Table 4.2 is 855kΩ and the magnetising reactance is 17 kΩ. The open circuit test of this PCPT generates mostly reactive power and only a small amount of real power losses (2%). This result satisfies the fundamentals of the power transformer design.

Table 4.3 Short circuit test results from the electrical model.

Short circuit test results		
Voltage on the outside winding	780	V
Inside winding current	65	A
Outside winding current	1.2	A
Apparent power	936	VA
Real power loss	505	W
The short circuit power factor	0.54	

The total copper losses of the PCPT are 505W. The winding resistance of the PCPT was determined to be 351Ω; and the leakage reactance is 547Ω from the short circuit model. Compared with the core resistance, the windings resistance of the PCPT is very low (0.04%). This value is very ideal for a power transformer design. Since this is an oil-immersed power transformer, a space is required between each winding wire layer for the insulation and the cooling channel. This increases leakage reactance, which also increases the total short circuit impedance. This can aid in limiting the short circuit current caused by a fault external to the transformer.

Table 4.4 1 p.u load test results from the electrical model.

Output results from the electrical model		
Flux density	1.74	T
Inside winding turns	260	
Outside winding turns	12454	
Inside winding current	65	A
Inside winding voltage	230	V
Outside winding current	1.65	A
Outside winding voltage	11033	V
Core loss	190	W
Winding loss	1081	W
Outside winding apparent power	18.2	kVA

Outside winding real power	16.3	kW
Outside winding power factor	0.9	
Inside winding apparent power	14.9	kVA
Inside winding real power	14.9	kW
Inside winding power factor	1	
Inside winding current density	5.2	A/mm^2
Outside winding current density	6	A/mm^2
Efficiency of transformer at rated load	91	%
Voltage regulation at rated load	7.2	%

The turns' ratio of the PCPT is 47.9; and the voltage ratio is 47.97 at 1 p.u load. These two values are expected to be different since this is a non-ideal transformer. However, the difference between these two values is only 0.14 %, and is within the tolerance range. Based on Table 4.4, the inverse of the current ratio is 0.0209. This result matches the inverse of the turns ratio which is 0.0189 based on Table 4.4. The core losses at 1 p.u load are 190 W; and both the winding losses at 1 p.u load are 1081W. The majority of losses for the PCPT are therefore the winding losses, being 5.7 times larger than the core losses. The current density of the PCPT for the inside winding is 5.2 A/mm^2; and the outside winding is 6 A/mm^2. The winding current density for a transformer is normally around about 3~4 A/mm^2 [15]. However, the allowable current density depends on the different cooling methods [15]. As long as the cooling model generates an acceptable result, 6.6 A/mm^2 for the inside winding and 4.94 A/mm^2 for the outside winding are the acceptable current densities for the two windings. For the PCPT, the efficiency is 92 %. This is lower than the average efficiency of a full core power transformer 98%~99% [16]. This is due to the relatively high winding losses. However, the efficiency of the PCPT is only 5 % lower than a normal full core transformer. Thus, for an emergency power transformer, it is still an acceptable result. The voltage regulation of the PCPT is 7.2%. This indicates the PCPT has reasonable short circuit impedance for limiting fault currents through the windings.

Table 4.5 Weight for each component for the PCPT from the electrical model.

The weight of each transformer component from the electrical model		
Core	10.5	kg
Both windings	16.34	kg
Total	26.84	kg

From Table 4.5, most of the PCPT weight is due to both windings (72 %), while the weight of the core is 28 % of the total weight.

4.3 Thermal Modeling Results

After determining the electrical performance and physical weight of the designed PCPT, the second step was to examine the thermal performance of the transformer by using the developed thermal model. The inputs of the thermal model which are the apparent power, the I^2R losses, the core losses, the weight of the core, and the core losses during over excitation can be obtained from the results given by the electrical model.

Table 4.6 PCPT thermal model input parameters.

Programme input	
Apparent power	18.2
Temperature base for losses at this kVA,˚C	75
I^2R losses, P_W, Watts	1080.5
Winding eddy losses, P_E, Watts	0
Stray losses, P_S, Watts	0
Core losses, P_{CR}, Watts	190
1 per unit kVA base for load cycle	18.61
Rated average winding temperature rise over ambient, ˚C	65
Tested or rated average winding temperature rise over ambient , $\Delta\Theta_{W/A,R}$,˚C	63
Tested or rated hot-spot temperature rise over ambient, $\Delta\Theta_{H/A,R}$, ˚C	80
Tested or rated top-oil temperature rise over ambient, $\Delta\Theta_{W/A,R}$, ˚C	55
Tested or rated bottom oil temperature rise over ambient, $\Delta\Theta_{W/A,R}$, ˚C	25
Rated ambient temperature, $\Theta_{A,R}$, ˚C	30
Winding conductor, 2=copper	2
Per unit eddy losses at winding hot-spot	0
Winding time constant, $t_{W,}$ minutes	1
Per unit winding height to hot spot, H_{HS}	1
Weight of core, M_{CC}, lb	59
Weight of tank and fittings, M_{Tank}, lb	15
Type fluid, 1=BIOTEMP®	1
Oil volume (US gallons)	20
Over excitation occurs, 0=yes, 1=yes	0
Time when over excitation occurs, h	0
Core loss during over excitation, $P_{C,OE,}$ W	190
Loading case,1or 2	2
Initial winding hot-spot temperature, $\Theta_{HS,}$˚C	20
Initial average winding temperature, $\Theta_{W,}$˚C	20
Initial top oil temperature, $\Theta_{TO,}$˚C	20
Initial top duct oil temperature, $\Theta_{TDO,}$˚C	20
Initial bottom oil temperature, $\Theta_{BO,}$˚C	20
Type cooling for load cycle , 1=OA	1
Print temperature Table,1=yes	1
Time increment for printing, minutes	60
Number of points on load cycle	24
Ambient temperature ˚C	20
Per unit of load	1

After inputing the values from Table 4.6 into the thermal model, the hot-spot, top oil, and bottom oil temperature can be generated, there are as shown in Figure 4.1.

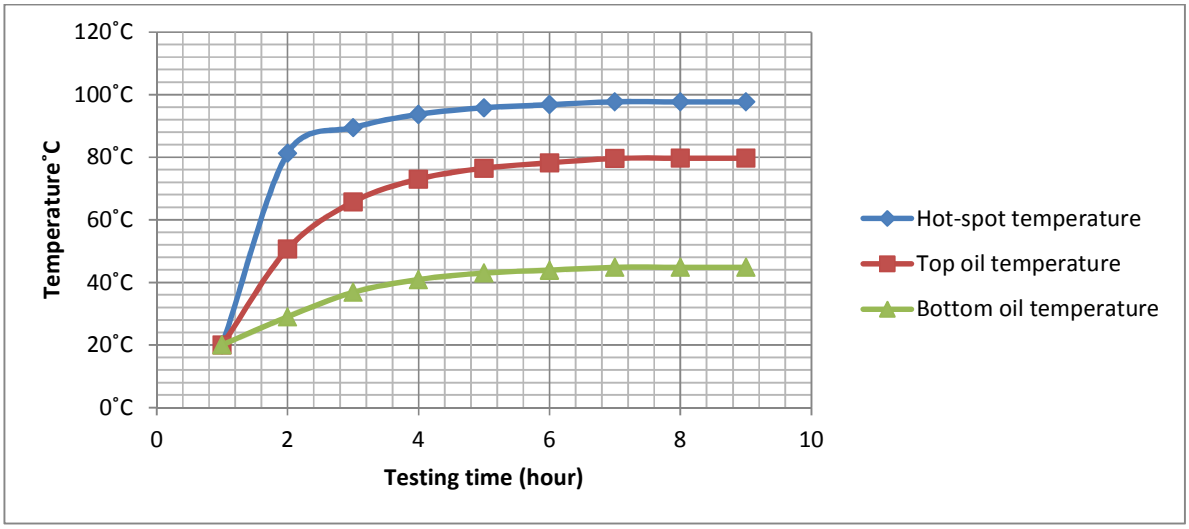

Figure 4.1 Hot-spot, top oil and bottom oil temperature generated by the thermal model.

The hot-spot temperature rises to 97 ˚C, and stays at this level after 6 hours. The top oil temperature reaches 78 ˚C; and the bottom oil temperature rises to 44 ˚C. This result shows that the PCPT is able to operate at 1 p.u. load continuously.

4.4 Construction of the Core, Windings and Tank

Since the results of both the thermal and the electrical model satisfied the design requirements, the actual transformer manufacturing process could be started. In general, in constructing any type of power transformer, there are three individual components that have to be built, and to be assembled together. These are the core, the windings, and the transformer tank.

4.4.1 Construction of the Core

The core of this particular power transformer is made from Kawasaki Steel. This is a new grain-oriented magnetic steel strip which has ultra–high flux density and low iron loss [9]. The thickness of the steel strip is 0.23 mm, and its width is 170 mm. There were two options to choose from build the transformer core. The first option was the parallel stacked [8], and the second option was radially stacked [2]. The diameter of the transformer core was only designed as 0.055m. This is too narrow to use radially stacked laminations since there are limited cutting tools. Therefore, the parallel stacked laminations are much more practical for this project. Since, the length of the core is 55 cm, and the diameter is 5.5 cm, as per the

design specified, the steel strip needed to be cut 55 cm long with various widths, and to be assembled into packets. Since the shape of the core is circular, the lamination packets were produced with different widths so that they build up a circular core as shown in Figure 4.2.

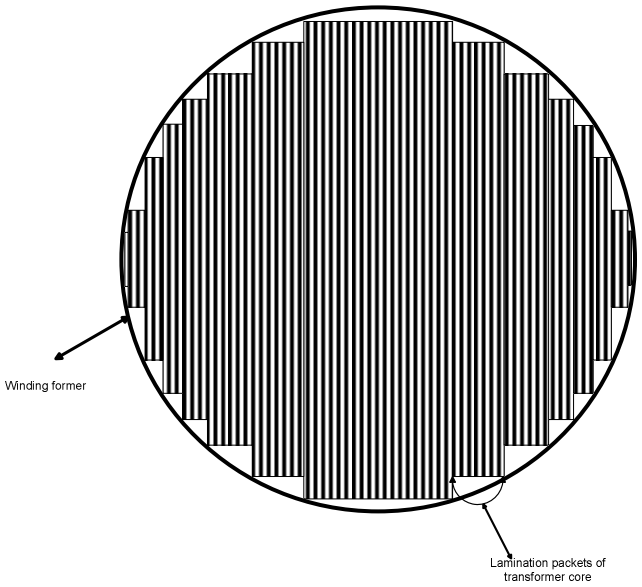

Figure 4.2 Top view of the circular core for the PCPT.

The total number of the laminations is 231 pieces as calculated from the computer model. The widths of the lamination packets were divided into 8 different sizes for ease of manufacturing. The stacking factor of the core is 0.935. This is lower than the design specification. The numbers of pieces of each width are listed in Table 4.7.

Table 4.7 Different widths of laminations and the quantities of each width.

Width of lamination (mm)	Quantity
55	60
50	50
45	40
40	26
35	15
30	15
25	15
20	10

After cutting all the laminations from the steel strip, the laminations were packed together tightly to produce a partial core as shown in Figure 4.3. The outside of the core was wrapped with Vida Polyester Glass Tape (VPGT) [17]. The VPGT shrinks when it is heated up so that the core was bound tightly. Insulation varnish was painted on the tape to increases the rigidity.

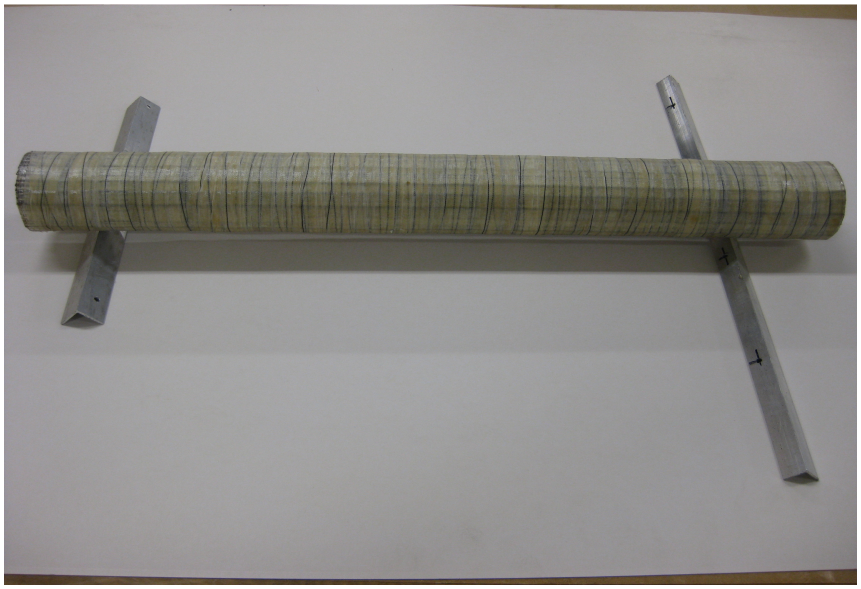

Figure 4.3 Core of the transformer.

4.4.2 Winding Construction

Once the core had been completed, the next critical components were the windings. The lengths of both the inside and outside winding are 55 cm as specified in the design. Construction of both windings is started with selecting the winding former, also known as the core winding insulation. The material used for the winding former was a fiberglass tube. There are four advantages for using this material as the winding former.

1. It has high rigidity and strength
2. It has a very low density
3. It is a very good insulation material
4. It has a high melting temperature (400˚C) relative to the operating temperature of the transformer.

The length of the fiberglass tube is 65 cm, and the diameter is 6 cm. Thus, the fiberglass tube is sufficiently wide and long for fitting in the transformer core. The extra length of the fiberglass tube allows for a physical support to connect the winding former and core with the bottom of the tank. The thickness of the fiberglass tube is 2 mm.

Nine fiberglass rods were glued to the outside of the winding former as shown in Figure 4.4. The first layer of the inside winding (4mm circular wire) was wound around the fiberglass

rods as shown in Figure 4.4. A second layer of fiberglass rods was glued to the winding layer; and then the second winding layer added.

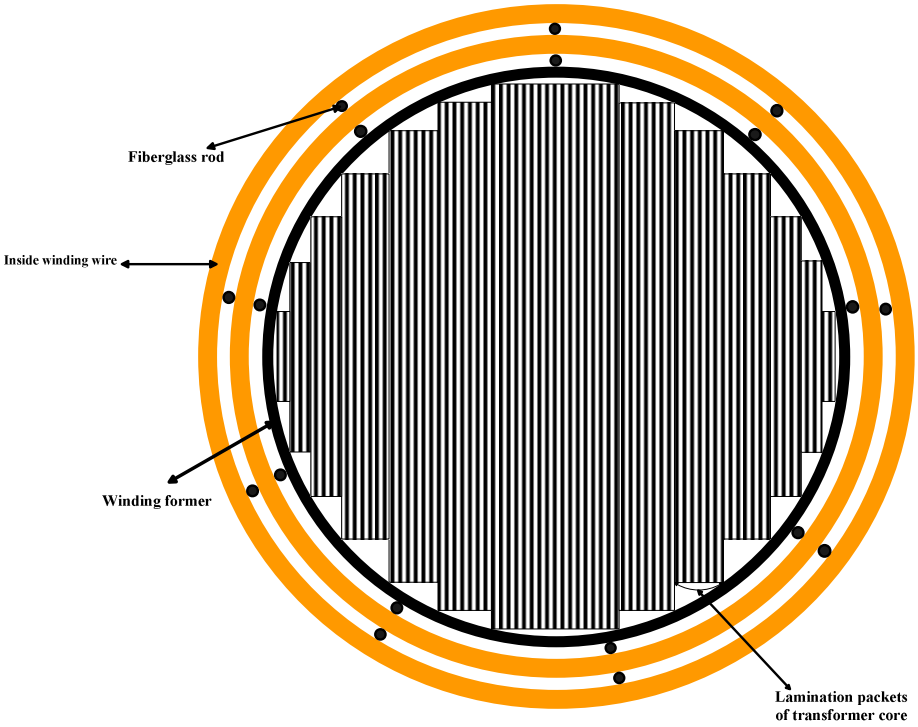

Figure 4.4 Inside winding construction layout.

Placing the fiberglass rods (1mm) between the winding layers creates an open construction space between each winding layer to allow the oil to circulate for cooling the windings.

The outside winding was then built around the inside winding. The voltage between two layers of the outside winding of was estimated to be 1.1 kV from the computer model. Therefore, adding 0.24 mm of Nomex/Myler/Nomex NMN [19] insulation paper between each two layers, provides a sufficient insulation level 16 kV [19] to prevent voltage breakdown between the layers. The outside winding structure is shown in Figure 4.5.

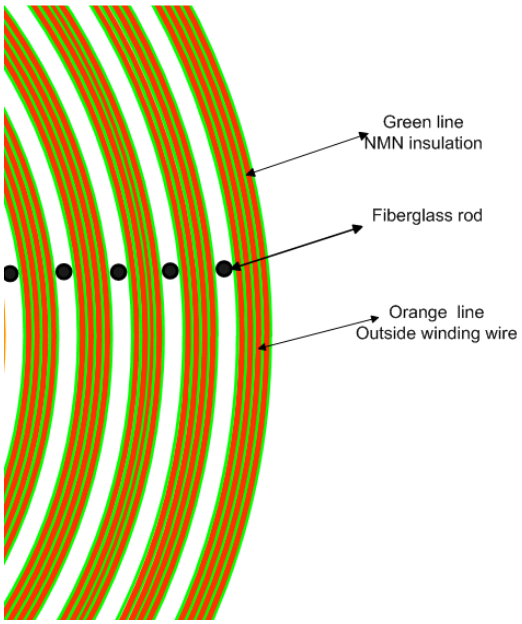

Figure 4.5 Outside winding structure layout.

Because the outside winding wire is so thin, 0.6 mm, it has little rigidity. Hence, fiberglass rods inserted to create space for cooling purposes, cannot be put in every layer. Instead, the fiberglass rods are placed every four outside winding layers; and insulation NMN layers supports the winding, and creates the cooling paths. The outside winding has a total of 17 layers with 12460 turns. A top view of both windings is shown in Figure 4.6.

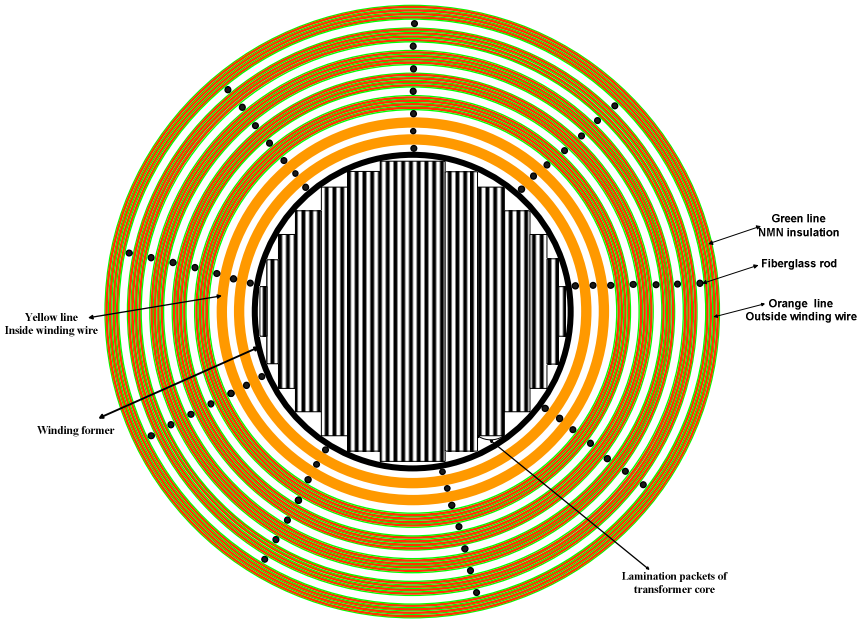

Figure 4.6 Top view of both windings and the core of the transformer.

The transformer windings were constructed using a lathe. The winding construction setup is shown in Figure 4.7.

Figure 4.7 The PCPT winding construction setup.

4.4.3 Overall Assembly of the Transformer Core and Winding in the Tank

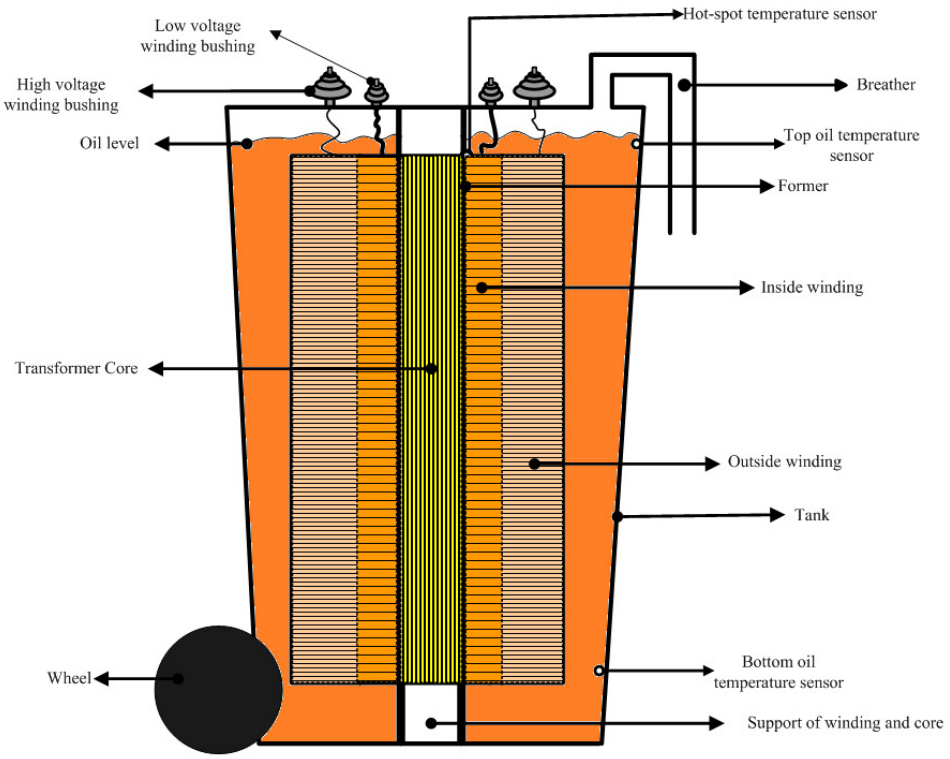

Figure 4.8 Overview of the PCPT.

After constructing the core and windings, the final stage of building the PCPT was obtaining a plastic wheely bin to use as the tank, and assembling them together as shown in Figure 4.8.

The reason for chosen the plastic tank is the flux path of the partial core transformer will conduct to the air, which is not same as the full core transformers. Therefore, the tank has to be non-metal materials; otherwise, the flux flows though the metal and generates the eddy loss. Eventually, the tank will heat up. The volume of the selected bin is 80L. The height of the bin is 85cm, the width is 45cm, and the breadth is 51cm. The bin size was selected to ensure there was sufficient space for fitting the transformer and 70L of oil.

For this project, BIOTEMP® was selected as the transformer oil for cooling and insulation purposes. BIOTEMP® is an advanced vegetable based dielectric insulating medium that was developed by ABB to be environmentally friendly. The fluid has excellent dielectric characteristics with high temperature stability, superior flash point, and fire resistance [12]. BIOTEMP® has excellent compatibility with solid insulating materials and is biodegradable in the short term.

Both the inside and outside windings are connected to bushings, which connect the windings to external cables. Also, on the lid top, a gas breather was installed using Polyvinyl chloride (PVC) pipe. The breather releases any moisture from the insulation; and the oil as it heats up. It also allows for the expansion of the oil as it gets hot, otherwise, the tank may explode with the increased oil pressure. There are also three thermal probes installed inside the tank and the windings for detecting the temperature of the transformer during long term operation. The completed PCPT is shown in Figure 4.9.

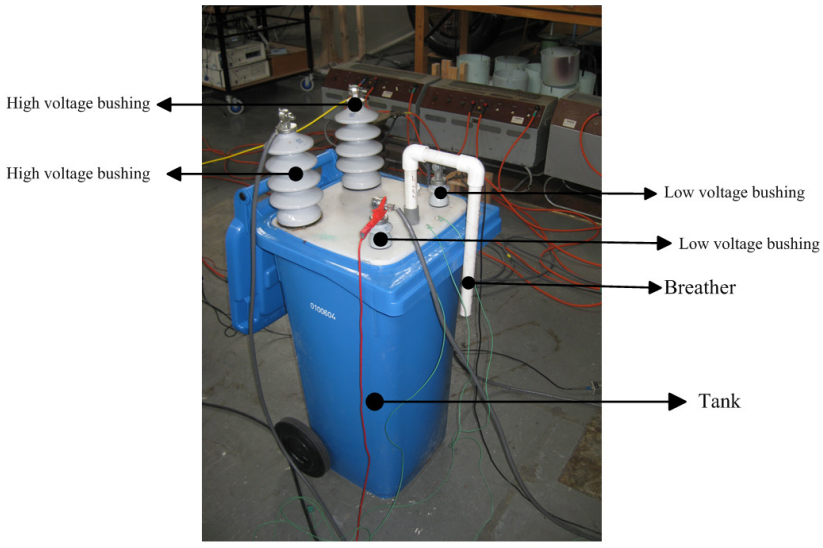

Figure 4.9 Completed PCPT sample.

4.5 Discussion and Conclusion

In chapter 4, a new PCPT was designed using the electrical and thermal models. The electrical model has the physical dimensions and the electrical performance for the PCPT. The thermal model calculated the winding hot-spot temperature rise from the given electrical performance and the physical dimensions. The designed PCPT has a flux density 1.74T. The voltage ratio was 11033V:230V. The power rating was 18.2kVA; and the real power delivered to the load was 14.9 kW. The inside winding current was 65A; and the outside winding current was 1.65 A. The inside winding current density was 5.2A/mm^2; and the outside winding current density was 5.3A/mm^2. The PCPT had 92% efficiency; and the voltage regulation was 7.2%. Based on the electrical performance of the PCPT, the thermal model generated a graph shown in Figure 4.1 which shows the hot-spot, top oil, and bottom oil temperatures. The hot-spot temperature rises to 97˚C and stayed at this level after 6 hours. The top oil temperature reached 78˚C and the bottom oil temperature rises to 44˚C. This result shows that the PCPT is able to operate at 1p.u load for a long operating time.

The PCPT was assembled after the separate construction of the core, the windings, and the tank. There were some issues encountered during the construction processes. During the core construction, the laminations packets were very difficult to line up to form a circular transformer core without proper machinery. For the windings, insulation paper overlap was another issue. Since NMN is very rigid, it is very difficult to fold around the transformer winding to form the overlap. A transformer insulation folding machine is required for overcome this problem.

The total number of the inside winding turns precisely matched the results calculated from the computer model. The result indicates that there is no space between each turn of the inside winding in the constructed transformer.

The plastic tank has an advantage of being light weight. However, the rigidity of the plastic is poor, the melting point is low, and the thermal insulation is very high. Therefore, a better transformer tank material is required for future construction of the PCPT.

CHAPTER 5
TESTING THE PARTIAL CORE POWER TRANSFORMER

5.1 Introduction

The electrical and thermal performances of the PCPT were estimated from the simulation models. However, after the construction of the partial core power transformer, the actual electrical and thermal performance results were obtained by performing a winding insulation test, a winding resistance test, an open circuit test, a short circuit test, a load circuit test, and a winding thermal test.

5.2 Winding Insulation Test

Transformers with two or more windings and a highest voltage equal to or greater than 3.6kV are required to withstand a winding insulation test [20]. Since, the partial core power transformer has a high voltage (HV) of 11kV, a winding insulation test is necessary.

The winding insulation test has three separate procedures. Each test was undertaken by injecting a dc voltage. The equipment used was a Megger insulation tester [21]. The first step is testing the insulation between the HV winding and the low voltage (LV) winding. The testing DC voltage was 5000V. The testing configuration is shown in Figure 5.1.

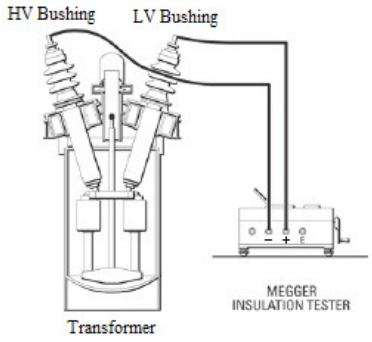

Figure 5.1 Setup for the testing the insulation between the HV winding and the LV winding.

The positive connection lead of the Megger meter was connected to a HV bushing on the transformer. The negative connection lead of the Megger meter was connected to the LV bushing on the transformer.

The second step was testing the HV winding insulation to the tank. The testing setup is illustrated in Figure 5.2.

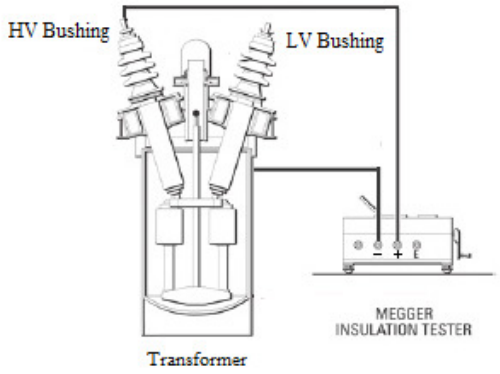

Figure 5.2 Setup for testing the insulation of the HV winding.

The positive connection lead of the Megger meter was connected to a HV bushing. The testing DC voltage was 5000V. The negative lead was connected to the surface of the tank as shown in Figure 5.2.

The last step was testing the LV winding insulation to the tank. The testing layout is illustrated in Figure 5.3.

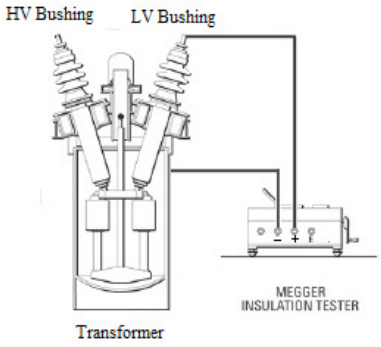

Figure 5.3 Setup for testing the insulation of the LV winding.

The positive lead of the Megger meter was connected to a LV bushing on the transformer. The testing DC voltage was 5000V. The negative lead was connected to the surface of the tank.

The time duration of each test was one minute. The results of the three tests are shown in the Table 5.1.

Table 5.1 Results of the insulation tests.

Insulation between the HV winding and the LV winding (GΩ)	>3
Insulation of the HV winding (GΩ)	>4
Insulation of the LV winding (GΩ)	>3

According to IEEE 62-1995 [22], the tested PCPT has a good insulation level for the HV winding, the LV winding, and between the HV winding and the LV winding.

5.3 Routine Tests

For any manufactured transformer, routine tests [20] are critical for determining the actual electrical performance. The routine tests give the overall electrical performance of the PCPT to compare with the modeling results. The routine tests are five independent tests [20] as listed.

a) Measurement of winding resistances

b) Measurement of voltage ratio

c) Measurement of no-load voltage and current

d) Measurement of short-circuit impedance

e) The load circuit test

5.3.1 Winding Resistance Test

This test used an mPK 254 digital micro-ohmmeter for recording the resistance of both windings. To do this test, the micro-ohmmeter was connected to the HV winding and then the LV winding separately. Each winding resistance was measured by injecting a 5A current from the micro-ohmmeter into the LV winding of the transformer, and a 1mA current into the HV winding of the transformer. The transformer was tested at 17˚C. The modeling results and the testing results are both shown in Table 5.2:

Table 5.2 Winding resistance comparison between computer modeling and the winding resistance test.

Description	**Computer model results**	**Test results**	**% difference**
HV winding (Ω)	244	290	19
LV winding (mΩ)	90	95	6

From Table 5.2, the resistance of the HV winding from the computer model is lower than the results from the winding resistance test. The main reason for the difference is the five oil gaps which are not included in the electrical model. These oil gaps increase the outside winding width. Hence, the total winding wire length is longer than the model predicts. Therefore, the resistance of the HV winding is increased by the extra length.

Also, the actual turns are more than the model estimated. The model design called for the outside winding to have 17 layers and 12454 turns in the model design, but the built value was 12460 turns. However, the effect at 0.05% is not very significant.

The two reasons explain why the measured winding resistance was higher than what the model estimated. For the LV winding side, both results from testing and modeling are much closer as shown in Table 5.2. This is because the LV winding only has two oil gaps and the diameter of the each oil gap is much smaller than the diameter of the LV winding wire. Therefore, the extra length for the LV winding would not be as much as the HV winding. Thus, the LV winding actual resistance is much closer to the result from the computer model.

5.3.2 Voltage Ratio and Open Circuit Test Results

The open circuit test determines the voltage ratio of a transformer as well as the VI curve. The VI curve is used for determining the operating region of the designed transformer at the required voltage level. The test circuit is shown in Figure 5.4.

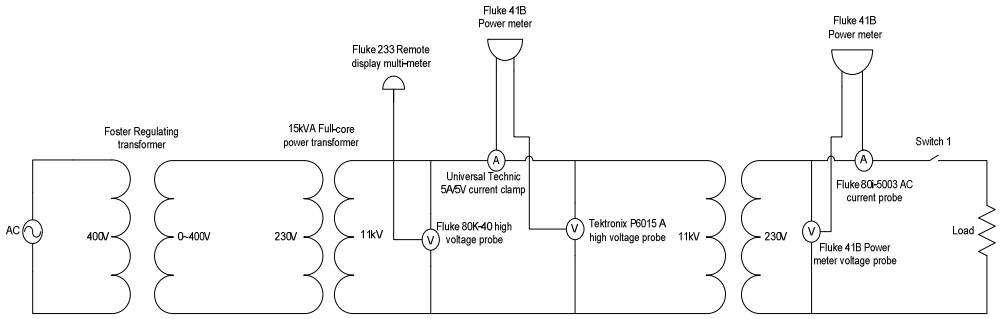

Figure 5.4 Open circuit test circuit.

The test AC power source is generated from a Foster regulating transformer (regulator) which is a 245kVA transformer with an output voltage range from 0 to 438 volts. In order to deliver a 11kV input to the partial core transformer, the output of the Foster regulator is connected to a 15kVA full core power transformer with a voltage ratio of 230V:11kV. A Fluke 233 remote display multimeter was used for monitoring the input voltage of the partial core transformer.

Both the HV and LV winding bushings were linked with FLUKE 41B power meters to record the current, voltage, power factor, and output power for both windings. Switch 1 was open for the open circuit test.

A Fluke 80K-40 high voltage probe with a high impedance [23] was connected to the Fluke 233 remote display multimeter (10MΩ input impedance) to measure the high voltage. A Tektronix P6015A high voltage probe with a low impedance was setup with the Fluke 41B power meter (with 5MΩ input impedance) [24]. The current probe on the HV side was a Universal Technic 5A/5V current clamp because the rated current in the HV winding is 1.36A. Since the rated current of the LV winding is 65A, the current clamp used on the LV winding was a Fluke 80i-5003 AC current probe which has an input range of 1A to 500A. The experimental results of the open circuit test are shown in Table 5.3.

Table 5.3 Open circuit results for the partial core power transformer.

Voltage of HV winding (V)	Current of HV winding (A)	Apparent power (VA)	Real power (W)	Power factor	Voltage of LV winding (V)
1181	0.07	83	5.8	0.07	23
2324	0.15	349	17.4	0.05	46
3582	0.22	788	39.4	0.05	69
4820	0.3	1446	57.8	0.04	93
6020	0.38	2288	91.5	0.04	116
7160	0.46	3294	132	0.04	139
8340	0.54	4504	180	0.04	162
9620	0.61	5868	235	0.04	185
10390	0.77	8000	320	0.04	208
10860	0.83	9014	361	0.04	215
11050	0.88	9724	389	0.04	220
11300	0.96	10848	434	0.04	225
11500	1.024	11776	471	0.04	230

Based on Table 5.3, a comparison between the model and the experimental results for the open circuit test at a LV winding voltage of 230V is shown in Table 5.4

Table 5.4 Comparison between model and experimental results for the open circuit test at a flux density of (1.81T).

Description (1.81 T)	**Computer model results**	**Experimental test results**	**% difference**
HV winding voltage (V)	11970	11500	-4
LV winding voltage (V)	230	230	0
HV winding current (A)	0.7	1.0	46
HV winding apparent power (VA)	8379	11776	40
HV winding power factor	0.016	0.04	150
Real power loss (W)	127	471	270

The voltage ratio at the rated secondary voltage is 11500V:230V. This result matches the ratio determined from the computer model of 11970:230 very well. However, Table 5.4 shows that there are significant differences between the experiment results and computer model results for the HV winding current, the HV winding apparent power, the HV winding power factor and the open circuit real power loss.

In order to investigate the cause of these significant differences, based on Table 5.4, the open circuit HV winding voltage is plotted against the HV winding current and the open circuit core losses in Figure 5.5 and Figure 5.6 respectively. The HV winding power factor against the HV winding voltage is plotted in Figure 5.7.

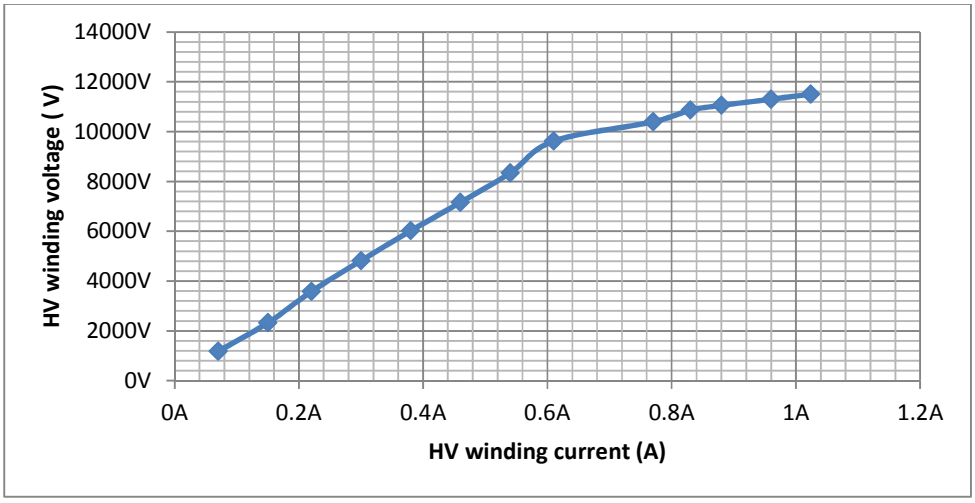

Figure 5.5 Open circuit HV winding voltage versus HV winding current.

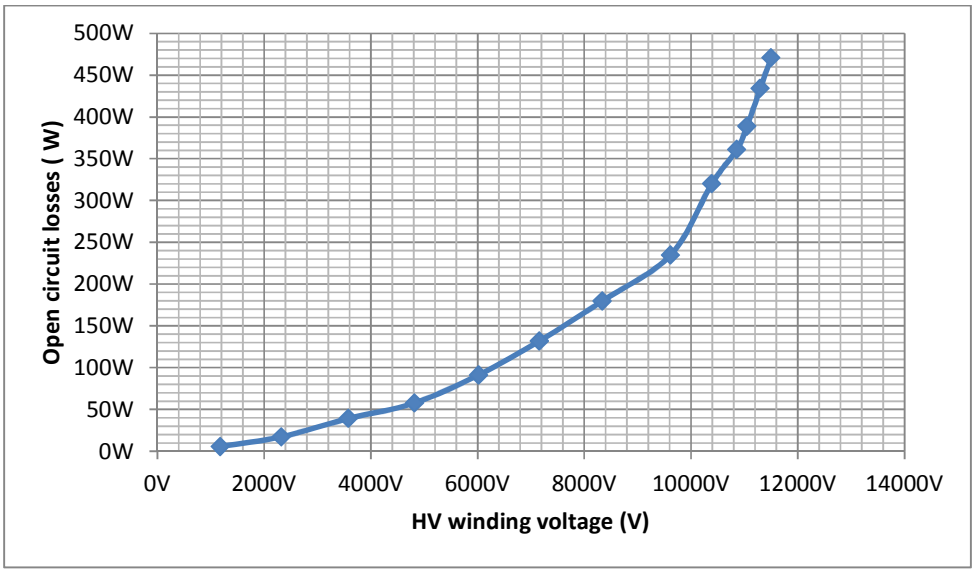

Figure 5.6 Open circuit losses versus voltage.

As Figure 5.5 shows, the knee point of the curve is located at 9620V and 0.65A. The cross section area of the core is less than the calculation from the model due to the cutting technique and the core stacking technique in the manufacturing. Therefore, the actual induction of the core is higher than calculated. Hance, the opearting voltage 11kV is above the knee point of the VI curve. The partial core transfomer operates in the saturation region when the input voltage is 11kV. This will cause the transfomer to draw more current from the supply than for a linear realtionship between the HV winding voltage and current. It also generates more core loss as shown in Figure 5.6. Hence, operating the transformer at the saturated region will reduce the overall efficiency.

In order to improve the overall efficiency of the transfomer, the transformer needed to operate more linearly. The cause of the transformer core saturation was the high flux density in the core, which was calculated to be 1.8T using the computer model. The flux density of the core can be reduced by increasing the cross-sectional area of the core by adding more laminiations. The diameter of the former is 6cm but the initial diameter of the core was 5.5cm in the original design specification. This gives a 0.5cm air gap; and the stacking factor drops to 0.83. Thus, extra laminiations can be physically added to fill the 0.5cm air gap inside the former, and improve the core stacking factor. The thickness of the laminiation steel is 0.023cm. To fill the air gap, a total 22 pieces of 5.5cm width laminiation steel were added. The stacking factor was increased to 0.93.

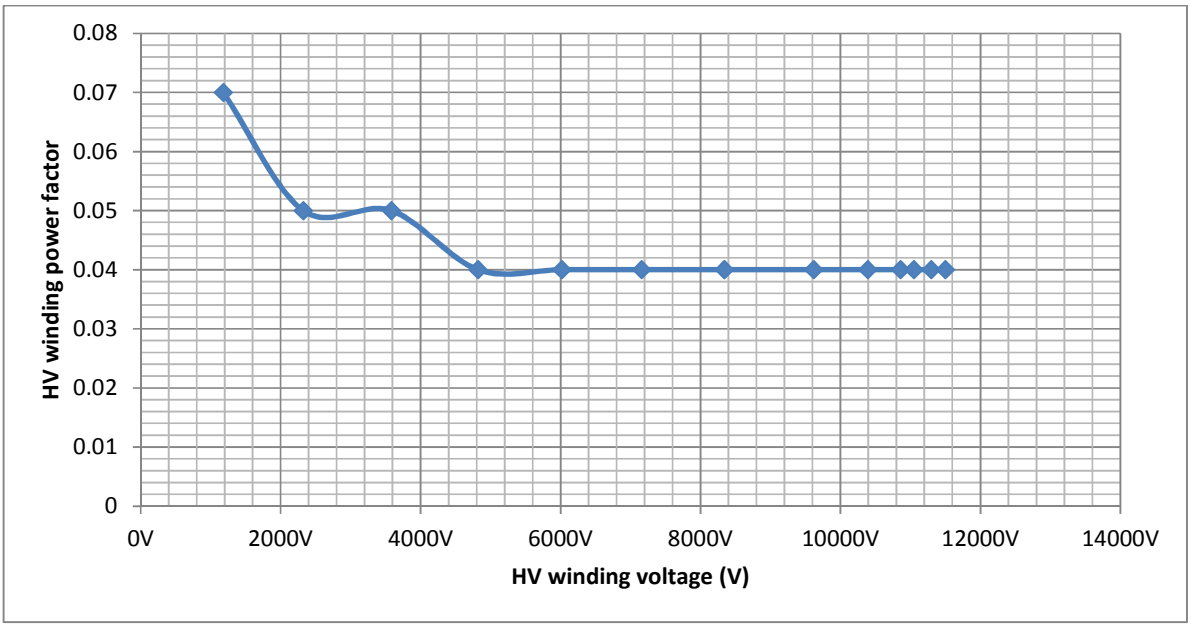

Figure 5.7 Open circuit HV winding power factor versus the HV winding voltage.

As shown in Figure 5.7, the HV winding power factor of the PCPT was 0.04 at 11kV while the computer model calculated it as 0.015, as shown in Table 5.4. The significant difference is due to the larger air gaps between the core and the winding former. This air gaps will reduce the effective permeability of the flux path, and will saturate the core since the reluctance of the air is much larger than the reactance of the steel, hence, increasing the reluctance which decreases the magnetising reactance. Therefore, the actual magnetising reactance is smaller than the model estimated, which is why the power factor of the core is larger than the model expected. By adding the extra laminations to fill the air gaps, the flux coupling will be improved, and will increase the magnetising reactance of the core to reduce the power factor. After increasing the diameter of the core. The core flux density was reduced to 1.48T. The new open circuit results are listed in the Table 5.5.

Table 5.5 New open circuit results with 1.48 T core flux density.

Voltage of HV winding (V)	Current of HV winding (A)	Apparent power (VA)	Real power (W)	Power factor	Voltage of LV winding (V)
458	0.056	26	1.0	0.04	9.5
1167	0.12	140	4.2	0.03	24
2105	0.18	379	7.6	0.02	44
3118	0.24	748	15.0	0.02	65
4032	0.3	1210	24.2	0.02	84
5067	0.36	1824	36.5	0.02	106
6049	0.43	2601	52.0	0.02	126
7075	0.48	3396	67.9	0.02	169
8106	0.61	4945	98.9	0.02	208
9010	0.66	5947	118.9	0.02	188
10060	0.7	7042	140.8	0.02	210
11112	0.76	8445	169	0.02	230

After decreasing the flux density, the VI curve is much more linearized up to 11kV as shown in Figure 5.8.

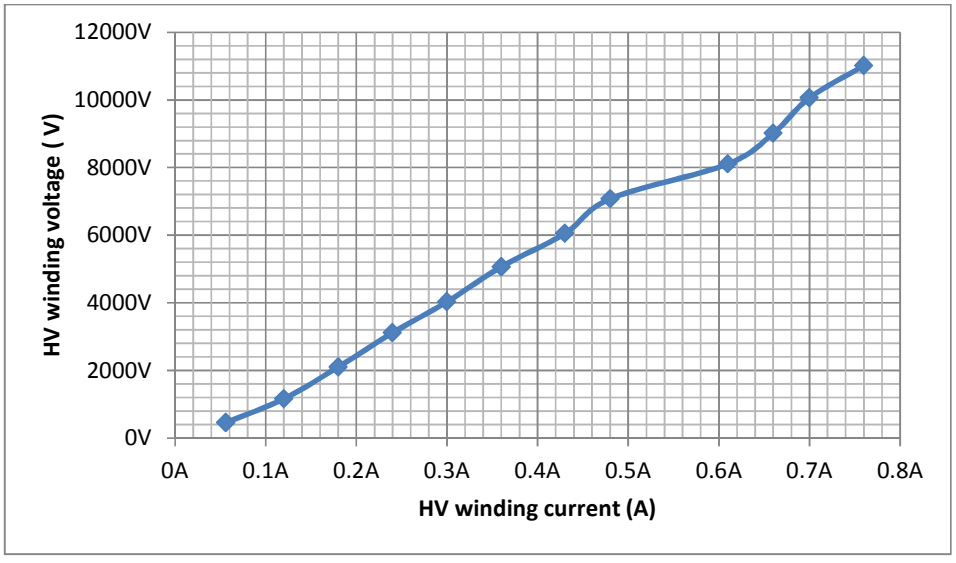

Figure 5.8 VI curve of the partial core power transformer with a calculated core flux density of 1.48T.

Since the transformer operates in the linear region, the HV winding draws less current 0.8A at 11kV than when the transformer operated in the saturation region as Figure 5.5 showed.

Also by adding steel laminations into the air gap, the core losses and the power factor of the HV winding are significantly reduced, as shown in Figure 5.9 and Figure 5.10 respectively.

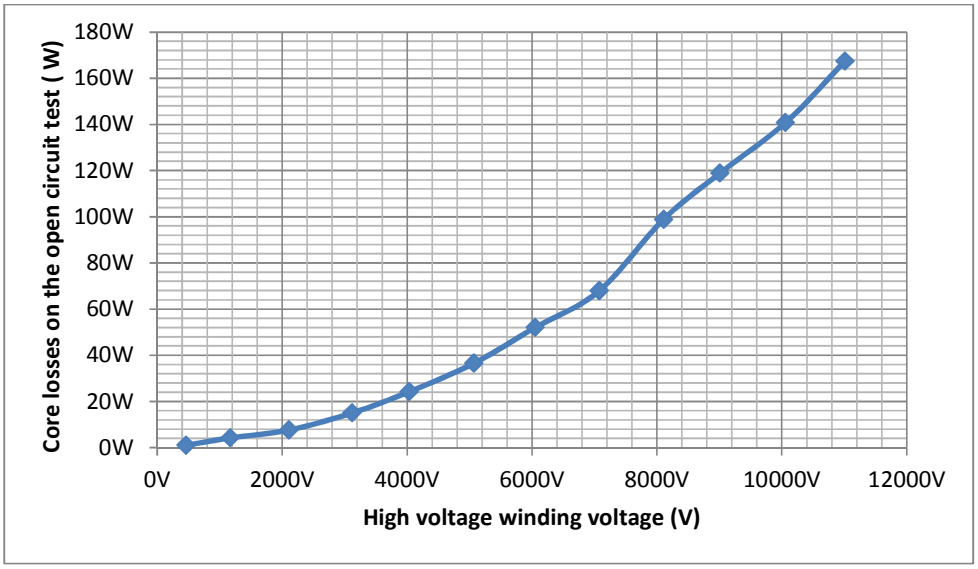

Figure 5.9 New core losses of partial core power transformer with a core flux density of 1.48.

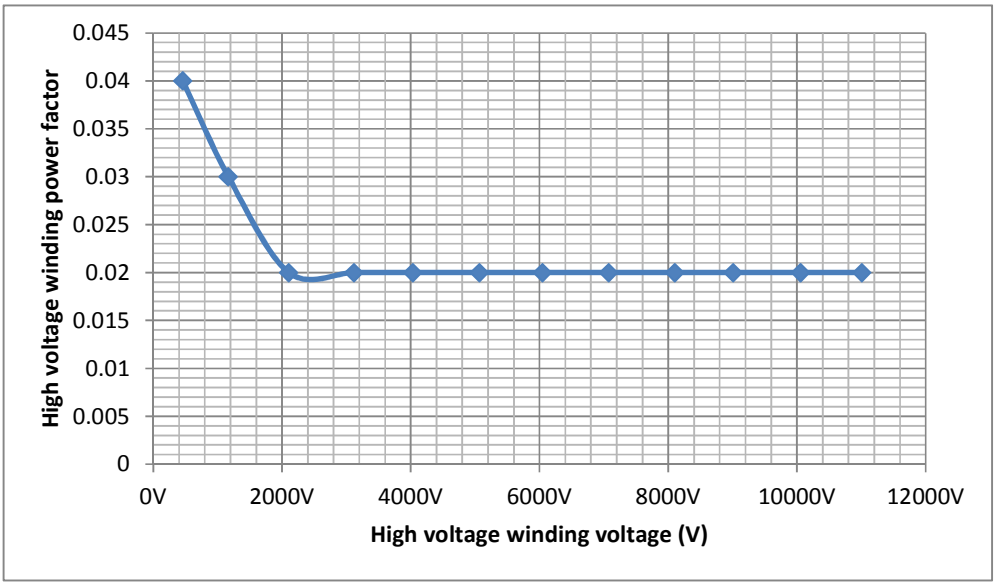

Figure 5.10 New power factor of HV winding a core flux density of 1.48T.

Figures 5.8, 5.9, and 5.10 illustrate that by eliminating the air gap, the calculated flux density is reduced from 1.89T down to 1.48T. The reduction of the flux density brings the PCPT operation into the linear region of the magnetisation curve. The high voltage winding draws

less current than when it was operating in the saturation region. Therefore, the open circuit losses are significantly reduced from 471W down to 167W. Furthermore, by adding extra laminations, the air gaps between the core and the winding former is much smaller. The effective permeability of the flux path is increased. Hence, the total reluctance of the core is decreased which increases the magnetising reactance. Therefore, the PCPT is operating in the linear region of the magnetisation curve. Also, increasing of the magnetising reactance reduces the power factor of the PCPT. The overall electrical performance of the PCPT has been significantly improved.

Table 5.6 Comparison for the new core of the open circuit test (1.48 T) between model results and experimental results.

Description	Computer model results	Experimental test results	% difference
HV input winding voltage (V)	11700	11112	6
LV output winding voltage (V)	230	230	0
HV winding current (A)	0.69	0.76	10
Apparent power (VA)	8000	8445	4.6
HV winding power factor	0.015	0.02	33
Real power loss (W)	120	169	39

From Table 5.6, the percentage difference between the computer model results and the experimental test results for all aspects are significantly reduced after filling the air gap with steel laminations. However, as shown in Figure 5.11, there will always be some air gaps between the core and former. These air gaps affect the HV winding power factor, the HV winding current and the losses. The results of the open circuit test show that the air gaps inside of the transformer have a significant impact on the overall performance of the transformer. The model does not include this air gap. Therefore, there will be some difference between the computer model results and the experimental test results.

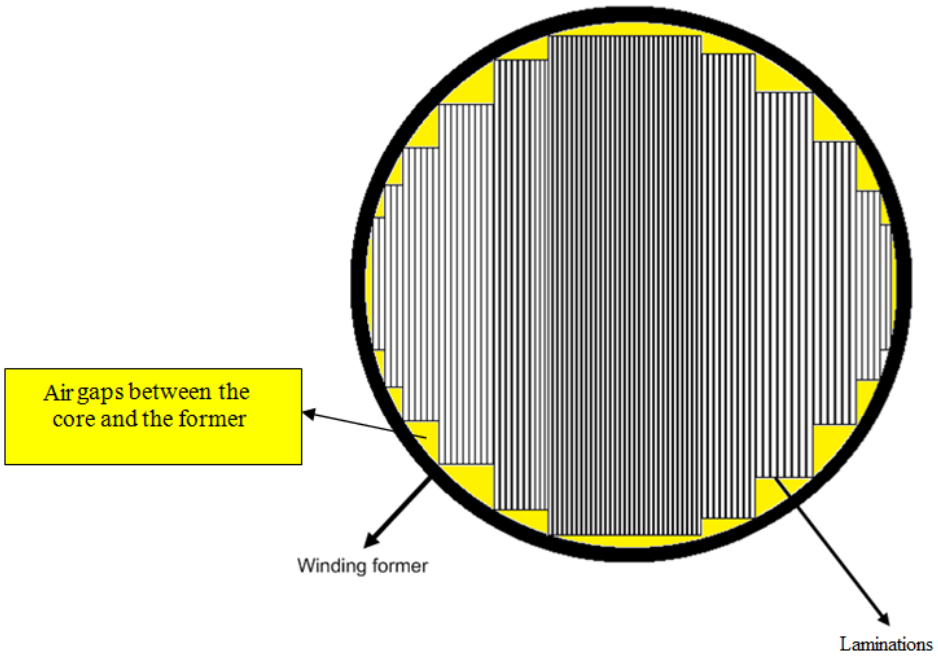

Figure 5.11 Top view of the circular core for the PCPT.

The magnetising reactance and total core resistance can be calculated from the HV input winding voltage, the HV winding current, and the HV winding power factor. Based on the measurements of the open circuit test, the magnetising reactance of the PCPT is 14.5kΩ and the total core resistance is 724.5kΩ. The total open circuit impedance is 14.5kΩ. From the calculation of the model, the magnetising reactance of the PCPT is 14kΩ, and the total core resistance is 780kΩ. The total open circuit impedance is 14kΩ from the model. The values of the magnetising reactance calculated from the model and the open circuit test are very close to each other. The difference in the total core resistance from the open circuit test and the model is due to the stacking factor of the core. In the model, the stacking factor was set too high (0.99) which assumes the lamination packs would form a perfect circle. However, the actual stacking factor is lower (0.93) as shown in Figure 5.11. In reality, there will be less steel to make the core than the model expects. It is possible to reflect this lower stacking factor into the design calculations

The open circuit real power losses are reduced from 471W when the PCPT was operated in the saturation region down to 167W after adding an extra 22 laminations. The HV winding resistance is 290Ω and the HV winding current is 1A when the PCPT was saturated. The actual core losses from when the PCPT was in the saturation region are 181W. After adding 22 laminations, the HV winding current is 0.76A; and the core losses drop to 169W. Hence,

the core losses are significantly decreased as the PCPT operates in the linear region rather than in the saturation region.

5.3.3 Short Circuit Test

The short circuit impedance of a transformer is obtained from the short circuit test. The LV winding is short circuited; and the HV winding voltage is quickly raised until the LV winding current is at its rated value [2]. The short circuit test layout is shown in Figure 5.12.

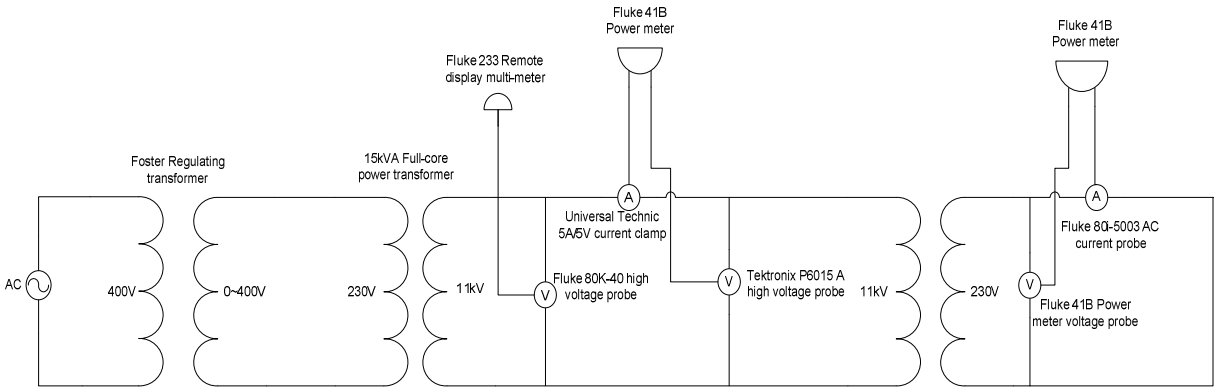

Figure 5.12 Short circuit PCPT test layout.

The short circuit test results are presented in Table 5.7.

Table 5.7 Short circuit test results for the partial core power transformer.

HV winding (V)	HV winding (A)	Apparent power (VA)	Real power (W)	Power factor	LV winding (A)
1100	1.48	1628	977	0.6	65

The total short circuit impedance of the PCPT at rated current can be calculated from these measurements. Based on Table 5.7, the total short circuit resistance is calculated as 446 Ω; and the total leakage reactance is calculated as 595 Ω. A comparison of the short circuit test results between the computer model and actual experiment are listed in the Table 5.8.

Table 5.8 Comparison between model and experimental results for the short circuit test.

Description	Computer model results	Experimental test results	% difference
HV winding current (A)	1.1	1.48	14
HV winding voltage (V)	860	1100	21
Short circuit impedance (Ω)	782	732	-6
HV winding power factor	0.73	0.6	-18
LV winding current (A)	65	65	0

The short circuit test impedance and the HV winding current results for both the modeling and from the experiment are very similar. The HV winding power factor experimental result is lower, because the leakage reactance for the model is smaller than the experimental test results. This is due to the oil gaps between each winding layer in the built transformer, however, in the model, each winding layer only has solid insulation. In the built transformer, there is an oil gap after every third-layer of the outside winding and after every layer of the inside winding. Therefore, the actual diameter of the free space between each winding is larger than that calculated from the model. This means that the actual leakage reactance as determined from the experiment is bigger than the model results. The electrical model needs to be modified by adding oil gaps in the winding design to better calculate the winding leakage reactance.

5.3.4 Load Circuit Test for PCPT

The load circuit test for the PCPT is shown in Figure 5.13.

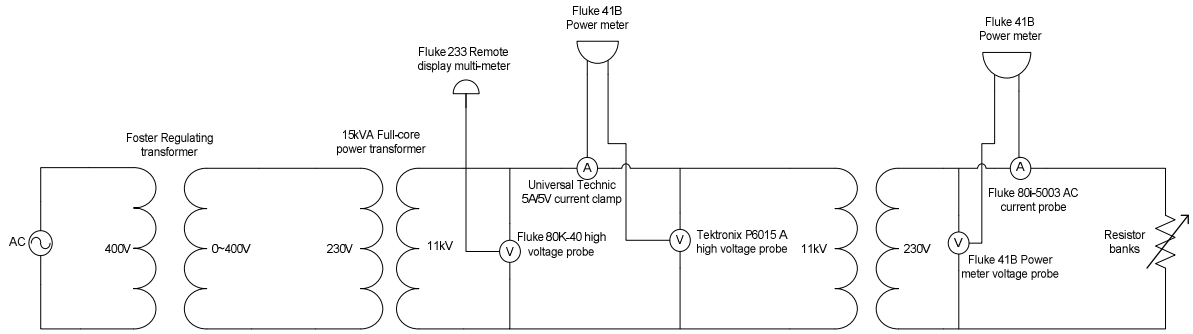

Figure 5.13 Layout of the load test circuit for PCPT.

The resistive load used in the load circuit test consisted of three, 5kW resistor banks in parallel. Each resistor bank had multiple parallel resistors that could be switched on and off. This setup allowed measuring the load circuit performance for different load conditions. In this test, the HV winding voltage was kept at 11kV for the different load conditions. The load test results are shown in Table 5.9.

Table 5.9 Load circuit test results for the partial core power transformer.

HV winding					LV winding					
Voltage (V)	Current (A)	Real power (W)	Power factor	Apparent power (VA)	Voltage (V)	Current (A)	Real power (W)	Power factor	Apparent power (VA)	Efficiency (%)
11000	0.76	167	0.02	8360	230	0	0	0	0	0
11000	0.79	2694	0.31	8690	220	10	2200	1	2200	82
11000	0.86	4825	0.51	9460	218	19	4142	1	4142	86
11000	0.96	6864	0.65	10560	216	28	6048	1	6048	88
11000	1.08	8791	0.74	11880	213	37	7881	1	7881	90
11000	1.22	10736	0.8	13420	211	46	9917	1	9917	92
11000	1.38	12751	0.84	15180	209	55	11495	1	11495	90
11000	1.54	14907	0.88	16940	207	65	13455	1	13455	90

The LV winding voltage can be plotted versus the LV winding current in Figure 5.14.

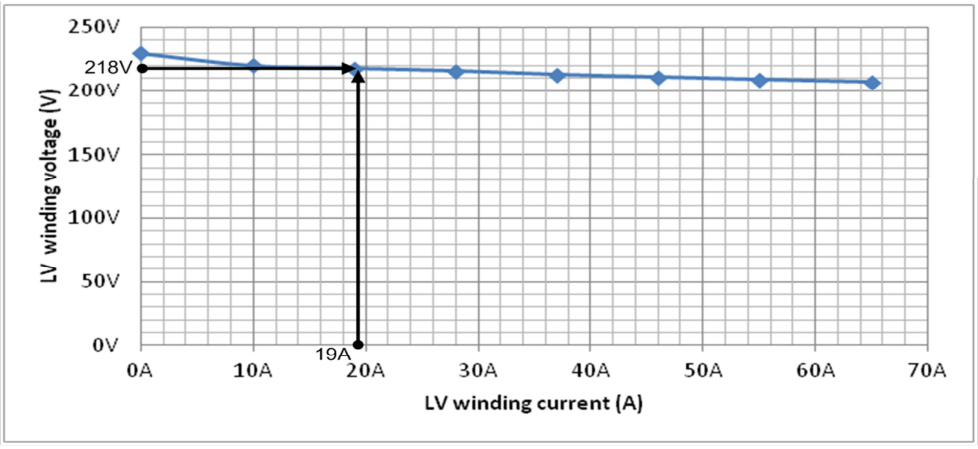

Figure 5.14 LV winding voltage versus LV winding current.

As illustrated in Figure 5.14, the LV winding voltage decreases when the LV winding current is increased. This is due to the voltage dropping through the LV winding impedances. In New Zealand, the home voltage level is within 6% of 230V [28]. Therefore, the minimum supply voltage has to above 218V [26]. Otherwise, it will cause a voltage regulation problem. The LV winding voltage of the PCPT drops to 218V when the load current is 19A as shown in Figure 5.14. For load currents greater than 19A, the LV winding voltage drops below 218V. Therefore, a tap change is required to increase the LV winding voltage.

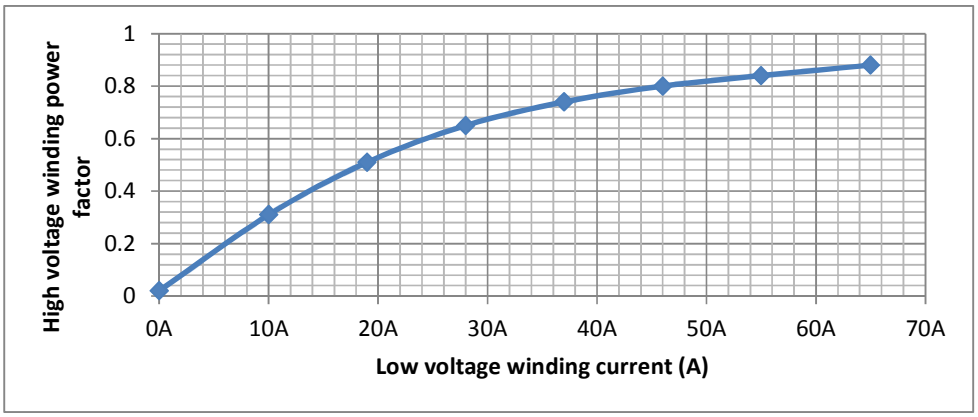

Figure 5.15 Transformer HV winding power factor plot at different load current level.

The transformer HV winding power factor is 0.88 at rated load as shown in Figure 5.15. The figure5.16 also shows that the HV winding power factor increases with increasing LV winding current.

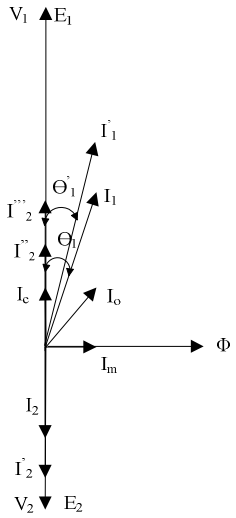

Figure 5.16 Phasor diagram for an initial and an increased resistive load [15]**.**

List of phasor diagram symbols

V_1 – HV winding voltage (supply voltage)

E_1 – HV winding emf

V_2 – LV winding terminal voltage (output voltage)

I_2 – LV winding load current

E_2 – LV winding emf

Φ – Magnetic flux

I_o – HV winding no-load current

I_m – HV winding magnetizing current

I_c – HV winding core loss current

I'_2 – Increased LV winding load current

I'_1 – Increased of the total HV winding current

I_1 – Total HV winding current (including I''_2 and I_o)

I''_2 – I_2 winding load current on HV winding

I'''_2 – I'_2 winding load current on HV winding

Θ_1 – HV winding power factor angle

Θ'_1 – New HV winding power factor angle

The short circuit impedance of the PCPT is 782Ω; and the open circuit impedance is 14kΩ. Hence, the winding resistance and leakage reactance are very small (only 5%) comparing with the core resistance and core magnetising reactance. Therefore, the influence of the winding resistance and leakage reactance with the HV winding power factor angle is negligible. The assumption was made such as V_1 is equal to E_1 and they are in phase as Figure 5.16 shown.

Once the load current I_2 is increased to I'_2, I''_2 also is increased to I'''_2. I_1 is the sum of vector I'_2 and I_o. I'_1 is the sum of vector I'''_2 and I_o. Hence, I'_1 is larger than I_1 and is also closer to V_1

as Figure 5.16 shown. Therefore, the HV winding power factor is increased when the LV winding load current increases.

Thus, the HV winding power factor is increased as Figure 5.15 shown.

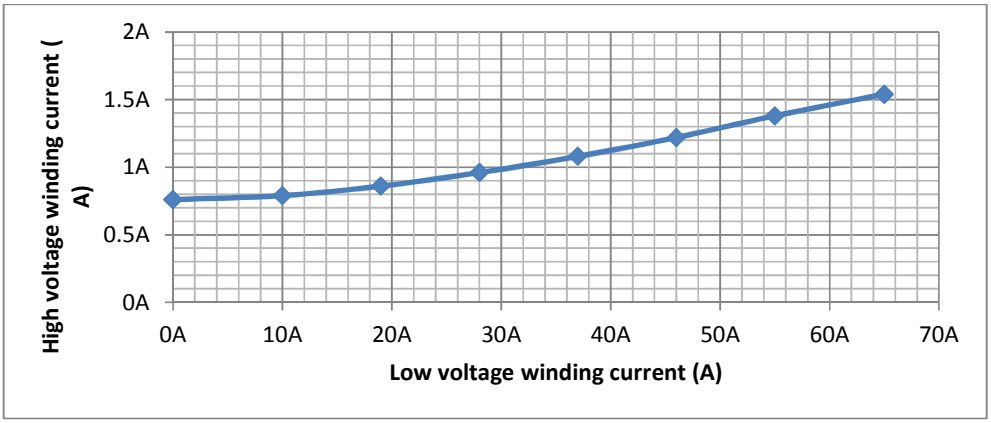

Figure 5.17 HV winding current versus LV winding current.

In an ideal transformer, the ratio between the HV winding current and the LV winding current is a constant value. Figure 5.17 shows the relationship between the measured HV winding current and the LV winding current. This is not constant nor a straight line. This is mainly due to the magnetising current of the PCPT dominating at low winding current values.

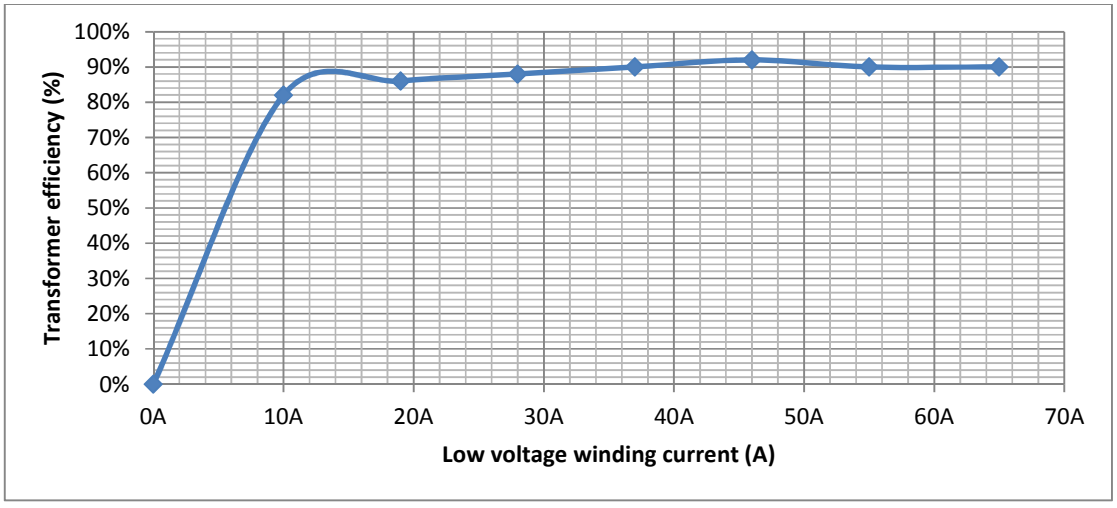

Figure 5.18 Transformer efficiency versus the load current.

As shown in Figure 5.18, the efficiency of the PCPT at rated load is 90%. The maximum efficiency of the PCPT is 92%, and this occurs when the load current is 46A. Theoretically, the maximum efficiency occurs when the core loss of the partial core power transformer is equal to the winding loss [8]. After the load exceeds 60A, the winding loss starts to dominate

the core loss, and the transformer efficiency starts to drop. The overall electrical performance of the PCPT is given in Table 5.10.

Table 5.10 Comparison of results from the electrical model and the experimental load circuit test at rated load for the partial core power transformer.

Description	Electrical model results	Experimental test results	% difference
HV winding voltage (kV)	11.1	11	-1
HV winding current (A)	1.65	1.54	-6.6
HV winding real power (kW)	16.6	15	-10
HV winding power factor	0.88	0.88	0
HV winding apparent power (kVA)	18.3	17	-7.1
LV winding voltage (V)	230	207	-10
LV winding current (A)	65	66	-1.5
LV winding real power (kW)	15	13.5	-10
LV winding power factor	1	1	0
Low voltage winding apparent power (kVA)	15	13.5	-10
Efficiency (%)	90	90	0
Voltage regulation (%)	7.4	10	35

The measured efficiency of the partial core power transformer is very close to that predicted from the model. However, the voltage regulation of the partial core power transformer (10%) is significantly higher than that predicted from the computer model. This is because the leakage reactances of the windings are higher than the values calculated from the computer model. This is because of the arrangement between the fiberglass rods and the winding layers, as explain in the short circuit test of section 5.3.3. Also the magnetising reactance of the core is lower than that calculated from the model. The cause of this is the air gap between the core and the winding former. Thus, the output voltage is lower than expected. Therefore, the LV winding apparent power and the real power are both lower than the values from the computer model.

5.4 Weight of Core Components

The model and measured values of the weights for both windings and the core are shown in Table 5.11.

Table 5.11 Computer model and measured values of the weights for the core components of the partial core power transformer.

Description	Electrical model	Measured	Difference %
Weight of the core (kg)	10.5	11.5	6.5
Weight of both windings (kg)	16.34	17	4
Total weight (kg)	26.34	28.5	8.2

The model predicts the physical weight for each component of the PCPT very closely to the actual values. The measured values are heavier due to the inclusion of insulation.

5.5 Winding Temperature Testing Results

The thermal performance of the partial core power transformer at 15kVA is calculated from the computer model. The calculated values for the hot-spot, top oil, and bottom oil temperatures from the thermal model are shown in Figure 5.19.

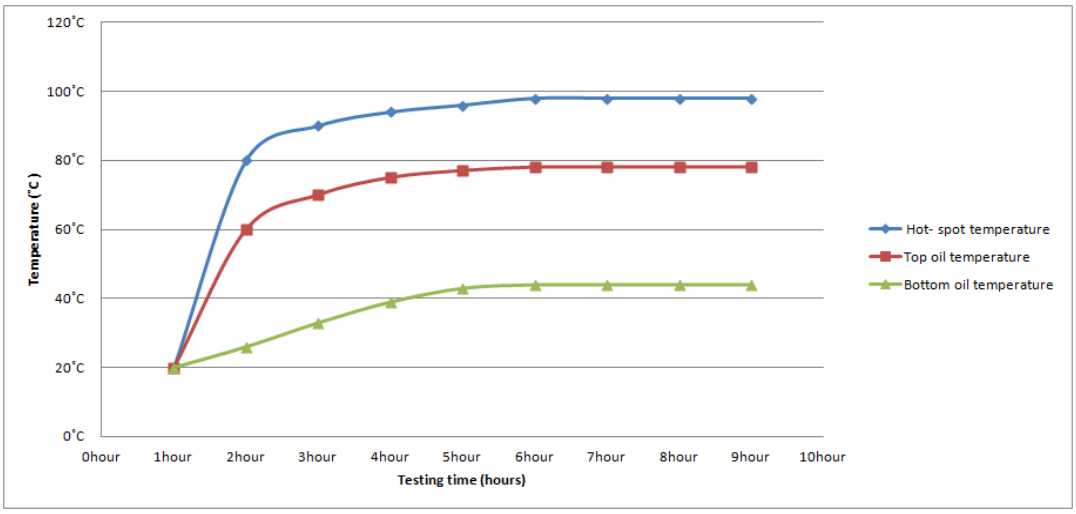

Figure 5.19 Hot-spot, top oil and bottom oil temperatures generated by the thermal model.

The hot-spot temperature is 97˚C after 6 hours; the top oil temperature reaches at 78˚C; and bottom oil temperature rises up to 44˚C. This result indicates that the designed partial core power transformer should be able to operate continuously at a 15kVA rating.

5.6 Experimental Winding Temperature Test

Three thermal sensors were installed inside the PCPT according to the IEC 60067-2 standard [14]. The locations of the three thermal sensors are shown in Figure 5.20.

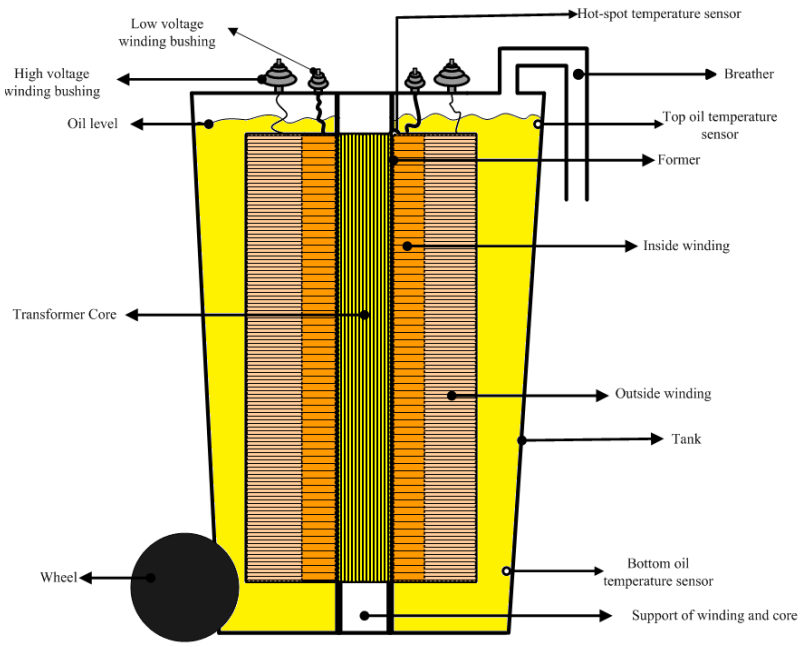

Figure 5.20 Side view of the partial core power transformer and the location of the three temperature sensors.

The hot-spot temperature sensor is located in the slot between the top of the first inside winding layer and the winding former. The top oil temperature sensor is located at the top inside of the bin. The bottom oil temperature sensor is set at the bottom inside of the bin. The measured temperatures for the partial core power transformer at a load of 15kVA are shown in Figure 5.21.

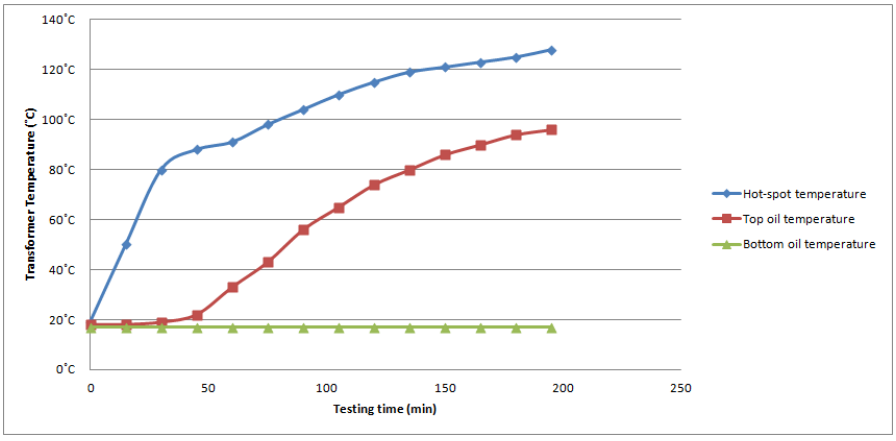

Figure 5.21 Measured hot-spot, bottom oil and top oil temperatures for the PCPT operating at 15kVA.

The hot-spot and top oil temperatures exceeded the thermal model predictions. The hot-spot temperature is about 130˚C; and the top oil temperature exceeded 95˚C after 195 minutes and

was still rising. In order to protect the plastic tank, the thermal experiment was stopped at this time. Therefore, the actual power rating of this partial core power transformer is lower than the estimated 15kVA for steady state operation.

The hot-spot temperature rises up very rapidly in the first 50 minutes. However, the top oil temperature does not respond in the same way. The bottom temperature stays at 20˚C for the first 50 minutes. The bottom oil temperature is still at 19˚C after 195 minutes, and is much lower than the model calculated. The reason for these values is the oil in the gaps between the windings does not have sufficient space to flow, and to circulate. The model expects oil circulation; and hence heat exchange between the top oil and bottom oil. However, there is no heat exchange between the top oil and bottom oil in reality. Thus, the oil circulation between the top oil and the bottom oil is very poor. Without any forced circulation, there will be little heat exchange between the top oil and bottom oil. Thus, the hot-spot and the top oil temperatures cannot be maintained at lower than 100˚C at 15kVA. Hence, the power rating has to be dropped so that the partial core power transformer operates within the 100˚C hot-spot constant temperature condition for continuous operation.

5.7 Finding a New Power Rating for the Designed PCPT.

In order to find a new power rating for the designed partial core power transformer, the load was varied from 0% of its nominal rating of 15kVA to 20%, 40%, 60%, 80%, and 90%. The hot-spot temperature was recorded every 10 minutes. The results are shown in Figure 5.22.

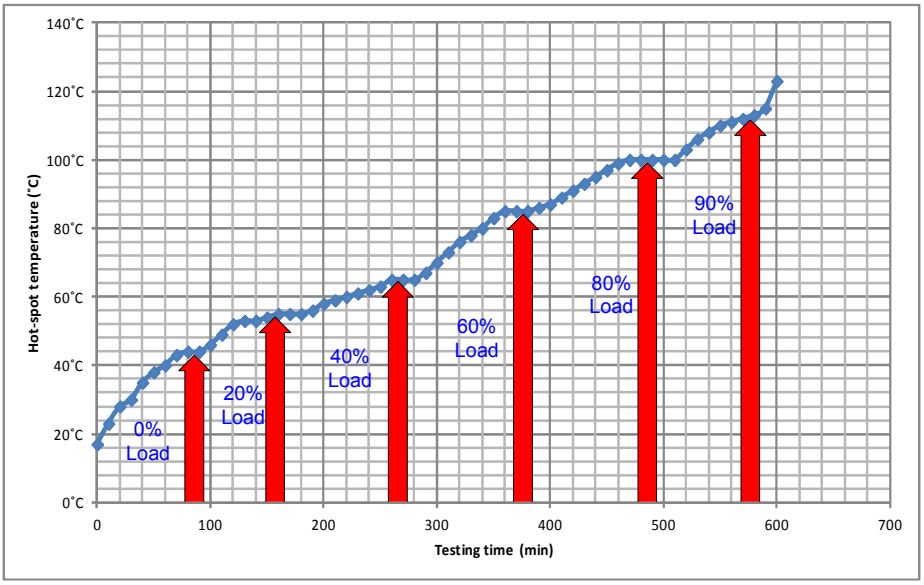

Figure 5.22 Hot-spot temperature for varying load.

The hot-spot temperature stays constant at 100˚C at 80% load for 40 minutes, and rises when more loads is added. Thus, the actual power rating of the partial core power transformer is 80% of 15kVA, being 12kVA.

The overall specification for the PCPT is listed in Table 5.12

Table 5.12 Overall specifications for the designed PCPT.

Power rating	(kVA)	12
Operating frequency	(Hz)	50
HV winding	(kV)	11
LV winding	(V)	230
Weight of the core	(kg)	11
Weight of both windings	(kg)	16
Weight of Container	(kg)	5
Volume of oil	(l)	75
Weight of oil	(kg)	60
Total weight	(kg)	92
Overall Efficiency	%	90
Regulation	%	10

5.8 Discussion and Conclusion

Eight different tests were applied to the PCPT to obtain its overall electrical performance. They were the winding insulation tests, the winding resistance test, the open circuit test, the short circuit test, the load circuit test, and the winding temperature rise test. Since the PCPT had cooling problems during the winding temperature rise test, a further thermal test had to be conducted to determine a new power rating for continuous operation.

The winding insulation tests illustrate that the insulation in the HV winding, the LV winding, and between the HV winding and the LV winding are all above 3GΩ, and they all have a very high resistance or insulation level.

The winding resistance test shows that there is a difference between the computer model results and the test results, especially for the HV winding resistance. This is due to two factors. The main factor is due to the addition of oil gaps between the inside and outside winding layers increasing the diameter of the windings. This increased the total lengths of the

winding wires, and hence increased the winding resistances. The oil gaps need to be added to the model to better evaluate the winding resistance. In addition, the actual outside winding turns were calculated from the model to be 12454 turns, but 12460 turns were actually wound during the manufacturing process.

The open circuit results show that the voltage ratio of the PCPT is 11970:230. This result matches the calculated values from the computer model reasonably well. Also from the open circuit test, the original flux density was too high (calculated to be 1.81 T) causing the PCPT to saturate at 10 kV. In order to reduce the flux density of the core, 22 extra 5.5 cm width pieces of steel lamination were added into the gap between the core and the winding former. The flux density of core dropped to 1.46 T, and the PCPT operated linearly to 11 kV. The new open circuit voltage ratio was 11112V:230V. The new test result matched the ratio determined from the computer model results of 11700V:230V. The difference is 5%. The overall electrical performance was improved significantly and the results between the experiment; and computer model were much closer. However, the HV winding power factor was still not quite same as the result calculated from the model. This is because a circular core made of lamination packets always has air gaps between the core and the winding former as shown in Figure 5.12. To overcome this problem, a rectangular core and winding former as shown in Figure 5.23 is a better design option to minimise the air gaps. However, this increases the winding wire length per turn, and increases the winding resistance, and may not necessarily lead to an overall better performance.

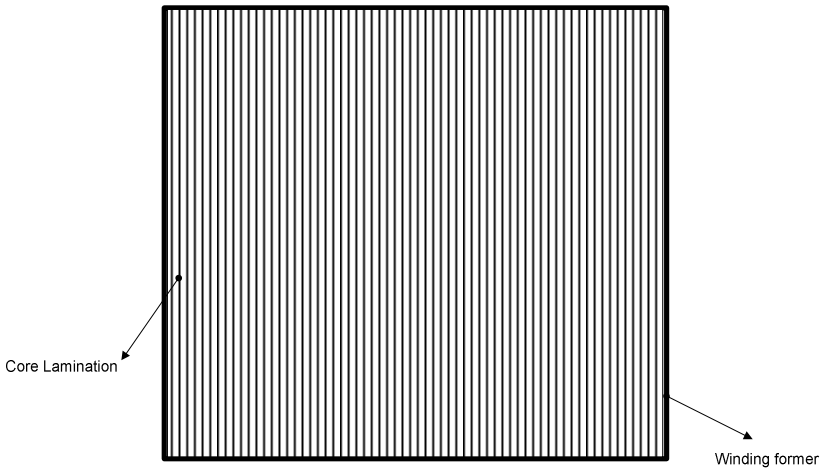

Figure 5.23 A rectangular core of a PCPT.

The short circuit impedances determined from the computer model and the short circuit test are very close to each other. The short circuit impedance calculated by the model is 782 Ω. The actual short circuit impendence from the measurements is 732 Ω. Inclusion of the oil gaps is critical for the electrical model to calculate a more accurate leakage reactance.

The results of the load circuit test are close for both the computer model and test. The voltage regulation was 10% in the load circuit test and 7.4% from the computer model. The cause of the difference is that the winding leakage reactance is higher than calculated from the model. Also, the magnetising reactance of the core is lower than the model calculated due to the air gaps between the core and winding former. This means more magnetising current to increase voltage drop in the primary winding.

There were three thermal probes used in the thermal test to obtain the temperatures for the winding hot-spot, the top oil, and the bottom oil. The model calculated that the hot-spot temperature stayed at 97˚C after 6 hours; with the top oil temperature reaching 78˚C, and the bottom oil temperature rising up to 44˚C. However, the hot-spot temperature exceeded 130˚C, and the top oil temperature climbed to 95˚C after 195 minutes during the winding thermal test. In order to protect the plastic bin from melting, the thermal test was stopped. The overheating was because the oil gaps are not wide enough to offer a sufficient space for the oil to circulate. Thus, there is no thermal circulation, and thus heat exchange between the bottom oil and the top oil. The temperature of the bottom oil did not change during the thermal test. However, further investigation is required to check the heat exchange between the bottom oil and the top oil by using the thermal imagining. The nominal power rating of the PCPT had to be decreased so that the PCPT could operate continuously. The new power rating of the partial core power transformer is 80% of 15kVA, or 12kVA. At that level, the hot-spot temperature stayed constant at 100˚C.

CHAPTER 6

DISCUSSION AND FUTURE WORK

6.1 General Conclusions

Both the electrical model and the thermal model for designing a PCPT are described in this thesis. The characteristics of BIOTEMP® were added into the thermal model. After completing the two-models, the PCPT was designed and constructed. The PCPT construction was divided into the core, windings and the tank construction. The final stage of construction was assembling all these components together as a unit. Testing of the PCPT was separated into several different individual tests. They were the winding insulation test, the winding resistance test, the open circuit test, the short circuit test and the load circuit test. The results of these tests were compared to the results from the models.

6.2 Electrical Model

In chapter 2, the basic principles and the modeling for an ideal partial core transformer was introduced. The modeling for the physical dimensions and the electrical performance of the non-ideal partial core transformer was then developed. The open circuit, short circuit and the load circuit test were well incorporated with the electrical performance of the partial core transformer in the model. However, when modeling the eddy current losses, the eddy current model used in this project was for full core transformers. The value for the eddy current resistance of the partial core transformers determined from test results was much smaller than that from the model. In order to account for this, a multiplication correction factor η was used in the model. This is not very accurate because the eddy current loss for the partial core transformers does not have a linear relationship with load. A more accurate model [9] has been developed and could be included in future work. The hysteresis power loss model used is based on the Steinmetz model which has two constants k and x. For the material used in the partial core transformers fabricated and tested at the University of Canterbury, the average value of x is 1.85. The k value is chosen as 0.11 in this project. It is the same as used in full core transformer models. However, the values of k for the different partial core transformers are significantly different [7]. This suggests that the Steinmetz hysteresis loss model may not directly apply to partial core transformers. A new mathematical expression for the constant value k is required for the partial core transformer design.

6.3 Thermal model

In chapter 3, the original full core transformer thermal model from the IEEE Guide for Loading Mineral-oil-Immersed Transformers [1] was successfully corrected. The error in the program input was discovered and fixed. It was due to the unmatched load cycle duration. Also, there were few coding errors which were corrected. These errors and their corrections are shown in Table 3.4. After correcting these errors, the modification of the thermal characteristics for BIOTEMP® were successfully programmed into the original model, based on a thermal characteristic comparison between BIOTEMP® and mineral oil. An existing PCPT was used to test the accuracy of the new thermal model.

The thermal model testing results showed that the model can accurately estimate the maximum hot-spot temperature for the tested PCPT. Having successfully developed and tested the model, the process of designing and manufacturing a new PCPT commenced. The variation of estimating the transient performance for the hot-spot temperature is something that is required to be solved in the future. However, it does not affect the steady state performance.

6.4 Transformer Design and Construction

In chapter 4, a new PCPT was designed using the electrical and thermal models. The electrical model is the physical dimensions and the electrical performance for the PCPT. The thermal model calculated the winding hot-spot temperature rise from the given electrical performance and the physical dimensions. The designed PCPT has a flux density of 1.48T. The voltage ratio was 11033V:230V. The power rating was 18.2kVA and the real power deliver to the load was 16.3kW. The inside winding current was 65A and the outside winding current was 1.65A. The inside winding current density was 5.2A/mm^2 and the outside winding current density was 6A/mm^2. The PCPT had 91% efficiency and the voltage regulation was 7.2%. Based on the electrical performance of the PCPT, the thermal model generated Figure 4.1 which shows the hot-spot, top oil and bottom oil temperature from the PCPT. The hot-spot temperature rose to 97˚C and stayed at this level after 6 hours. The top oil temperature reached 78˚C and the bottom oil temperature rose to 44˚C. This result shows that the PCPT is able to operate at 1per unit load for a long operating time.

A few issues were encountered during the construction processes of the PCPT. During the core construction, the laminations packets were very difficult to line up as a circular transformer core without appropriate machine assistance. Insulation paper overlap was

another issue. Since NMN is a very rigid paper, it is very difficult to fold around the transformer winding and cause the overlap.

The oil gaps added between the winding layers have an influence on the leakage reactance and the winding resistance which was discovered by the winding resistance test and the short circuit test. To achieve a more accurate electrical performance from the computer model, the oil gaps need to be included in the winding design component of the computer model.

6.5 Transformer testing and results

The last part of the project was testing the PCPT, and was analysing the results from several different tests. Seven different tests were applied to the PCPT to obtain the overall electrical performance of the PCPT.

1. The winding insulation test.
2. The winding resistance test.
3. The open circuit test.
4. The short circuit test.
5. The load circuit test.
6. The winding temperature rise test.
7. Reduced load temperature rise test.

The winding insulation tests determine the insulation resistance of the HV winding, the LV winding and between the HV winding and the LV winding. All the insulation results were above 3 GΩ, showing very high resistance or insulation level.

The winding resistance test showed that there was a difference between the computer model results and the test results, especially for the HV winding resistance. The main factor was the oil gaps between inside and outside winding layers increasing the diameter of the windings.

The open circuit results showed that the voltage ratio of the designed PCPT was 11112V:230V. The test result matched the ratio detemined from the computer model results of 11700V:230V. The open circuit power factor was 0.02 which means the core real power loss is very low and therefore the core resistance is high relative to the magnetisation reactance. Based on the measurements of the open circuit test, the magnetising reactance of the PCPT is 14.5 kΩ with the total core resistance of 724.5 kΩ. The total open circuit impedance is 14.5 kΩ.

The short circuit impedances determined from the computer model and the short circuit test are very close to each other. The short circuit impedance calculated by the model is 782 Ω. The actual short circuit impendence calculated from the short circuit test is 732 Ω. However, inclusion of the oil gaps in electrical model will allow a more accurate leakage reactance to be calculated.

The load circuit test gives the PCPT electrical performance at 1 p.u. resistive load. The HV winding voltage was 11 kV and the LV winding voltage was 207V. The HV winding current was 1.54A and the LV winding circuit was 66A. The HV apparent power was 17 kVA and the real power was 15 kW. The HV winding power factor was 0.88 and the LV winding real power was 13.4kW. The efficiency of the PCPT was 90% and the voltage regulation was 10%. The measured result of the load circuit test is close to that determined from the computer model. The voltage regulation was 10% in the load circuit test and 7.4% from the computer model. This is due to the winding leakage reactance being higher than calculated from the model. Also, the magnetising reactance of the core is lower than the model that calculated due to the air gaps between the core and winding former, causing an increase in magnetising current and primary winding voltage drop.

The results of the winding temperature test on load showed that the hot-spot temperature was 130˚C and the top oil temperature 95˚C after 195 minutes, and they were still rising. In order to protect the plastic tank, the thermal experiment was stopped. The actual power rating of this partial core power transformer is lower than the estimated 15kVA for steady state operation. From the thermal results, it was determined that, there was not enough circulation of oil between the core windings, and heat exchange between the bottom oil and the top oil.

Since the 15kVA power rating could not be reached, a new power rating for the designed partial core power transformer was determined. The load was varied from 0% of its nominal rating of 15kVA to 20%, 40%, 60%, 80% and 90%. The hot-spot temperature was recorded every 10 minutes. The hot-spot temperature stayed constant at 100˚C at 80% load for 40 minutes and increased with more loads rather than stay constant. Thus, the actual power rating of the partial core power transformer was 80% of 15kVA, being equal to 12kVA.

6.6 Future work

Mathematical models of winding eddy current losses and stray losses for partial core transformer have not been developed in the electrical model. Inclusion of these two models generate more accurate thermal performance is future work.

The IEEE thermal model was used to model the heat dissipation of transformers which the metal tanks and radiators. In this project, a plastic tank was used and radiators were not added to the transformer. Heat dissipation through metal is much faster than heat dissipation through plastic and radiators also accelerates the heat dissipation of the transformer. Hence, the thermal model needs to account for the plastic tank and the partial core transformer without the radiators.

Base on the results from the thermal winding test, the PCPT overheating problem is caused by no oil circulating between the top and the bottom of the tank, and the slow thermal reaction of the top oil. To overcome these problems, there are some modifications that can be applied on the PDPC physical design for the future work.

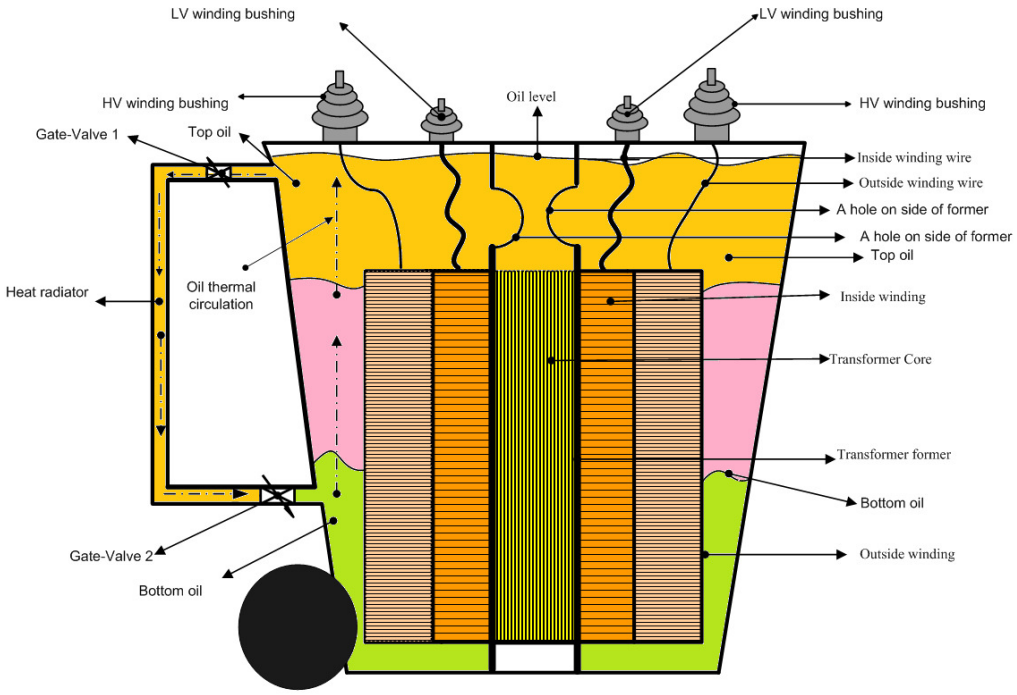

Figure 6.1 Thermal improved partial core power transformer.

The first option is increasing the length of the tank as shown in Figure 6.1. Since the length of the tank is increased, the greater volume of the relatively cooler top oil will cover the top of the hot-spot location for steadying the hot-spot temperature.

The second option is drilling holes through the top of the winding former to allow the top cold oil to cool the core as shown in Figure 6.1. Also need holes at the bottom of the former to allow the oil to circulate about the core.

The third option is to reduce the length of the transformer windings so that the transformer has more layers on both inside and outside windings. More layers of both windings allow the construction of more oil gaps to increase circulation of the hot oil inside the windings. Therefore, the winding temperature will be reduced. However, this option has the disadvantage of increasing the leakage reactance of the windings and hence the voltage regulation. Therefore, the maximum number of oil gaps allowed in the transformer design has been calculated using the computer model to determine an acceptable voltage regulation. The oil gaps have to be added to the computer model to estimate the total leakage reactance.

The fourth option is adding a heat radiator for the tank. The heat radiator design is shown in Figure 6.1. There are two gate valves used in the heat radiator design. When the transformer has operated for 20 minutes, the top gate valves and bottom gate valves are both opened to allow the hot top oil to flow though the radiator down to the bottom of the radiator. Then, the bottom valve is opened to allow the warm hot top oil to flow and mix with the cold bottom oil. As the cooling perspective, the more heat radiators were added on the transformer, the better cooling results were achieved. Since the top oil is warmer than the bottom oil, the top warm oil is able to push the cold bottom oil to the high position inside of the tank. Both valves can be controlled electronically. The top oil and bottom oil circulation is created by natural convection according to this configuration as shown in Figure 6.1.

The last option is changing the tank material. A plastic tank is used in this project. An advantage of the plastic tank is that it is highly insulated. However, the plastic tank has a high thermal isolation characteristic. Therefore, a better heat exchange material could be considered to replace the plastic as the material for making the transformer tank. However, this needs to be non-metallic to avoid induction heating of the tank.

APPENDIX A LIST OF FIGURES

Figure 1.1 Flow chart of the project overview. 2
Figure 2.1 3D model of a partial core resonant transformer [2]. 6
Figure 2.2 Partial core transformer cross sectional view [1]. 6
Figure 2.3 An ideal partial core transformer. 7
Figure 2.4 Equivalent circuit of a non-ideal partial core transformer operating at low frequency [8]. 10
Figure 2.5 Transformer equivalent circuit referred to the primary side [8]. 11
Figure 2.6 Centre limb of a partial core transformer showing component dimensions and material properties [8]. 12
Figure 2.7 Dimensions of a partial core transformer. 15
Figure 2.8 Calculate the leakage reactance for both windings [8]. 18
Figure 2.9 Axial flux view of the core for the partial core transformer [8]. 20
Figure 2.10 Magnetic circuit of the partial core transformer. 21
Figure 2.11 Open circuit transformer equivalent circuit [8]. 24
Figure 2.12 Short circuit transformer equivalent circuit [8]. 26
Figure 2.13 Loaded circuit transformer equivalent circuit [8]. 27
Figure 3.1 Graphical representation of the hot-spot temperature and its components. 32
Figure 3.2 Graphical presentation of the top and bottom oil temperatures. 33
Figure 3.3 A side view of the tested after PCPT. 46
Figure 3.4 Hot-spot temperature for both experiment and computer model. 49
Figure 4.1 Hot-spot, top oil and bottom oil temperature generated by the thermal model. 56
Figure 4.2 Top view of the circular core for the PCPT. 57
Figure 4.3 Core of the transformer. 58
Figure 4.4 Inside winding construction layout. 59
Figure 4.5 Outside winding structure layout. 60
Figure 4.6 Top view of both windings and the core of the transformer. 60
Figure 4.7 The PCPT winding construction setup. 61
Figure 4.8 Overview of the PCPT. 61
Figure 4.9 Completed PCPT sample. 62
Figure 5.1 Setup for the testing the insulation between the HV winding and the LV winding. 65
Figure 5.2 Setup for testing the insulation of the HV winding. 66
Figure 5.3 Setup for testing the insulation of the LV winding. 66
Figure 5.4 Open circuit test circuit. 68
Figure 5.5 Open circuit HV winding voltage versus HV winding current. 70
Figure 5.6 Open circuit losses versus voltage. 71
Figure 5.7 Open circuit HV winding power factor versus the HV winding voltage. 72
Figure 5.8 VI curve of the partial core power transformer with a calculated core flux density of 1.48T. 73
Figure 5.9 New core losses of partial core power transformer with a core flux density of 1.48. 74
Figure 5.10 New power factor of HV winding a core flux density of 1.48T. 74
Figure 5.11 Top view of the circular core for the PCPT. 76
Figure 5.12 Short circuit PCPT test layout. 77
Figure 5.13 Layout of the load test circuit for PCPT. 78
Figure 5.14 LV winding voltage versus LV winding current. 79
Figure 5.15 Transformer HV winding power factor plot at different load current level. 80
Figure 5.16 Phasor diagram for an initial and an increased resistive load [15]. 80
Figure 5.17 HV winding current versus LV winding current. 82

Figure 5.18 Transformer efficiency versus the load current. 82
Figure 5.19 Hot-spot, top oil and bottom oil temperatures generated by the thermal model..... 84
Figure 5.20 Side view of the partial core power transformer and the location of the three temperature sensors..... 85
Figure 5.21 Measured hot-spot, bottom oil and top oil temperatures for the PCPT operating at 15kVA. 85
Figure 5.22 Hot-spot temperature for varying load. 86
Figure 5.23 A rectangular core of a PCPT..... 88
Figure 6.1 Thermal improved partial core power transformer..... 95

APPENDIX B LIST OF TABLES

Table 3.1 Temperatures for calculating viscosity for the PCPT thermal model. 42
Table 3.2 Specific heat and constants for BIOTEMP® viscosity calculation..... 42
Table 3.3 Exponent temperature parameter for ONAN cooling method [11]..... 42
Table 3.4 Thermal program coding errors, adjustment and their corrections. 43
Table 3.5 Thermal program modification for BIOTEMP®. 43
Table 3.6 Design specification of the PCPT..... 44
Table 3.7 1 p.u load circuit test results from the electrical model. 45
Table 3.8 Weights for each component of the PCPT generated by the electrical model..... 45
Table 3.9 Input specification for PCPT of the developed thermal model. 47
Table 3.10 Initial loading case input setting. 48
Table 4.1 Design specification for the PCPT. 51
Table 4.2 Open circuit results from computer modeling. 52
Table 4.3 Short circuit test results from the electrical model. 53
Table 4.4 1 p.u load test results from the electrical model. 53
Table 4.5 Weight for each component for the PCPT from the electrical model. 54
Table 4.6 PCPT thermal model input parameters. 55
Table 4.7 Different widths of laminations and the quantities of each width. 57
Table 5.1 Results of the insulation test. 67
Table 5.2 Winding resistance comparison between computer modeling and the winding resistance test. 67
Table 5.3 Open circuit results for the partial core power transformer. 69
Table 5.4 Comparison between model and experimental results for the open circuit test (1.81T). 70
Table 5.5 New open circuit results with 1.48 T core flux density. 73
Table 5.6 Comparison for the new core of the open circuit test (1.48 T) between model results and experimental results. 75
Table 5.7 Short circuit test results for the partial core power transformer. 77
Table 5.8 Comparison between model results and experimental results for the short circuit test. 78
Table 5.9 Load circuit test results for the partial core power transformer. 79
Table 5.10 Comparison of results from the electrical model and the experimental load circuit test at rated load for the partial core power transformer. 83
Table 5.11 Computer model and measured values of weight for transformer core components in the partial core power transformer. 84
Table 5.12 Overall specifications for the designed PCPT..... 87

APPENDIX C THERMAL PROGRAM CODE

```
10 REM PROGRAM LOADT,9-15-1993

20 DEFINT I-N: DIM TIM (100), PUL (100), AMB (100), TIMP (1500)

30 PRINT "ENTER INPUT DATA FILENAME"

40 INPUT F2$

50 PRINT "ENTER OUTPUT FILENAME"

60 INPUT F1$

70 OPEN F2$ FOR INPUT AS #2

80 OPEN F1$ FOR OUTPUT AS #1

90  INPUT #2, LN, XKVA1, TKVA1, PW, PE, PS, PC

100 INPUT #2, LN, XKVA2, THKVA2, THEWA, THEHSA, THETOR, THEBOR, TAR

110 INPUT #2, LN, MC, PUELHS, TAUW, HHS

120 INPUT #2, LN, WCC, WTANK, MF, GFLUID

130 INPUT #2, LN, MCORE, TIMCOR, PCOE

140 INPUT #2, LN, LCAS

150 ON LCAS GOTO 170, 160

160 INPUT #2, LN, THS, TW, TTO, TTDO, TBO

170 INPUT #2, LN, MA, MPR1, DTP, JJ

180 FOR J = 0 TO JJ

190 INPUT #2, LN, TIM(J), AMB(J), PUL(J)

200 TIM(J) = 60 * TIM(J)

210 NEXT J

220 CLOSE #2

230 PT = PW + PE + PS + PC

240 PRINT #1, "PROGRAM LOADT, VERSION 1.1, 9-15-1993"

250 PRINT #1, "TRANSFORMER TEMPERATURE CALCULATION WITH
VARIABLE"
```

```
260 PRINT #1, "LOAD AND AMBIENT TEMPERATURE USING BOTTOM OIL RISE"
270 PRINT #1, "DUCT OIL RISE, RESISTANCE CHANGE WITH TEMPERATURE"
280 PRINT #1, "CORRECTIONS FOR FLUID VISCOSITY FOR OA, FA, AND NON-"
290 PRINT #1, "DIRECTED FOA COOLING MODES. NO VISCOSITY CORRECTION"
300 PRINT #1, "FOR DIRECTED FOA COOLING MODE."
310 PRINT #1,
320 PRINT #1, "INPUT DATA FILENAME IS "; F2$
330 PRINT #1, "OUTPUT DATA FILENAME IS "; F1$
340 PRINT #1,
350 PRINT #1, "KVA BASE FOR LOSS INPUT DATA = "; XKVA1
360 PRINT #1, "TEMPERATURE BASE FOR LOSS INPUT DATA = "; TKVA1; "C"
370 PRINT #1, "WINDING I SQUARE R = "; PW; "WATTS"
380 PRINT #1, "WINDING EDDY LOSS = "; PE; "WATTS"
390 PRINT #1, "STRAY lOSSES = "; PS; "WATTS"
400 PRINT #1, "CORE LOSS = "; PC; "WATTS"
410 PRINT #1, "TOTAL LOSSES = "; PT; "WATTS"
420 PRINT #1,
430 ON MC GOTO 440, 460
440 PRINT #1, "WINDING CONDUCTOR IS ALUMINUM"
450 TK = 225: CPW = 6.798: GOTO 480
460 PRINT #1, "WINDING CONDUCTOR IS COPPER"
470 TK = 234.5: CPW = 2.91: GOTO 480
480 PRINT #1, "PER UNIT EDDY LOSS AT HOT SPOT LOCATION = "; PUELHS
490 PRINT #1, "WINDING TIME CONSTANT = "; TAUW; "MINUTES"
500 PRINT #1, "PER UNIT WINDING HEIGHT TO HOT SPOT = "; HHS
510 PRINT #1,
520 PRINT #1, "WEIGHT OF CORE & COILS = "; WCC; "POUNDS"
```

```
530 PRINT #1, "WEIGHT OF TANK AND FITTINGS = "; WTANK; "POUNDS"
540 PRINT #1, "GALLONS OF FLUID = "; GFLUID
550 ON MF GOTO 1, 560, 580, 600
560 CPF = 15.21: RHOF = .031621: C = 2800: B = .0054292
570 PRINT #1, "COOLING FLUID IS BIOTEMP®": GOTO 620
580 CPF = 11.49: RHOF = .0347: C = 1782.3: B = .12127
590 PRINT #1, "COOLING FLUID IS SILICONE": GOTO 620
600 CPF = 14.55: RHOF = .03178: C = 4434.7: B = 7.343E-05
610 PRINT #1, "COOLING FLUID IS HTHC"
620 PRINT #1,
630 PRINT #1, "ONE PER UNIT LOAD. = "; XKVA2; " KVA"
640 ON MA GOTO 650, 680, 710, 740
650 X = .5: YN = .8: Z = .5: THEDOR = THETOR
660 PRINT "COOLING MODE IS OA"
670 PRINT #1, "COOLING MODE IS OA": GOTO 770
680 X = .5: YN = .9: Z = .5: THEDOR = THETOR
690 PRINT "COOLING MODE IS FA"
700 PRINT #1, "FORCED AIR (FA) COOLING": GOTO 770
710 X = .5: YN = .9: Z = 1: THEDOR = THEWA
720 PRINT "COOLING MODE IS NON-DIRECTED FOA"
730 PRINT #1, "NON-DIRECTED FORCED OIL (NDFOA) COOLING": GOTO 770
740 X = 1: YN = 1: Z = 1: THEDOR = THETOR
750 PRINT "COOLING MODE IS DIRECTED FOA"
760 PRINT #1, "DIRECTED FOA COOLING (DFOA)"
770 PRINT "NOMINAL VALUE OF Y EXPONENT IS"; YN
780 PRINT "DO YOU WISH TO CHANGE? TYPE Y FOR YES AND N FOR NO"
790 INPUT F3$
```

```
800 IF F3$ = "Y" THEN GOTO 820
810 GOTO 840
820 PRINT "INPUT DESIRED VALUE OF Y EXPONENT"
830 INPUT YN
840 PRINT "PROGRAM IS RUNNING"
850 PRINT #1, "EXPONENT OF LOSSES FOR AVERAGE FLUID RISE = "; YN
860 TWR = TAR + THKVA2: TWRT = TAR + THEWA
870 THSR = TAR + THEHSA: TTOR = TAR + THETOR
880 TBOR = TAR + THEBOR: TTDOR = THEDOR + TAR
890 TWOR = (HHS * (TTDOR - TBOR)) + TBOR
900 TDAOR = (TTDOR + TBOR) / 2: TFAVER = (TTOR + TBOR) / 2
910 XK2 = (XKVA2 / XKVA1) ^ 2: TK2 = (TK + TWR) / (TK + TKVA1)
920 PW = XK2 * PW * TK2: PE = XK2 * PE / TK2: PS = XK2 * PS / TK2
930 PT = PW + PE + PS + PC
940 IF (PE / PW) > PUELHS THEN PUELHS = PE / PW
950 TKHS = (THSR + TK) / (TWR + TK): PWHS = TKHS * PW
960 PEHS = PUELHS * PWHS
970 PRINT #1, "AT THIS KVA LOSSES AT"; TWR; "C ARE AS FOLLOWS:"
980 PRINT #1, "WINDING I SQUARE R = "; PW; "WATTS"
990 PRINT #1, "WINDING EDDY LOSS = "; PE; "WATTS"
1000 PRINT #1, "STRAY LOSSES = "; PS; "WATTS"
1010 PRINT #1, "CORE LOSSES = "; PC; "WATTS"
1020 PRINT #1, "TOTAL LOSS = "; PT; "WATTS": PRINT #1,
1030 PRINT #1, "AT THIS KVA INPUT DATA FOR TEMPERATURES AS FOLLOWS:"
1040 PRINT #1, "RATED AVERAGE WINDING RISE OVER AMBIENT = "; THKVA2;
"C"
1050 PRINT #1, "TESTED AVERAGE WINDING RISE OVER AMBIENT = "; THEWA;
"C"
```

```
1060 PRINT #1, "HOTTEST SPOT RISE OVER AMBIENT = "; THEHSA; "C"
1070 PRINT #1, "TOP FLUID RISE OVER AMBIENT = "; THETOR; "C"
1080 PRINT #1, "BOTTOM FLUID RISE OVER AMBIENT = "; THEBOR; "C"
1090 PRINT #1, "RATED AMBIENT TEMPERATURE = "; TAR; "C"
1100 IF MCORE < 1 GOTO 1140
1110 PRINT #1, "CORE OVEREXCITATION OCCURS AT "; TIMCOR; "HOURS"
1120 PRINT #1, "CORE OVEREXCITATION LOSS IS "; PCOE; "WATTS"
1130 GOTO 1150
1140 PRINT #1, "CORE OVEREXCITATION DOES NOT OCCUR"
1150 IF MPR1 < 1 GOTO 1230
1160 PRINT #1,
1170 PRINT #1, " (LOAD-TEMPERATURE TABLE ON PAGE TWO)"
1180 FOR I = l TO 15
1190 PRINT #1,
1200 NEXT I
1210 PRINT #1, " LOAD TEMPERATURE TABLE"
1220 PRINT #1,
1230 TIMCOR = 60 * TIMCOR
1240 DT = .5
1250 IF (TAUW / DT) > 9 THEN GOTO 1270
1260 DT = DT / 2: GOTO 1250
1270 XMCP = (PE + PW) * TAUW / (TWRT - TDAOR): WWIND = XMCP / CPW
1280 IF WWIND > WCC GOTO 2260
1290 WCORE = WCC - WWIND: CPST = 3.51: WFL = GFLUID * 231 * RHOF
1300 SUMMCP = (WTANK * CPST) + (WCORE * CPST) + (WFL * CPF)
1310 DEF FNV (B, C, TMU) = B * EXP(C / (TMU + 273!))
1320 T = (TWRT + TDAOR) / 2: VISR = FNV(B, C, T)
```

```
1330 T = (THSR + TWOR) / 2: VIHSR = FNV(B, C, T)
1340 TMP = 0: IF MPR1 < 1 THEN DTP = 15
1350 KK = INT((TIM(JJ) / DTP) + .01)
1360 FOR K = 0 TO KK
1370 TMP = TMP + DTP: TIMP(K) = TMP
1380 NEXT K
1390 PRINT #1,
1400 C$ = "##.### ##.### ##.# ###.# ###.# ###.# ###.#"
1410 IF MPR1 < 1 THEN GOTO 1450
1420 PRINT #1, " TIME    PU    AMB    HS    TOPO  TOPDO DOTO"
1430 PRINT #1, " HOURS  LOAD  TEMP  TEMP  TEMP  TEMP  TEMP"
1440 PRINT #1,
1450 ON LCAS GOTO 1460, 1480
1460 THS = THSR: TW = TWRT: TTO = TTOR: TTDO = TTDOR: TBO = TBOR
1470 MPR = 0: JLAST = 2: GOTO 1490
1480 MPR = MPR1: JLAST = 1
1490 TFAVE = (TTO + TBO) / 2: TWO = TBO + (HHS * (TTDO - TBO))
1500 FOR JJJ = 1 TO JLAST
1510 IF JJJ = 2 THEN MPR = MPR1
1520 THSMAX = THS: TIMHS = 0: TTOMAX = TTO: TIMTO = 0
1530 J = 0: K = 0: TIMS = 0: TIMSH = 0: ASUM = 0
1540 IF MPR < 1 THEN GOTO 1560
1550 PRINT #1, USING C$; TIMSH; PUL(0); AMB(0); THS; TTO; TTDO; TBO
1560 TIMS = TIMS + DT
1570 IF TIMS > TIM(J + 1) THEN J = J + 1
1580 IF TIMS > TIM(JJ) THEN GOTO 2120
1590 TIMSH = TIMS / 60
```

```
1600 IF ABS(TIM(J + 1) - TIM(J)) < .01 THEN J = J + 1

1610 SL = (PUL(J + K + 1) - PUL(J + K)) / (TIM(J + 1) - TIM(J))

1620 PL = PUL(J + K) + (SL * (TIMS - TIM(J + K)))

1630 SLAMB = (AMB(J + K + 1) - AMB(J + K)) / (TIM(J + 1) - TIM(J))

1640 TA = AMB(J + K) + (SLAMB * (TIMS - TIM(J + K)))

1650 TDAO = (TTDO + TBO) / 2

1660 TKW = (TW + TK) / (TWR + TK)

1670 QWGEN = PL * PL * ((TKW * PW) + (PE / TKW)) * DT

1680 IF TW < TDAO THEN GOTO 1750

1690 ON MA GOTO 1700, 1700, 1700, 1730

1700 T = (TW + TDAO) / 2: VIS = FNV(B, C, T)

1710 QWLOST = (((TW - TDAO) / (TWRT - TDAOR)) ^ 1.25) * ((VISR / VIS) ^ .25) *
(PW + PE) * DT

1720 GOTO 1770

1730 QWLOST = ((TW - TDAO) / (TWRT - TDAOR)) * (PW + PE) * DT

1740 GOTO 1770

1750 QWLOST = 0

1760 IF TW < TBO THEN TW = TBO

1770 TW = (QWGEN - QWLOST + (XMCP * TW)) / XMCP

1780 DTDO = (TTDOR - TBOR) * ((QWLOST / ((PW + PE) * DT)) ^ X)

1790 TTDO = TBO + DTDO: TDAO = (TTDO + TBO) / 2

1800 TWO = TBO + (HHS * DTDO): TKHS = (THS + TK) / (THSR + TK)

1810 IF (TTDO + .1) < TTO THEN TWO = TTO

1820 IF THS < TW THEN THS = TW

1830 IF THS < TWO THEN THS = TWO

1840 QHSGEN = PL * PL * ((TKHS * PWHS) + (PEHS / TKHS)) * DT

1850 ON MA GOTO 1860, 1860, 1860, 1890
```

```
1860 T = (THS + TWO) / 2: VISHS = FNV(B, C, T)

1870 QLHS = (((THS - TWO) / (THSR - TWOR)) ^ 1.25) * ((VIHSR / VISHS) ^ .25) *
(PWHS + PEHS) * DT

1880 GOTO 1900

1890 QLHS = ((THS - TWO) / (THSR - TWOR)) * (PWHS + PEHS) * DT

1900 THS = (QHSGEN - QLHS + (XMCP * THS)) / XMCP

1910 QS = ((PL * PL * PS) / TKW) * DT

1920 QLOSTF = (((TFAVE - TA) / (TFAVER - TAR)) ^ (1 / YN)) * PT * DT

1930 IF MCORE < 1 THEN GOTO 1960

1940 IF TIMS < TIMCOR THEN GOTO 1960

1950 QC = PCOE * DT: GOTO 1970

1960 QC = PC * DT

1970 TFAVE = (QWLOST + QC + QS - QLOSTF + (SUMMCP * TFAVE)) / SUMMCP

1980 DTTB = ((QLOSTF / (PT * DT)) ^ Z) * (TTOR - TBOR)

1990 TTO = TFAVE + (DTTB / 2): TBO = TFAVE - (DTTB / 2)

2000 IF TBO < TA THEN TBO = TA

2010 IF TTDO < TBO THEN TTDO = TBO

2020 AX = (15000 / 383) - (15000 / (THS + 273))

2030 A = EXP(AX): ASUM = ASUM + (A * DT)

2040 IF THS < THSMAX THEN GOTO 2060

2050 THSMAX = THS: TIMHS = TIMSH

2060 IF TTO < TTOMAX THEN GOTO 2080

2070 TTOMAX = TTO: TIMTO = TIMSH

2080 IF TIMS < TIMP(K) THEN GOTO 1560

2090 IF MPR < 1 THEN GOTO 2110

2100 PRINT #1, USING C$; TIMSH; PL; TA; THS; TTO; TTDO; TBO

2110 K = K + 1: GOTO 1560
```

```
2120 NEXT JJJ
2130 TIMS = TIMS - DT: ASUM = ASUM / 60: AEQ = ASUM / TIMSH: PRINT #1,
2140 PRINT #1, "TEMPERATURES DURING LOAD CYCLE:"
2150 PRINT #1, "MAX. HOT SPOT TEMP. = "; THSMAX; "AT "; TIMHS; "HOURS"
2160 PRINT #1, "MAX. TOP FLUID TEMP. = "; TTOMAX; "AT "; TIMTO; "HOURS"
2170 PRINT #1, "FINAL HOT SPOT TEMP. ="; THS
2180 PRINT #1, "FINAL AVE. WIND. TEMP. ="; TW
2190 PRINT #1, "FINAL TOP OIL TEMP. ="; TTO
2200 PRINT #1, "FINAL DUCT OIL TEMP. ="; TTDO
2210 PRINT #1, "FINAL BOT. OIL TEMP. ="; TBO
2220 PRINT #1, "EQUIVALENT AGING = "; ASUM; "HOURS"
2230 PRINT #1, "LOAD CYCLE DURATION = "; TIMSH; "HOURS"
2240 PRINT #1, "EQUIVALENT AGING FACTOR = "; AEQ; "PER UNIT"
2250 GOTO 2290
2260 PRINT "WINDING TIME CONSTANT TOO HIGH"
2270 PRINT #1, "CHANGE INPUT TO LOWER VALUE"
2280 PRINT "CHANGE INPUT TO LOWER VALUE IN INPUT FILE"; F2$
2290 CLOSE #1
2300 END
```

REFERENCES

[1] Liew, M.C. and Bodger, P.S., "Reverse design transformer modelling", 6th National NZ Postgraduate Conference, University of Canterbury, Christchurch, NZ, 19-21 November, 1999.

[2] Bell, S.C. (2008). High-voltage partial-core resonant transformers. University of Canterbury, PhD thesis.

[3] Bodger, P. S. and Enright, W. G. (2004). A resonant transformer for high voltage testing of generator stators. Australian Journal of Electrical and Electronics Engineering, 1(3):179–185.

[4] Bodger, P. S., Enright, W. G., and Ho, V. (2005). A low voltage, mains frequency, partialcore, high temperature, superconducting transformer. In Australasian Universities Power Engineering Conference (AUPEC), volume 1, pages 73–78, Hobart, Australia.

[5] Lynch, K., Bodger, P. S., Enright, W. G., and Bell, S. C. (2007). Partial core transformer for energization of high voltage arc-signs. In 15th International Symposium on High Voltage Engineering, Ljubljana, Slovenia. Paper T3.304, CD-ROM.

[6] Bell, S. C., Enright, W. G., Tunstall, K. R., and Bodger, P. S. (2007). Lightning arc drawings - dielectric barrier discharges for artwork. In 15th International Symposium on High Voltage Engineering, Ljubljana, Slovenia. Paper T9.305, CD-ROM.

[7] Bodger, P. S. and Liew, M. C. (2002). Reverse as-built transformer design method. International Journal of Electrical Engineering Education (IJEEE), 39(1):42–53.

[8] Liew, M. C (2001). Reverse Design Transformer Modeling Technique with Particular Application to Partial Core Transformers. University of Canterbury, PhD thesis,

[9]Kawasaki Steel Corporation (1997). New Grain-Oriented Magnetic Steel Strip with ultra-high flux density and low iron loss.

[10] Huo XiTing (2009), New Model of Eddy Current Loss Calculation and Applications for Partial Core Transformers, University of Canterbury, ME thesis.

[11] IEEE Standards Board (1995) “IEEE Guide for Loading Mineral-Oil-Immersed Transformers”

[12] BIOTEMP® Biodegradable Dielectric Insulating Fluid. ABB. (2/29/2012). http://www.nttworldwide.com/docs/BIOTEMP-ABB.pdf

[13] Pierce, L. W, ‘‘An Investigation of the Thermal Performance of an Oil Filled Transformer Winding,’’ IEEE Transactions on power delievery,Vol,7,no.3,pp.1345-1358,July 1992.

[14] IEC60067-2 Power transformer Temperature rise (1994)

[15] Martin J. Heathcote, CEng, FIEE (Twelfth edition), The J & P Transformer Book. (1998)

[16] ABB, Distribution transformer national efficiency standards. (2/29/2012)

http:// www05.abb.com/global/scot/scot252.../1luj460200-lte_doe_bro.pdf

[17] Safety- from the generation of electricity to its use (2/29/2012), http://www.krempel-group.com/englisch/home/products/electrical-insulations/insulating-sleevings-tapes-and-cords.html

[18] Kevin Schmit and Baton Rouge, (1998). LA fiberglass reinforced plastic (FRP) piping systems designing process/ facilities piping systems with FRPA comparison to traditional metallic materials. http:// www.fiberbond.com/docs/LoadingConditions.pdf (2/29/2012)

[19] NMN/NPN Dexlu Item No: D030103, Suzhou Dexlu Material &Tech Co.Ltd. (2/29/2012). http://www.dexlu.cn/flexible/NMN-6640.html

[20] IEC 60076-1 International standards Power transformers General (2004).

[21] Megger. The Complete Guide to Electrical Insulation Testing (2/29/2012) http://www.omnicontrols.com/articles...ch_in_Time.pdf

[22]IEEE 62-1995 Guide for Diagnostic Field Testing of Electric Power Apparatus-Part 1:

Oil Filled Power Transformer, Regulators, and Reactors (1995)

[23] Fluke instruction sheet Model 80k-40 high voltage probe (2/29/2012)

http://cef.uca.edu.sv/labsfisica/fisica%20III/80k40___iseng0900.pdf

[24]Fluke 41B power meter manual (2/29/2012)

http://www.fluke.com/fluke/usen/Discontinued-Products/41B.htm?PID=54783

[25] Giorgio Bertotti, General Properties of Power Losses in Soft Ferromagnetic Materials,

IEEE Transactions on Magnetics, vol. 24, no. 1, January 1988, pp. 621- 630.

[26] Mains Electricity (4/19/2012) Http://en.wikipedia.org/wiki/Mains_electricity.

[27] Mains electricity by country (23/08/2012) http://en.wikipedia.org/wiki/Mains_electricity_by_country.

[28] Mains electricity (04/02/2012)

http://en.wikipedia.org/wiki/Mains_electricity.